

New aspects of quality control of pharmaceutical tablets
with special focus on enzyme tablets

Dissertation

with the aim of achieving a doctoral degree
at the Faculty of Mathematics, Informatics and Natural Sciences

Department of Chemistry

Universität Hamburg

submitted by

Marten Klukkert

Hamburg 2015

Reviewer of the thesis:

Professor Dr. Claudia S. Leopold

Professor Dr. Hans-Ulrich Moritz

Thesis defense committee:

Professor Dr. Claudia S. Leopold

Professor Dr. Sascha Rohn

Dr. Werner Pauer

Date of thesis defense:

26th November 2015

Acknowledgements

The experimental part of this work was prepared from January 2011 until December 2014 at the Department of Chemistry, division of Pharmaceutical Technology, University of Hamburg, on the initiative and under supervision of Professor Dr. Claudia S. Leopold.

First, I would especially like to thank Prof. Dr. Leopold for leaving me this interesting research topic and for the chance to being a member of her research group. I deeply appreciated the provided scope and freedom to do research and that she always had an open door to discuss scientific approaches and to give guidance.

Furthermore, I am deeply grateful to Prof. Dr. Dr. h.c. Thomas Rades from the University of Copenhagen for being co-supervisor of my work and proofreading of this thesis. I really enjoyed the inspiring discussions with him, his effort for the joint research projects, and the warm welcome to his group during my research visits at the University of Copenhagen.

Moreover, I thank Prof. Dr. Hans-Ulrich Moritz for evaluating my thesis and Dr. Werner Pauer for serving as a member of the examination committee. Special thanks to Prof. Dr. Sascha Rohn for the interesting discussions on protein analysis and for also being member of the examination committee.

Furthermore, I am grateful to Dr. Albrecht Sakmann for his engagement regarding my work and the good working climate. Petra Borbe and Kai Braunschweig are thanked for their assistance with regard to enzymatic activity determinations and tableting experiments.

Moreover, I thank Associate Prof. Dr. Marco van de Weert and Dr. Mathias Fanø from the University of Copenhagen for the friendly welcome in their lab and their help regarding acquisition and interpretation of the differential scanning calorimetry and size-exclusion data, respectively. Associate Prof. Dr. Jens Michael Carstensen from the Technical University of Denmark is deeply thanked for kindly supplying the VideometerLab UV imager and the interesting discussions on image analysis.

Moreover, I like to thank Prof. Dr. Jukka Rantanen and Dr. Jian-Xiong Wu from the University of Copenhagen for the fruitful imaging research collaborations. I really appreciated Jians advice with regard to multivariate data and image analysis and the discussions with him really got me enthusiastic about this field of research. Furthermore, I like to thank Dr. Morten Allesø and Uffe Teis Savre from Lundbeck A/S for the chance to use the NIR imager and for their assistance in acquiring the NIR images.

In addition, I would like to thank my colleagues from the pharmaceutical technology research group, especially Dr. Marc Michaelis, Dr. Ines Saniocki, Andreas Beyer, Dr. Robert Wulff, and Anna Novikova for the productive scientific discussions, the nice working atmosphere, and the good times during the conference journeys. Special thanks go to my former colleague Dr. Sönke Carsten Rehder for his deep interest in my work and the various productive discussions about project planning and data analysis.

I am furthermore grateful to the University of Hamburg, the German Academic Exchange service, the GlaxoSmithKline foundation, the German Chapter of the Controlled Release Society, as well as the Analysis and Pharmaceutical Quality section of the American Association of Pharmaceutical Scientists for the financial support of my research visits and congress participations.

I dearly thank Milana, my parents, and my brother for their interest in my work, their endless understanding, and their support in all situations of life. Their encouragement significantly contributed to the success of this work.

Summary

Manufacturing of pharmaceutical tablets is usually a multistep process including compaction of the powder blend, tablet coating, and packaging. Lately, tableting has become an attractive formulation alternative for protein Active Pharmaceutical Ingredients (APIs) as promising approaches for oral delivery and bioavailability of biomacromolecules have been developed. Thus, there is an increasing interest in the effect of the compaction pressure on the integrity of protein APIs. Therefore, in the first chapter of this work the influence of the compaction pressure during tableting on the conformation and thermal stability of trypsin, a model protein API, was investigated. The study revealed that with increasing compaction pressure the enzymatic activity of trypsin decreases, accompanied by conformational alterations in the solid state, which were found to be partially reversible upon tablet reconstitution in water. The irreversible conformational changes could be accurately determined qualitatively and quantitatively by aqueous state infrared spectroscopy and could be used as estimate for trypsin enzymatic activity. Furthermore, it was shown that trypsin thermal stability was reduced by the applied compaction pressure, as demonstrated by a significantly reduced folding reversibility after denaturation.

Caused by the Quality by Design (QbD) and Process Analytical Technology (PAT) frameworks launched by the regulatory authorities from 2004 on, pharmaceutical manufacturers successively change their quality control strategy from testing representative samples in laboratories to monitoring product quality in the manufacturing line. This so-called real-time sample characterization allows to correlate the determined product specifications with the manufacturing parameters and to establish a feedback control system that is beneficial for process understanding and control. For this purpose, spectral imaging techniques have been shown to be attractive alternatives to traditional quality control procedures, as they are non-destructive, do not require sample preparation, and provide spatially resolved spectral information. In this context, the second goal of this work was to

investigate the suitability of multispectral UV imaging as a reliable and rapid technique for quality control of tablets. Image analysis routines should be established having potential for real-time tablet characterization. Upon compaction, stresses applied to the tablet formulation influence the physicochemical properties of the prepared tablets. Therefore, in the second chapter of this work the applicability of multispectral UV imaging for determination of quality-relevant chemical and physical tablet attributes was investigated. Based on UV images, the tablet (protein)-API content and hardness could be assessed, splintering of tablets could be detected and qualitative as well as quantitative information about the surface density distribution was obtained.

To guarantee the desired tablet performance and to ensure patient safety it is essential to detect cracks on the tablet surface as well as to verify intactness and readability of imprinted codes. Therefore, one aim of the third study described in this work was to monitor these tablet attributes by UV imaging. Furthermore, during tablet packaging it is required to control correct filling of blister packs and to prevent cross contamination in the production line. Therefore, another goal of this study was to apply UV imaging to detect tablets in blister packs as well as to characterize blister packs according to the type of the packaged tablets and the used blister sealing foil. It could be shown that UV imaging allows accurate detection of cracks and imprint defects. In addition, it could be confirmed, that UV imaging is a valuable technique to detect tablets within blisters as well as to classify blister packs based on the type of the tablets therein and the type of the blister sealing foil.

Coating is another common tablet manufacturing step, as coatings may control the API release, facilitate the tablet intake, and improve tablet appearance. Thus, in the fourth chapter of this work, the applicability of UV imaging was investigated in terms of evaluation of tablet coating intactness and texture. Based on UV images, different types of coating layer defects could be detected, distinguished, and localized. In addition, UV imaging allowed differentiation of tablets with a homogeneous coating from those with an unacceptably inhomogeneous coating texture.

Zusammenfassung

Die Herstellung pharmazeutischer Tabletten ist üblicherweise ein mehrstufiger Prozess, der Vorgänge wie das Tablettieren an sich, das Überziehen der Tabletten sowie deren Verpackung einschließt. In letzter Zeit hat sich die Tablettierung zu einem attraktiven alternativen Verfahren zur Formulierung von Protein-Arzneistoffen entwickelt, da vielversprechende Ansätze zur Verbesserung der oralen Bioverfügbarkeit von Proteinen entwickelt wurden. Hieraus resultiert ein wachsendes Interesse am Einfluss der Tablettierung auf die physikochemischen Eigenschaften von Proteinen. Daher wurde im ersten Kapitel dieser Arbeit der Einfluss des Pressdrucks auf die Konformation und die thermische Stabilität von Trypsin, einem Modellprotein, untersucht. Die Studie hat gezeigt, dass dessen enzymatische Aktivität mit steigendem Pressdruck abnimmt und mit Konformationsänderungen im festen Aggregatzustand des Proteins einhergeht, die jedoch bei Rekonstitution der Tabletten in Wasser teilweise reversibel sind. Die irreversiblen Konformationsänderungen konnten qualitativ und quantitativ präzise durch Infrarotspektroskopie der Proteinlösungen bestimmt und anhand dieser die Trypsin-Aktivität abgeschätzt werden. Weiterhin konnte gezeigt werden, dass der Tablettierdruck die thermische Stabilität von Trypsin reduziert, was anhand einer reduzierten Reversibilität der Faltung nach Denaturierung belegt wurde.

Bedingt durch die Quality by Design (QbD) und Process Analytical Technology (PAT) Initiativen der Regulierungsbehörden die seit dem Jahr 2004 veröffentlicht wurden, ändert sich schrittweise die Strategie der pharmazeutischen Hersteller hinsichtlich der Kontrolle der Produktqualität. Die konventionelle Analytik von repräsentativen Produktmustern in Qualitätskontrolllaboren wird ergänzt um Methoden, die es erlauben, die Produktqualität bereits innerhalb der Fertigungslinie zu erfassen. Eine solche Probencharakterisierung in ‚Echtzeit‘ ermöglicht eine Korrelation zwischen den erfassten Produktspezifikationen und den Herstellungsparametern und ermöglicht die Etablierung eines Feedback-Kontrollsystems zur gezielten Steuerung des Prozesses. Zu diesem Zweck haben sich spektrale Imaging Methoden als

wertvolle Alternativen zu herkömmlichen Qualitätskontroll-Methoden erwiesen, da sie nicht-zerstörend und ohne weitere Probenvorbereitung räumlich aufgelöste spektrale Informationen liefern. Ein weiteres Ziel dieser Arbeit war es daher, die Eignung des multispektralen UV-Imaging als zuverlässige und schnelle Methode zur Qualitätskontrolle von Tabletten zu untersuchen. Hierbei sollten Bildauswerterroutinen eingesetzt werden, die Potential zur Charakterisierung von Tabletten in Echtzeit haben. Beim Tablettieren werden durch die auf das Tablettiergut einwirkenden Kräfte die physikochemischen Eigenschaften der hergestellten Tabletten beeinflusst. Daher wurde im zweiten Kapitel dieser Arbeit untersucht, ob sich mittels UV-Imaging qualitätsrelevante chemische und physikalische Tabletteneigenschaften bestimmen lassen. Anhand der UV-Bilder konnten einerseits chemische Informationen über den (Protein)-Arzneistoffgehalt bestimmt werden sowie physikalische Parameter wie die Härte der Tabletten erfasst, Absplitterungen detektiert und qualitative als auch quantitative Informationen über den Dichteverlauf an der Tablettenoberfläche gewonnen werden.

Um die gewünschten Tabletteneigenschaften und damit die Patientensicherheit zu gewährleisten, ist es zudem notwendig, Risse auf der Tablettenoberfläche zu erkennen und die Unversehrtheit und Lesbarkeit von Einprägungen sicherzustellen. Ein Ziel der im dritten Kapitel dieser Arbeit beschriebenen Studie war es daher, diese Oberflächenmerkmale durch UV-imaging zu bestimmen. Zudem ist während des Verpackungsprozesses von Tabletten die korrekte Füllung der Blister sicherzustellen und eine Kreuzkontamination in der Produktionslinie zu verhindern. Ein weiteres Ziel dieser Studie war es daher, anhand der UV-Bilder eingeblisterte Tabletten zu detektieren, sowie Blister anhand der Art der verpackten Tabletten und der verwendeten Siegelfolie zu charakterisieren. Es zeigte sich, dass UV-Imaging eine präzise Erkennung von Rissen sowie Defekten an Einprägungen ermöglicht. Zudem stellt UV-Imaging eine geeignete Methode zum Detektieren verblisteter Tabletten sowie zur Klassifizierung von Blistern anhand der Art der sich darin befindlichen Tabletten und der verwendeten Siegelfolie dar.

Das Überziehen von Tabletten ist ein weiterer häufig durchgeführter Prozessschritt der Tablettenherstellung, da Überzüge z.B. der Steuerung der Arzneistofffreisetzung, sowie der Erleichterung der Tabletteneinnahme oder der Verbesserung des Erscheinungsbilds der Tabletten dienen. Im vierten Kapitel dieser Arbeit wurde die Eignung des UV-imaging zur Untersuchung der Unversehrtheit und Oberflächenbeschaffenheit von Tablettenüberzügen untersucht. Anhand der UV-Bilder konnten verschiedene Arten von Defekten des Überzugs detektiert, unterschieden und lokalisiert werden. Zudem konnten Tabletten mit einem homogenen von solchen mit inakzeptabel inhomogenen Überzug unterschieden werden.

Contents

Acknowledgements.....	III
Summary.....	V
Contents	X
List of Figures.....	XV
List of Tables	XIX
List of Abbreviations	XX
1 Introduction.....	1
1.1 Relevance of pharmaceutical tablets	2
1.1.1 General aspects.....	2
1.1.2 Oral delivery of biomacromolecules	4
1.2 Tablet manufacturing and quality control in context with the QbD and PAT initiatives	7
1.3 Product quality attributes during tablet manufacturing.....	11
1.3.1 Assessment of relevant tablet quality attributes.....	11
1.3.2 Tablet quality attributes and related process parameters	13
1.3.3 Specific aspects of the manufacturing of tablets containing biomacromolecules	18
1.4 Analytical techniques for quality control during tablet manufacturing	20
1.4.1 Process monitoring in context with the QbD and PAT initiatives.....	20
1.4.2 Spectroscopic methods.....	24
1.4.2.1 General aspects	24
1.4.2.2 Mid-infrared spectroscopy	25
1.4.2.3 Near-infrared spectroscopy	26
1.4.2.4 Raman spectroscopy	27
1.4.2.5 Application of spectroscopic methods for non-destructive tablet quality control.....	28
1.4.2.6 Structural characterization of biomacromolecules by mid-infrared spectroscopy	30
1.4.3 Spectral imaging techniques.....	34
1.4.3.1 General aspects	34
1.4.3.2 Working principles of spectral imaging techniques	36

1.4.3.3	Application of spectral imaging techniques for non-destructive quality control of tablets.....	38
1.4.3.4	UV imaging for quality control	41
1.5	Analysis of spectral data sets.....	44
1.5.1	Spectral data analysis pathway and preprocessing.....	44
1.5.1.1	Centering and scaling.....	47
1.5.1.2	Baseline correction and normalization.....	49
1.5.1.2.1	Offset correction.....	50
1.5.1.2.2	Area normalization	50
1.5.1.2.3	SNV correction	50
1.5.2	Uni- and multivariate analysis	52
1.5.2.1	General aspects.....	52
1.5.2.2	Principal Component Analysis.....	54
1.5.2.3	Partial Least Squares Regression	57
1.5.3	Pattern recognition techniques	60
1.5.3.1	General aspects.....	60
1.5.3.2	k-Nearest Neighbor.....	61
1.5.3.3	Soft Independent Modelling by Class Analogy	63
1.6	Objectives of this work.....	66
2	Materials and Methods	68
2.1	Materials	69
2.1.1	Active Pharmaceutical Ingredients	69
2.1.2	Tableting excipients	69
2.1.3	Chemical reagents	69
2.1.4	Bulk tablets.....	70
2.1.5	Packaging material	70
2.2	General methods	71
2.2.1	Tableting.....	71
2.2.2	UV imaging.....	71
2.2.3	Photographic imaging	72
2.2.4	Image analysis and statistics	73
2.2.5	Pattern recognition.....	73

2.3	Specific methods of ‘Influence of tableting on the conformation and thermal stability of trypsin as a model protein’	76
2.3.1	Preparation of tablets.....	76
2.3.2	Assay of trypsin activity	76
2.3.3	Fourier transform infrared spectroscopy	77
2.3.4	Liquid-state differential scanning calorimetry.....	79
2.4	Specific methods of ‘UV Imaging for fast and non-destructive quality control of chemical and physical tablet attributes’	81
2.4.1	Preparation of tablets.....	81
2.4.2	Hyperspectral near-infrared spectroscopic imaging.....	84
2.4.3	Image analysis and related statistics.....	85
2.4.3.1	General aspects	85
2.4.3.2	Estimation of the tablet API content.....	85
2.4.3.3	Evaluation of tablet hardness	87
2.4.3.4	Evaluation of tablet intactness and surface density profile.....	87
2.4.4	Pattern recognition	88
2.4.5	Radial tensile strength of the tablets.....	89
2.5	Specific methods of ‘Non-destructive quality control of tablets and blister packs by UV imaging’.....	90
2.5.1	Sample preparation.....	90
2.5.2	Photographic imaging	90
2.5.3	Image analysis and related statistics.....	90
2.5.3.1	General aspects	90
2.5.3.2	Characterization of blister packs.....	91
2.5.3.2.1	General aspects	91
2.5.3.2.2	Pattern recognition.....	91
2.5.3.3	Evaluation of imprint intactness	92
2.5.3.4	Detection of cracks.....	93
2.6	Specific methods of ‘Rapid assessment of tablet film coating quality by multispectral UV imaging’	94
2.6.1	Preparation of tablets.....	94
2.6.2	Pan coating	94
2.6.3	Photographic imaging	95
2.6.4	Photometric stereo.....	95
2.6.5	Image Analysis and related statistics.....	95
2.6.5.1	General aspects	95

2.6.5.2	Evaluation of tablet coating layer intactness	96
2.6.5.3	Evaluation of tablet coating texture	98
3	Results and Discussion	100
3.1	Results and discussion of ‘Influence of tableting on the conformation and thermal stability of trypsin as a model protein’	101
3.1.1	Influence of tableting on trypsin bioactivity.....	101
3.1.2	Influence of tableting on the conformation of trypsin.....	103
3.1.2.1	Structural characterization by FTIR spectroscopy.....	103
3.1.2.2	Quantification of the reversibility of pressure-induced conformational changes of trypsin	105
3.1.2.3	Principal Component Analysis of the aqueous state spectral dataset	107
3.1.2.4	Partial Least Squares Regression of the aqueous state spectral dataset	109
3.1.3	Influence of tableting on the transition temperature of unfolding and folding reversibilities of trypsin	112
3.1.4	Conclusion.....	115
3.2	Results and discussion of ‘UV Imaging for fast and non-destructive quality control of chemical and physical tablet attributes’	117
3.2.1	Estimation of the tablet API content.....	117
3.2.2	Estimation of the radial tensile strength of tablets.....	120
3.2.3	Evaluation of tablet intactness and surface density profiles.....	123
3.2.3.1	Quantification of surface density inhomogeneity	129
3.2.4	Conclusion.....	131
3.3	Results and discussion of ‘Non-destructive quality control of tablets and blister packs by UV imaging’	133
3.3.1	Verification of blister pack filling.....	133
3.3.2	Characterization of blister packs	135
3.3.2.1	General aspects.....	135
3.3.2.2	Pattern recognition	137
3.3.3	Visual inspection of unblistered tablets	140
3.3.3.1	Imprint intactness	140
3.3.3.2	Tablet surface cracks.....	143
3.3.4	Conclusion.....	147

3.4	Results and discussion of ‘Rapid assessment of tablet film coating quality by multispectral UV imaging’	148
3.4.1	Detection, differentiation, and localization of coating defects	148
3.4.2	Evaluation of tablet coating texture	156
3.4.3	Conclusion	161
4	References	162
5	Appendix	195
A	Curriculum vitae	196
B	Conference contributions and publications	197
C	Hazardous materials	200
D	Declaration on oath / Eidesstattliche Versicherung	202

List of Figures

Figure	Caption	Page
1	Tablet manufacturing flow chart.	7
2	Implementation principles of process analyzers.	22
3	FTIR-ATR spectrum of bovine trypsin.	31
4	Assignment of bands within the amide I infrared spectrum to protein secondary structures.	32
5	Three-dimensional spectral data cube obtained by NIR imaging.	34
6	Visualization of image acquisition methods (FOV: field of view).	36
7	Data analysis pathway of (a) single-point and (b) imaging spectroscopic datasets.	44
8	Unprocessed (a) and mean centered (b) UV spectra of tablets prepared at different compaction pressures.	47
9	Unprocessed (a) and SNV corrected (b) NIR absorbance spectra.	51
10	Overview of uni- and multivariate analysis.	52
11	Illustration of a principal component data space.	55
12	Data matrices of PCA.	56
13	Underlying structure of a PLS Regression model.	58
14	(a) Working principle of the UV imager, (b) Multispectral UV imager, (c) Resulting three-dimensional data array of a tablet.	72
15	Imaging data analysis pathway for evaluation of tablet API content, hardness, intactness, and surface density profile.	86
16	(a) Enzymatic activity of trypsin as a function of the applied compaction pressure during tableting. Results are calculated as means \pm SD ($n \geq 3$). (b) Solid state and (c) Aqueous state amide I spectra of trypsin. Only representative spectra of unprocessed and 382 MPa samples are shown.	102

Figure	Caption	Page
17	The area overlap approach applied to a representative compacted trypsin sample and the mean spectrum of unprocessed trypsin (n=3). The gray area corresponds to the area overlap of the two solid state spectra.	105
18	(a) From top to bottom: difference spectrum of amide I spectra of a heat-denatured sample and unprocessed trypsin; difference spectrum of a sample compacted at 382 MPa and unprocessed trypsin; PCA loadings plot of PC-1. (b) PCA scores plot for trypsin secondary structure changes during tableting.	108
19	PLS Regression plot (R ² of calibration: 0.988, slope: 0.988, RMSECV: 0.47 %) of predicted activity according to the aqueous state FTIR spectral dataset (predicted activity loss) vs. activity loss according to the USP photometric reference method (measured activity loss).	110
20	Representative example of consecutive calorimetric heating scans for unprocessed trypsin. Thermograms were recorded at a heating rate of 1 K/min and subsequently concentration normalized. ΔH: calorimetric enthalpy; T _m : transition temperature of unfolding.	113
21	(a) Representative mean UV absorbance spectra of tablets with different amylase contents (b) PCA loadings plots (c) PCA scatter plot for tablets with different amylase contents (d) PLS Regression plot (R ² of calibration: 0.991, slope: 0.991) of the predicted amylase content of the tablets based on the mean UV absorbance spectra as a function of the tablet amylase content (RMSEP: 3.1 %).	118
22	(a) Representative mean UV absorbance spectra of tablets with a different RTS as determined by a hardness tester (b) PCA loadings plots (c) PCA scatter plot for tablets with a different RTS (d) PLS Regression plot (R ² of calibration: 0.972, slope: 0.972) of the predicted RTS of trypsin tablets based on the mean UV absorbance spectra as a function of the measured RTS (RMSEP: 0.36 MPa).	121
23	Analysis of UV images of tablets prepared at different compaction pressures. Columns from left to right correspond to the PCA score images of PC-1, mean UV spectra of representative tablet regions, loadings plots of PC-1, and relative SD of PC-1 scores of the concentric subunits as a function of the tablet radius (thickness of subunits: 2 pixels).	124

Figure	Caption	Page
24	Analysis of NIR images of tablets prepared at different compaction pressures. Columns from left to right correspond to the PCA score images of PC-1, mean NIR absorbance spectra of representative image regions, loadings plots of PC-1, and relative SD of PC-1 scores of the concentric subunits as a function of the tablet radius (thickness of subunits: 4 pixels).	127
25	(a) Representative UV images of partly or completely filled blister packs that contain tablets 'B' and/or tablets 'D'. The blister packs were either unsealed (I) or sealed with PVC PH 154 foil (II), PCTFE/PVC foil (III), or PVC PH 132 foil (IV). (b) Binary images of the blister packs with tablets being highlighted (red).	134
26	(a) Representative mean UV spectra of tablets 'B' (—) and 'D' (---) within blister packs. (b) PCA loadings plots of PC-1 and PC-2. (c) PCA scores plot of mean UV spectra of tablets 'B' (●) and 'D' (▲) within blister packs.	136
27	Image analysis of tablets 'A' with either intact (a) or defect (b and c) imprint. Columns from left to right correspond to photographic images (I), 365 nm gray scaled UV images (II), PC-1 scores images resulting from application of PCA to the UV images (III), binary images obtained by setting a hard threshold in the scores images (IV), processed binary images (V).	141
28	(a) Representative mean UV absorbance spectra of high- and low-intensity pixels (refer to Fig. 27: column III) of tablet 'A' with intact imprint. (b) Loadings plot of PC-1.	142
29	Image analysis of tablets 'C' with cracks on the surface. Rows from top to bottom correspond to photographic images (a), 365 nm UV images (b), PC-1 scores images obtained from application of PCA to the UV images (c), and binary images resulted from application of an edge detection algorithm to the scores images (d).	144
30	(a) Representative mean UV absorbance spectra of high- and low intensity pixels (refer to Fig. 29c) of tablet 'C' with cracks on the surface. (b) Loadings plot of PC-1.	146
31	(a) Mean UV absorbance spectra of an uncoated and a coated ASA tablet, respectively (b) PCA (Table 5: model 1) scatter plot applied to all pixels of uncoated and coated ASA tablets (c) Loadings plot of PC-1 and PC-2.	149

Figure	Caption	Page
32	Image analysis of representative ASA tablets with either homogeneous or inhomogeneous coatings. Columns from left to right correspond to photographic images (I), UV images at 365 nm (II), PCA (Table 5: model 1) scatter plots (III), binary images obtained from application of an edge detection algorithm on PC-1 (Table 5: PCA model 1) scores images (IV) binary images with pixels assigned to the class of uncoated ASA tablet pixels (Table 5: PCA model 2) being highlighted (V).	151
33	Image analysis of representative ASA tablets with an acceptably homogeneous (a) or an inhomogeneous (b) coating texture. Columns from left to right correspond to photographic images (I), photometric stereo darkfield images (II), UV images at 365 nm (III), and PC-1 scores images (IV).	156
34	(a) Mean UV spectra of high and low PC-1 score intensity pixels (b) Loadings plot of PC-1 (c) Deviation of the average score variation (\bar{X}_a) of 11 test tablets from the mean reference \bar{X}_a of tablets with the desired coating texture.	158

List of Tables

Table	Caption	Page
1	Excerpt of a Quality Target Product Profile of a tablet formulation.	12
2	Examples of pharmaceutical process parameters and related product quality attributes.	14
3	Overview of the compaction experimental setup.	82
4	SIMCA classification model.	92
5	PCA models applied to the UV images for detection, differentiation, and localization of coating defects. Prior to PCA all spectral datasets were mean-centered.	97
6	Area overlap (%) of normalized amide I spectra dependent on the applied compaction pressure. The area overlap is calculated in relation to a mean spectrum of unprocessed trypsin in the solid state and in the aqueous state, respectively. Results are calculated as means \pm SD (n=3).	106
7	Transition temperature (T _m) of unfolding and folding reversibility after thermal denaturation of trypsin samples in dependence of the applied compaction pressure. Results are calculated as means \pm SD (n=3).	113
8	Classification according to the SIMCA model. Tablets were assigned to class 1 and class 2 based on their intactness and surface density profiles.	128
9	Classification table of blister packs according to the tablet composition and sealing foil.	138

List of Abbreviations

API	Active Pharmaceutical Ingredient
ASA	Acetylsalicylic acid
ATR	Attenuated total reflection
BAEE	Benzoyl-L-arginine ethyl ester hydrochloride
CCD	Charge-coupled Device
CGMP	Current Good Manufacturing Practice
CI	Chemical Imaging
CMA	Critical Material Attributes
CPP	Critical Process Parameters
DSC	Differential scanning calorimetry
EDQM	European Directorate for the Quality of Medicines and HealthCare
FDA	Food and Drug Administration
FTIR	Fourier transform infrared
GI	Gastrointestinal tract
GLP-1	Glucagon-like-peptide-1
GMP	Good Manufacturing Practice
ICH	International Conference on Harmonisation of Technical Requirements for Registration of Pharmaceuticals for Human Use
KNN	k-Nearest Neighbor
LV	Latent variable
MCC	Microcrystalline cellulose
MCR	Multivariate Curve Resolution
MgSt	Magnesium stearate
MIR	Mid-infrared
NIR	Near-infrared

PAT	Process Analytical Technology
PC	Principle component
PCA	Principle Component Analysis
PCTFE	Polychlorotrifluoroethylene
PEG	Polyethylene glycol
Ph. Eur.	European Pharmacopoeia
PLS	Partial Least Squares
PVA	Polyvinyl alcohol
PVC	Polyvinyl chloride
QbD	Quality by Design
QTPP	Quality Target Product Profile
RMSEC	Root mean square error of calibration
RMSECV	Root mean square error of cross validation
RMSEP	Root mean square error of prediction
roiD	Region of increased density
rSD	Relative standard deviation
RTS	Radial tensile strength
SEC	Size Exclusion Chromatography
SIMCA	Soft Independent Modelling by Class Analogy
SNV	Standard Normal Variate
T_m	Transition temperature
USP	United States Pharmacopeia
UV	Ultraviolet
VIS	Visible
%ao	Percentage of area overlap

1 Introduction

1.1 Relevance of pharmaceutical tablets

1.1.1 General aspects

Pharmaceutical products are predominantly taken orally because of the easy way of administration as well as a higher safety compared to other routes of administration (1, 2). Tablets represent the predominant dosage form for pharmaceutical APIs with a market share of about 80 % and are particularly attractive in terms of an usually fast and straightforward manufacturing process, the ease of handling during shipping, storage, and administration, as well as a high stability of the formulation and lower costs compared to other dosage forms (3–5).

From a technological perspective, tablets are attractive because the physicochemical properties of the compacts can be specifically tailored to the demands of the patients and customers by a variety of well-established technologies. For instance, coatings can be applied to the tablets to facilitate the intake, provide taste masking, protect moisture or light sensitive APIs from the environment, as well as to control drug release (6–10). In addition, the opportunity to modify the appearance of tablets is interesting for pharmaceutical manufacturers in terms of marketing as well as patient compliance (11, 12). Moreover, the possibility to apply imprinted codes indicating the tablet composition and strength of the dose allow to unambiguously identify dosage forms (11, 13).

Thus, there are several advantages of tablets emphasizing their predominant role within the market for oral dosage forms. In this context, considerably effort has been made throughout decades to understand the tableting process and the influence of associated stress on the quality of the resulting compact. Although the basic principle

of compaction and powder particle deformation is well-understood (1, 14–18), a paradigm change with regard to tablet quality control (19–21) as well as the compaction properties of newly developed APIs and excipients require further distinct research in the field of tableting.

1.1.2 Oral delivery of biomacromolecules

Traditionally, tablets as oral formulations have been more or less limited to small molecular APIs due to the limited absorption of macromolecules in the gastrointestinal tract (GI) (22). However, in recent years considerably effort has been made in improving oral delivery and bioavailability of biomacromolecules potentially allowing a systemic therapy by this route (22–25). In this context, there are several challenges that have to be overcome for an efficient oral therapy with biomacromolecules. First, the three-dimensional structure of biomolecules is often sensitive to environmental conditions such as salt concentration, pH value as well as digesting enzymes, and thus has to be protected during its gastrointestinal transport (22, 26, 27). In the case of tablets, protection of the tablet core can be realized by application of an enteric coating (25). However, the main challenge for oral delivery of biomacromolecules remains the poor permeation of the APIs through the intestinal barrier and thus its systemic availability (22, 25). In this regard, the ideal drug delivery formulation protects the biomacromolecule against deleterious environmental conditions on its route to the intestine and increases its dissolution rate as well as absorption in the intestine, while showing a low toxicity (27).

To improve oral delivery of biomacromolecules, several new drug delivery approaches have been developed in the last years. For instance, an innovative tablet formulation consisting of biomacromolecules as API, a permeation enhancer as well as citric acid in the core of the tablet coated with an enteric polymer, has been developed (25, 28, 29). The working principle of this formulation strategy is based on the protective effect and the delayed release provided by the enteric coating (28). In

addition, the permeation enhancer facilitates the paracellular transport of the biomacromolecules by loosening the tight junctions, while citric acid lowers the pH after drug release in the intestine leading to a reduction of the activity of surrounding proteases and peptidases and prevention of biomacromolecule degradation (28). In a Phase III clinical trial such a formulation containing salmon calcitonin was superior regarding increase of bone mineral density compared to a nasal formulation or a placebo (30).

Moreover, tablets containing biomolecules such as insulin, Glucagon-like-peptide-1 (GLP-1), low-molecular weight heparin, or an oral Gonadotrophin-releasing hormone antagonist, together with surfactant-like permeation enhancers, e.g. medium-chain fatty acids, which are generally regarded as safe by the US Food and Drug Administration (FDA), are under investigation (25, 31). With this technique, a heparin bioavailability of 5-9 % could be achieved (32). Furthermore, an oral formulation with GLP-1 has recently successfully passed Phase II clinical trials (33). However, it is worth mentioning that the safety of permeation enhancers is still under debate as they potentially promote absorption of toxic substances from the GI tract (25, 34).

Another promising approach for oral delivery of biomacromolecules is a colon specific delivery system consisting of a tablet with a multilayer coat and lactulose in the core (25). The inner layer consists of an acid-soluble polymer and the outer layer of an enteric-soluble polymer separated from each other by an Hypromellose film (25, 35). Thus, during its route through the GI tract, the tablet core is protected from the acidic environment of the stomach by the outer enteric coating, while the inner coating layer provides protection within the alkaline environment in the intestine. At

the target side of the colon, environmental bacteria degrade the lactulose to short chain fatty acids, which lowers the local pH leading to dissolution of the inner coating layer and thus drug release (25).

Besides the demonstrated delivery approaches, several other promising approaches for oral delivery of biomacromolecules are in the pipeline and are summarized in the literature (22, 25, 27, 29, 36). Obviously, tableting becomes a potential formulation strategy for these APIs. Consequently, the influence of the tableting process and the associated stress with regard to the integrity and stability of biomacromolecules is of increasing interest.

1.2 Tablet manufacturing and quality control in context with the QbD and PAT initiatives

Tablet manufacturing is commonly a multistep process including operations such as powder blending, granulation, compaction, tablet coating and packaging (Fig. 1) (37). The production environment is highly regulated by the Good Manufacturing Practice (GMP) frameworks launched by the regulatory authorities, such as the FDA and the European Medicines Agency (EMA) (38–40). These frameworks quote minimum requirements for adequate manufacturing of pharmaceuticals to ensure product quality and patient safety by regulating aspects such as personnel responsibilities and qualifications, production organization, equipment and facility standards, as well as product control, packaging, labeling, distribution and documentation (38–42).

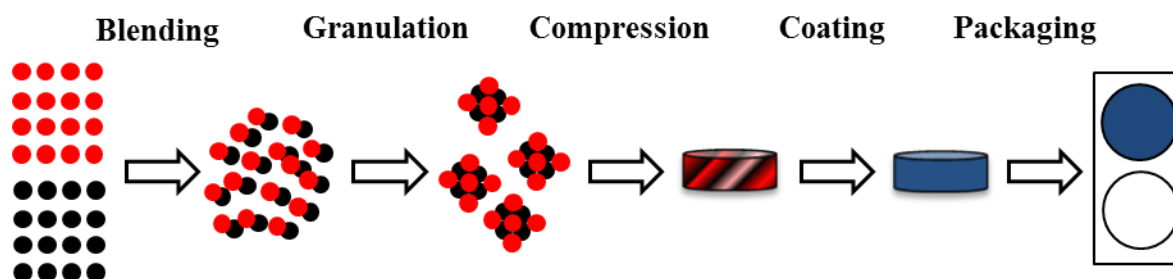


Fig. 1: Tablet manufacturing flow chart.

The manufacturing environment is more strictly regulated compared to other industries with regard to changes of the processes and operational parameters, as these are usually accompanied by a renewal of the approval by the regulatory authorities or the provision of supplements (43, 44). Such a highly regulated product environment shows advantages with regard to product quality and patient safety, but has also led to an innovation gap in the pharmaceutical industry with regard to the

improvement of production and associated quality control procedures (20, 45, 46). Nowadays, tablet manufacturing is accomplished batch-wise with the quality of the prepared products being ensured by removing a small number of representative products from the production line and analyzing them in separated laboratories (5, 43, 44).

To modernize pharmaceutical manufacturing, in 2004 the FDA launched two initiatives: the 'Pharmaceutical CGMPs for the 21st Century: A Risk-Based Approach' (19) and 'Guidance for Industry: PAT — A Framework for Innovative Pharmaceutical Development, Manufacturing, and Quality Assurance' (20). These initiatives and related globally recognized guidelines (47) intend to optimize the regulatory framework of pharmaceutical manufacturing and to introduce innovation into pharmaceutical processing (45). Thus, product quality as well as production efficiency should be increased and may allow to overcome the increasing cost pressure within the pharmaceutical industry (45). The initiatives inspire pharmaceutical manufacturers to design their manufacturing processes based on the latest scientific findings to ensure that product quality is built into the process and that the risk caused by insufficient quality of the products or processes is minimized (19, 20, 45).

To achieve the goal of producing a constantly high product quality more efficiently, a thorough understanding of the process is required and can be achieved by real-time or near real-time control of the relevant process parameters (19, 20). Therefore, the FDA promotes the implementation of process analyzers that allow timely monitoring

of the desired product attributes instead of solely testing end product quality in laboratories (20).

According to the FDAs PAT framework, the use of real-time or near real-time process analyzers for acquisition of product and process data that is sufficient for assuring product quality can further verify conformity of the prepared batches with the regulatory requirements and thus be the basis for real-time parametric release of the prepared products (20, 48). Real-time release implies that products are approved by the Qualified Person before obtaining analytical results of final product testing based on the documentation which verifies production according to predefined process parameters (5). This is considered an attractive strategy for obtaining a more cost-efficient manufacturing process (49).

Besides optimization of traditional batchwise production, the QbD and PAT initiatives launched by the regulatory authorities are furthermore essential to overcome the challenges of another emerging trend in the pharmaceutical industry, i.e. the change from batchwise or semi-continuous to continuous manufacturing (5, 20, 50). In batchwise production, all materials are being charged at the beginning and discharged after completion of the process, such as, for example, the powder blending, lyophilization, and wet granulation processes. In contrast, continuous manufacturing comprises simultaneous and continuous charging and discharging of raw materials and final products (51, 52). An intermediate way is semi-continuous manufacturing, e.g. roller compaction and tablet compaction with the material flow comparable to continuous manufacturing but the process being operated only for a limited period of time (52). Traditionally, pharmaceutical unit operations are

performed batch-based for reasons of quality control and uncertainty with regard to the judgment of the regulatory authorities (5, 20). In this regard, processes such as milling, spray drying, and tablet compaction, which are naturally continuous or semi-continuous and are thus predestinated for being combined to establish continuous manufacturing, are stopped after a predefined period of time to be in line with other batch-wise production processes (5, 53). Continuous production processes are well-established in e.g. the food industry and have shown to be advantageous compared to batch-based processes in terms of high throughputs, high yields, reduced waste, and thus decreased costs (5, 51, 54). Furthermore, the same equipment can be used for the production of varying product quantities with the advantage to minimize time- and cost-intensive process scale up (54). However, continuous manufacturing requires comprehensive process understanding and control by continuous monitoring of material properties and product attributes to guarantee uniform quality of the final products (20, 52).

1.3 Product quality attributes during tablet manufacturing

1.3.1 Assessment of relevant tablet quality attributes

In context with the PAT and QbD frameworks of the regulatory authorities adequate control of the product attributes and process parameters in every tablet manufacturing step is essential to build quality into the process and guarantee performance of the final products (19, 20, 44, 47, 48). A prerequisite for ensuring uniform product quality during manufacturing is to specify those properties of intermediates and the product that are important with respect to the final product quality and are thus intended to be achieved during processing (48). Traditionally, production processes are performed for a predefined period of time irrespective of the physicochemical characteristics of the input materials which may, however, vary slightly from batch to batch. In contrast, in the PAT framework the process end point should be determined quality- rather than time-based (20). Therefore, during pharmaceutical development Quality Target Product Profiles (QTPP) are established, which are '*A prospective summary of the quality characteristics of a drug product that ideally will be achieved to ensure the desired quality, taking into account safety and efficacy of the drug product*' according to the ICH pharmaceutical development guideline (47). For a tablet formulation, the QTPP can contain among others attributes as listed in Table 1 (55–57).

The QTPP scheme is the starting point for definition of Critical Quality Attributes (CQAs) of the dosage form (47, 58). A CQA is '*A physical, chemical, biological, or microbiological property or characteristic that should be within an appropriate limit, range, or distribution to ensure the desired product quality*' (47). Thus, CQAs define

those product attributes that have to be met to ensure patient safety and product efficacy (58).

Table 1: Excerpt of a Quality Target Product Profile of a tablet formulation.

Product Attribute	Target
Potency	200 mg, range 90 – 110 %
Content Uniformity	In agreement with Ph. Eur./USP criteria
Tablet appearance	Unit integrity Coated Identification and dose differentiation by imprint
Stability	36 months at room temperature
Container closure system	Suitable to preserve stability

After defining the product attributes that should be met, it is important to develop a robust manufacturing process leading to the desired product quality. In this regard, material attributes (Critical Material Attributes, CMA) and process parameters (Critical Process Parameters, CPP) that could affect final product quality and need to be controlled during manufacturing have to be identified (47, 58). In this context, criticality is generally defined as a function of risk and based on the interaction of process parameters or material attributes with the CQAs of the products and thus a high probability to obtain product failures (47, 48, 59). Relevant material attributes and process parameters should be included in the process design space (47). For efficient process control, it is essential to ensure that the predetermined CMAs, CPPs, or CQAs are within the defined limits and it is often beneficial to monitor additional attributes and parameters to verify a uniform and high quality of the prepared products according to the respective QTPP or product specification (44, 47, 48).

1.3.2 Tablet quality attributes and related process parameters

To monitor the tablet manufacturing process and control that the prepared tablets are within the specifications defined by the Pharmacopoeias, determination of various physicochemical quality attributes of the intermediate and final products is desirable (44, 48, 60). Table 2 gives an overview on process parameters of potential tablet manufacturing processes and related product quality attributes.

At the beginning of the tablet manufacturing line, one important parameter to monitor is the uniformity of the powder blend upon mixing to guarantee content uniformity of the tablets (48). Subsequently, during fluid bed granulation, it is essential to control the particle size distribution, as the size of the granules strongly influences their flowability and thus processability upon compaction (44). Generally, although product quality attributes are verified at defined points in the production line, they can be negatively affected by subsequent processing. For instance, movement and vibration of the hopper as well as shear applied to the powder blend by the feed frame of the tablet press may negatively affect powder blend homogeneity (61–63). Thus, real-time monitoring of the distribution of the ingredients within the prepared tablets allows continuous control of the related machine parameters and is beneficial to ensure tablet content uniformity (20, 44, 64). In this context, it is furthermore advantageous to control tablet hardness immediately after compaction, because it has been shown that the shear stress of the feed frame may lead to over-lubrication of the powder blend resulting in inadequate hardness and an altered dissolution behavior of the prepared tablets (65–67).

Table 2: Examples of pharmaceutical process parameters and related product quality attributes.

Pharmaceutical process	Process parameters	Product quality attributes
Powder blending	Blender geometry Load level Blending time Blender speed	Blend uniformity Particle size distribution
Granulation High-shear or fluid bed	Impeller speed Chopper speed Vessel temperature Product temperature Spray rate Nozzle geometry Inlet air temperature Inlet air volume	Particle size distribution Moisture content
Compaction	Hopper design Hopper vibration Feed frame speed Compaction pressure Turret rotation speed Tablet cylindrical height Filling depth	Visual appearance Tablet weight Ingredient distribution Content uniformity Tablet hardness Tablet intactness Density distribution Friability
Tablet coating Pan or fluid bed	Spray rate Nozzle geometry Inlet air temperature Inlet air volume Product temperature Pan rotation speed	Visual appearance Coating intactness Coating uniformity Coating mass/thickness Friability

*modified from (44)

Furthermore, tablet hardness often strongly depends on the rotor speed of the tablet press and could be also used for real-time adjustment of this machine parameter (68). In general, hardness of the tablets determined shortly after compaction is a good estimate for the robustness of the compacts during their life cycle, even if relaxation phenomena upon storage are accompanied by changes in the tablet properties (60). In addition, to effectively control the tableting process it is favorable to verify the physical intactness of the prepared compacts in the production environment. Phenomena such as sticking of the powder blend to the punches may occur upon compaction and are strongly dependent on the tableting parameters, e.g. compaction pressure and/or speed of the torque drive (68, 69). Sticking is pronounced around imprinted codes resulting from shear forces at the lateral parts of the codes (70) and may be accompanied by inadequate appearance of the tablets as well as hardly readable imprints. Consequently, customer acceptance as well as patient compliance and safety is reduced (13, 71).

To guarantee physical stability of the tablets, it is furthermore beneficial to determine their surface density profile, as it is well-known that die wall friction occurring upon compaction can be accompanied by undesired density variations in the compacts (72, 73). Friction between the powder and the die particularly occurs if powder blend lubrication is insufficient, e.g. at low lubricant levels, as well as at high compaction pressures (72–74). In these cases, tablets with high density regions in the upper edge and a lower density in the lower edge have been obtained (72, 73), which show a higher tendency for deficiencies such as capping or lamination (14, 75, 76). Therefore, examination of the tablet surface density may be advantageous for control

of the compaction pressure as well as regulation of the feeder speed as the latter may affect lubrication (65, 66).

Another commonly performed tablet manufacturing step is tablet coating (44). Quality control as part of this unit operation has to assure coating intactness, as coating failures may result from e.g. tablet twinning or insufficient flexibility of the coating film (9) and could be associated with a reduced stability of the API due to degradation by environmental factors and may lead to dose failures and dumping upon ingestion (7, 9, 77). Furthermore, a homogeneous surface texture of the applied coating has to be assured to guarantee the desired dissolution profile and ensure customer acceptance and patient compliance (6). Thus, determination of these tablet quality attributes and establishment of a feedback control system by linking these product attributes to parameters of the ongoing process, e.g. the spray rate and inlet temperature, is attractive for pharmaceutical manufacturers in terms of improvement of the patient safety and avoidance of legal consequences (44, 77).

At the end of the tablet manufacturing line, packaging of the prepared tablets has to be monitored (39). The objectives of quality control procedures are to verify that the desired type and amount of tablets is correctly filled into the desired type of packaging material, e.g. blister foils and cavities (39). Processing of the desired type of primary packing material is crucial as it has been reported to potentially affect the physicochemical stability of the enclosed product (78, 79). Real-time monitoring of the packaging process is advantageous, because it allows to detect cross-contamination of either the tablet formulation or the packaging material during the

time course of processing and thus enables to immediately stop the machines and to replace the equipment of the production line.

1.3.3 Specific aspects of the manufacturing of tablets containing biomacromolecules

During the different steps of tablet manufacturing, several types of stress such as temperature, pressure, and friction are applied to the tablet mass (16, 74, 80). For biomacromolecules, external stress factors have been shown to be critical, because their functionality depends on the integrity of their complex three-dimensional structure (81), which is potentially altered during pharmaceutical processing (82–84). Alterations in their conformation may be accompanied by a reduction of their biological activity and might lead to undesirable immune responses upon ingestion as a consequence of aggregate formation (81, 85, 86). From that perspective, identification and thorough understanding of the process parameters that potentially affect the integrity of biomacromolecules upon tablet manufacturing is crucial for product quality. In previous studies it has been shown that dependent on the type of process and its parameters, conformational changes may be reversible upon reconstitution, as shown for freeze- and spray-drying processes (87–89), but could also be partially or even completely irreversible (90, 91).

Several studies have been performed to investigate the influence of the compaction step on the integrity of biomacromolecules. It has been demonstrated that compaction reduces the enzymatic activity of e.g. catalase and α -amylase dependent on the applied pressure (92, 93). Furthermore, the structural integrity of proteins such as recombinant human deoxyribonuclease (94), lactobacillus proteins (95), α -chymotrypsinogen (96), lysozyme (96), as well as trypsin (84) has been shown to be more or less changed as a function of compaction pressure. Thus, the compaction pressure has been identified as a critical parameter with regard to the integrity of

biomacromolecules. However, the extent of reversibility of these compaction induced structural changes as well the influence of tableting on further important quality attributes of biomacromolecules such as the transition temperature (T_m) of unfolding and the folding reversibility after thermal unfolding remains unclear.

1.4 Analytical techniques for quality control during tablet manufacturing

1.4.1 Process monitoring in context with the QbD and PAT initiatives

To fulfill the objectives of the QbD and PAT concepts of the regulatory authorities that *'quality should not be tested into products; it should be built in'*, thorough understanding and control of manufacturing processes and related parameters is required (19, 20, 47). Therefore, as described in the previous section, a design space should be established that defines the range of process parameters leading to the desired product quality (44, 48). To set up such a design space and control the process based on this framework, real-time monitoring of relevant tablet attributes is beneficial as it allows to correlate the obtained information with parameters of the running process as well as with the clinical performance of the products. Thus, a feedback control system based on real-time process analyzers can be effectively used for process understanding during process development, for gaining additional knowledge during scaling-up, as well as for process control and troubleshooting during full-scale manufacturing (20, 97, 98).

As mentioned before, quality control has been traditionally performed by withdrawal of a small number of samples from the production stream and their analysis in spatially separated laboratories (39, 44, 46). In this regard, quality control is usually based on analytical procedures that capture only one quality attribute at a time. For instance, techniques such as high-performance liquid chromatography or photometry are applied for control of the tablet API content, tablet crushing strength is measured to evaluate tablet hardness, coating intactness is investigated by disintegration

testing, and the visual appearance of the tablets and of adequate blister pack filling is verified by manual inspection (48, 64). In the case of biomacromolecular APIs such as trypsin, the functionality may be affected by pharmaceutical processing and is traditionally evaluated by e.g. photometric wet assays (84, 99). These quality control procedures have been shown to be effective for assessment of tablet quality but are usually time- and labor-consuming and destructive (98). Consequently, such procedures, which are performed off-line the manufacturing stream (Fig. 2a), are accompanied by high costs and are usually not suited for real-time control of high-speed processes such as tablet manufacturing due to the time gap between processing and quality control, which prevents implementation of a feedback control system (98, 100).

To achieve efficient real-time or near real-time monitoring of the different processes during tablet manufacturing, analytical techniques are required that allow straightforward sampling and to capture the desired tablet attributes with similar accuracy but within a fraction of time compared to the traditional quality control routines (20, 98). According to the FDAs PAT framework, real-time process monitoring can be achieved by analytical tools that allow at-line, on-line, or in-line measurements rather than off-line data acquisition (Fig. 2) (20).

In the case of at-line measurements, the samples are removed from the process line and analyzed in the production environment within the time course of processing (20, 101). Thus, the reaction time for readjustment of process parameters after detection of an insufficient product quality attribute is markedly lower compared to off-line quality control.

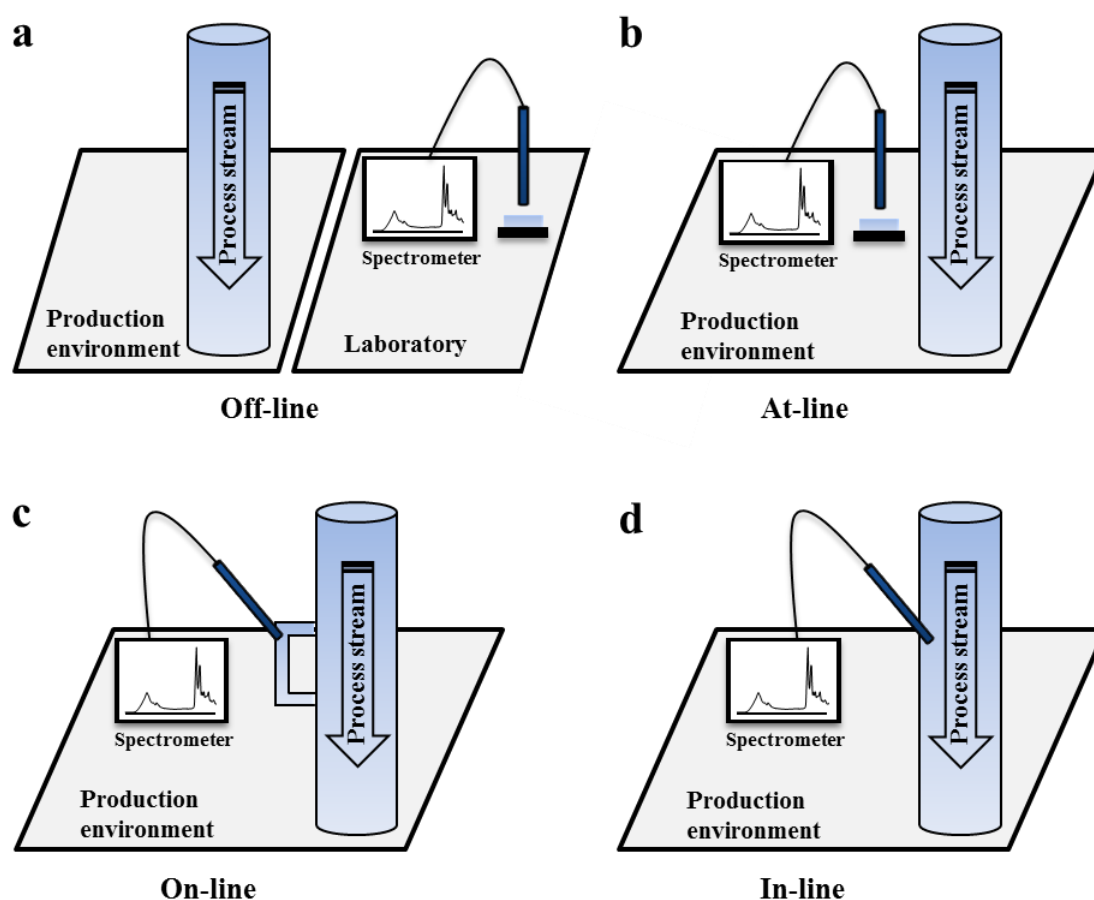


Fig. 2: Implementation principles of process analyzers; modified from (101).

During on-line measurement samples are temporarily separated from the material stream, directed to the analytical device via a sampling loop, and fed back into the process after data acquisition (20, 101). During in-line process monitoring the sampling probe is directly placed into the production vessel or machine capturing the material attributes directly in the product stream (20, 101).

Comparing off-line and real-time measurement techniques, the latter show the advantage of a timely and fast data acquisition, which is the basis for process control via a feedback control system and the establishment of a quality-based instead of a time-based process endpoint, which may be accompanied by a shorter process time

and consequently a higher yield (20, 98). Furthermore, real-time process analyzers do not require any sample preparation, which reduces the operational error upon quality control and potentially allows automation of product analysis (98). However, it has to be mentioned that implementation of such techniques in the production environment as well as their maintenance is markedly more complex compared to traditional off-line quality control systems (98).

In general, process analyzers that provide multivariate rather than univariate information on the samples are desirable for real-time quality assurance (20). In this regard, spectroscopic techniques such as near-infrared (NIR) or Raman spectroscopy have been widely investigated and, in combination with chemometrics, proven to be well-suited for fast, accurate, and even simultaneous determination of various physicochemical tablet attributes (46, 102–111).

1.4.2 Spectroscopic methods

1.4.2.1 General aspects

Spectroscopic techniques such as mid-infrared (MIR), NIR, and Raman spectroscopy have been proven to be well-suited for quality control of tablets (46, 109, 112, 113). These techniques have been used for years as stand-alone instruments in analytical laboratories, as the obtained spectra contain valuable information on the physicochemical properties of the analyzed samples (114, 115). Although marked differences exist between these techniques, their working principles are all based on the monitoring of spectra at defined frequencies resulting from the vibration and bending of molecules (114–117). Atomic nuclei undergo periodic motions by *‘moving together or apart along a straight-line vector and they rotate, they vibrate, they wag, and they bend relative to their centers of gravity’* (118). Although marked differences exist between the vibrational techniques, compared to other commonly used analytical procedures such as chromatography, mass spectrometry, or titration, these spectroscopic methods allow a fast data acquisition as well as a straightforward and non-destructive sampling dependent on the sampling device (46, 116, 117). Furthermore, these techniques provide multivariate rather than univariate information on the samples, which often allows to capture several physicochemical sample attributes with one measurement and potentially substitutes several univariate analytical procedures (46, 119–121). These aspects are beneficial in terms of routine quality control and turn spectroscopic techniques, particularly NIR (46, 109, 122) and Raman spectroscopy (46, 111, 121, 122), into attractive PAT tools.

1.4.2.2 Mid-infrared spectroscopy

Mid-infrared (MIR) spectroscopy covers the range between 4000 and 400 cm^{-1} of the electromagnetic spectrum (117). The two main advantages of MIR spectroscopy are its high sensitivity as well as the high information content of the obtained spectra (123). The position of the absorption bands in the spectrum reflects the chemical composition of the analyzed sample, while the intensity of the peaks is related to the concentration of the different compounds (117). Furthermore, MIR spectroscopy is sensitive with regard to the hydrogen bonding pattern within and between the molecules which influences for instance the peak widths (117). In addition, the spectrometer can be equipped with several sampling devices such as diffuse reflectance, attenuated total reflection (ATR), and (flow-through) transmission cells allowing the investigation of solid, semi-solid, as well as liquid samples (115, 117). However, sampling is not as straightforward as with NIR or Raman spectroscopy because previous preparation steps such as sample dilution are required dependent on the type of sample (116, 124, 125). In addition, remote sampling with fiber optics is more complex compared to other vibrational spectroscopic techniques (116). Consequently, MIR is usually not the first choice as a PAT tool compared to NIR or Raman spectroscopy (21, 46). Another general drawback of MIR spectroscopy is that the measurement of complex mixtures or aqueous samples can become challenging due to overlapping of peaks or interfering water, which may complicate the extraction of the desired information on a specific compound from the spectra. However, this disadvantage can be circumvented by proper data processing (117).

1.4.2.3 Near-infrared spectroscopy

Near-infrared (NIR) covers the spectral range between the mid infrared and the visible region of the electromagnetic spectrum corresponding to the wavenumber region between 12500 and 4000 cm^{-1} (116).

In recent years, NIR spectroscopy has become the power horse within the pharmaceutical industry for routine quality control and especially as process analyzer for real-time process monitoring (46, 109, 126, 127). The main reasons are the ease of sampling and of transferring the NIR light from the instrument to the process stream via fiber optics, as well as the high speed of data acquisition (109, 116). Another advantage of NIR compared to MIR spectroscopy is the comparably low absorption coefficient, which is accompanied by a markedly higher penetration depth of NIR compared to MIR radiation allowing to analyze even solid samples that are strong absorbing or leading to pronounced scattering of the incoming light (109). However, it is worth to mention that the typically broad, overlapping NIR absorption bands that are markedly weaker compared to MIR spectroscopy are accompanied by a lower sensitivity and structural selectivity of NIR compared to MIR spectroscopy (109, 116). This fact usually requires the application of multivariate models to link spectral information to physicochemical properties of the samples (109, 116) as well as reference techniques for establishment of calibration models (116).

1.4.2.4 Raman spectroscopy

In contrast to MIR and NIR spectroscopy which are considered as absorption techniques, Raman spectroscopy is a scattering technique usually capturing spectra in the energy range between 4000 and 50 cm^{-1} (116). Raman and MIR spectroscopy are complementary analytical techniques. While Raman spectroscopy is more sensitive to symmetric vibrations of non-polar groups of molecular structures, IR spectroscopy is more sensitive to symmetric vibrations of polar groups (124). Thus, molecules which are less sensitive to radiation in the MIR range can often be accurately characterized by Raman spectroscopy (124).

Similarly to NIR spectroscopy, Raman spectroscopy is particularly attractive for process analysis because of the ease of sampling and the straightforward attachment of fiber optic probes to process vessels (116, 121). Furthermore, the high information content of Raman spectra make distinct correlations between the obtained spectra and the molecular structure feasible (115, 124). Moreover, in contrast to MIR spectroscopy, Raman spectroscopy is insensitive to water allowing a direct measurement of aqueous samples (124). However, fluorescence may hamper the acquisition of high quality spectral data (116).

1.4.2.5 Application of spectroscopic methods for non-destructive tablet quality control

NIR and Raman spectroscopy have been proven to be particularly suited for real-time monitoring of the tableting process as well as determination of various physical and chemical tablet attributes. For example, NIR spectroscopy has been successfully applied to the feed frame of a tablet press for real-time monitoring of blend homogeneity (62, 128). Furthermore, tablet hardness could be non-destructively estimated based on NIR spectra. It has been shown that differences in the tablet surface texture are accompanied by spectral baseline shifts rather than distinct spectral differences. These baseline shifts allow a physical characterization of the samples by chemometrical methods such as Principal Component Analysis (PCA) and Partial Least Squares (PLS) Regression (102, 129–131). Furthermore, NIR spectroscopy combined with chemometrics has been shown to be suitable for determination of the tablet API content (102, 119, 120, 130, 132).

For monitoring of the tablet coating process, NIR spectroscopy has been successfully applied to fluid bed as well as pan coating processes and has been used together with multivariate data analysis as a PAT tool for the investigation of the coating layer thickness, mass of coating material, and coating uniformity (105, 106, 110, 132–135). At the end of the tablet manufacturing line, NIR spectroscopy has been effectively used for control of tablet packaging: the identity of tablets inside blister packs could be non-invasively determined from the NIR spectra (136, 137). In this context, a systematic classification of blistered tablets based on the tablet formulation could be achieved with pattern recognition methods such as Soft Independent Modelling by Class Analogy (SIMCA) (138). Furthermore, NIR spectroscopy has been proven to be a

convenient analytical method to monitor continuously operated manufacturing processes (139–142).

Raman spectroscopy combined with multivariate techniques such as PCA and PLS has been demonstrated to be well-suited for off-line, at-line, and on-line monitoring of the API content in tablets (143–145). In addition, physical tablet attributes, namely tablet porosity and hardness, could be assessed based on Raman spectra (146, 147). Furthermore, Raman spectroscopy together with PLS has been shown to be a sensitive tool for determination of the thickness of the applied coating and proven to be a suitable PAT tool for the tablet coating process (103, 104, 148). Moreover, Raman spectra together with related classification techniques have been demonstrated to allow reliable identification of tablets based on their composition (149).

Comprehensive overviews on the widely used spectroscopic methods for quality control during in the context of pharmaceutical processing are summarized in the literature (46, 109, 111, 150, 151).

1.4.2.6 Structural characterization of biomacromolecules by mid-infrared spectroscopy

Quality control of biomacromolecules is often complex and requires the application of various analytical methods to investigate their physicochemical stability (82, 152–154). In this context, the secondary structure of the molecules is of particular interest as it is linked to their biological functionality (153). Besides analytical methods such as circular dichroism (155), X-ray crystallography (156), and nuclear magnetic resonance spectroscopy (157), Fourier transform (mid-) infrared spectroscopy (FTIR) spectroscopy is a well-established experimental method for analysis of the secondary structure of biomacromolecules (153, 158–161). FTIR spectroscopy has the advantage of a straightforward and fast sampling, a large application range with regard to the size of the biomolecules as well as the possibility of a structural characterization of the biomolecules irrespective of their physical state (153, 158, 159, 162). For example, infrared spectra of biomacromolecules can be acquired in the solid as well as in the liquid state and thus allow the determination of the secondary structure under different environmental conditions (87, 163).

Structural characterization of biomacromolecules by FTIR spectroscopy is based on its sensitivity to the molecular geometry and hydrogen bonding pattern of molecules (159). The polypeptide backbone of biomolecules lead to nine characteristic bands within the MIR range referred to as amide A, B, and I-VII bands (Fig. 3) (160). A correlation between the obtained spectra and the molecular structure could be confirmed by the assignment of bands in the infrared spectra to information obtained by X-ray analysis of molecules with known three-dimensional structure (164).

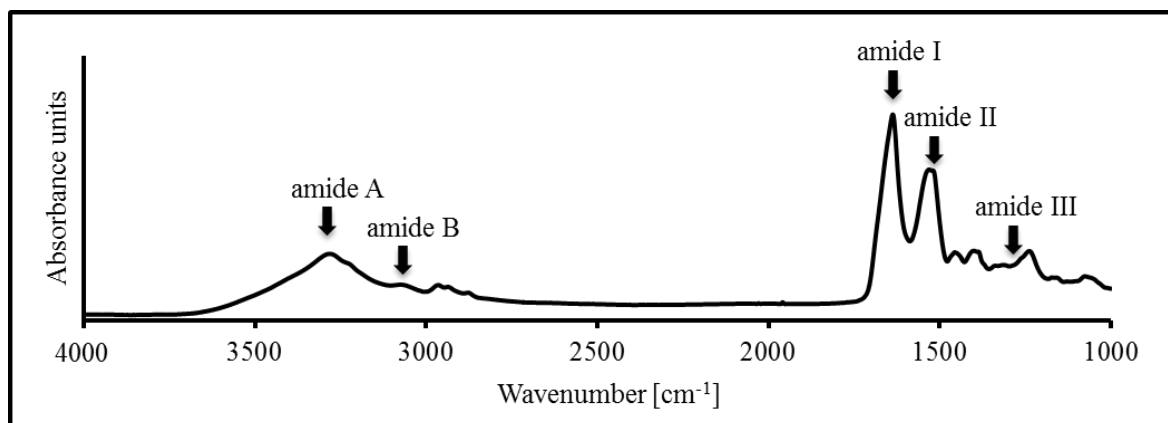


Fig. 3: FTIR-ATR spectrum of bovine trypsin.

Among the infrared bands the most intense and frequently used spectral region for secondary structure analysis is the amide I band ($1700\text{--}1600\text{ cm}^{-1}$) (153, 160). The amide I band mainly originates from the C=O stretching vibration of the peptide linkages (159) and has been shown to be particularly sensitive to the secondary structure of biomolecules (158, 160). The C=O stretching vibration is dependent on the geometric orientation of the peptide linkages, which differs significantly among the various secondary structures (159, 161). In this context, a basic assumption is that the C=O stretching vibration exhibits virtually the same molar absorptivity in all conformations allowing the spectral intensity to be related to the percentage of the secondary structural elements in the molecule (159). Thus, distinct frequencies within the amide I band can be attributed to different secondary structures of the biomacromolecule such as α -helix, β -sheet, β -turn and random coil (158, 160, 161). An overview on the assignment of defined bands to the different secondary structures is given in Fig. 4 and summarized in the literature (154, 165). However, the frequencies that represent the different structural elements overlap and therefore result in a broad amide I band as shown in Fig. 3. Thus, to establish a distinct correlation between the MIR spectral bands and the secondary structure, spectral

processing or multivariate data analysis techniques are usually required (159). In this context, band-narrowing techniques such as Fourier Self-Deconvolution or derivatisation as well as multivariate techniques such as PCA and PLS Regression have been successfully applied to characterize the secondary structure pattern (84, 153, 161, 166–168).

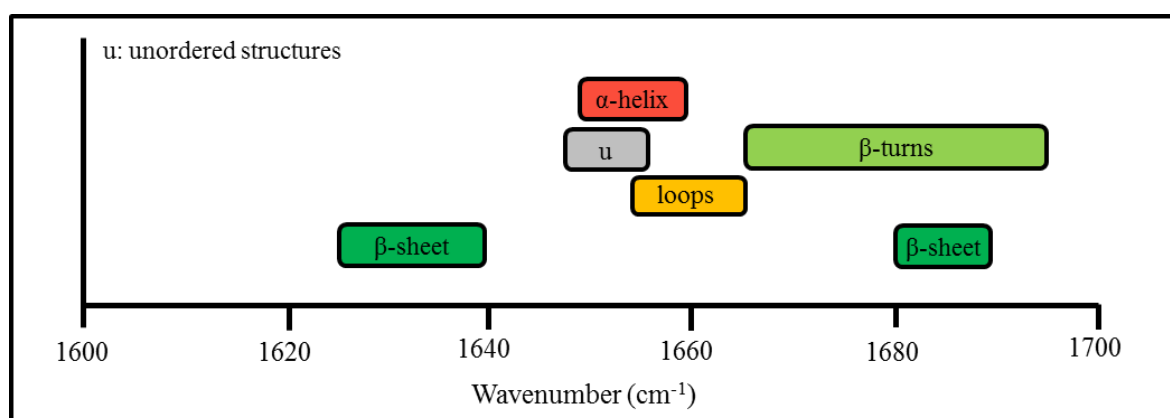


Fig. 4: Assignment of bands within the amide I infrared spectrum to protein secondary structures; modified from (160).

Traditionally, one limitation for determination of the secondary structure of biomacromolecules from the amide I band has been interfering water in aqueous environments (161, 165). This drawback has been circumvented by the use of deuterated water which is insensitive to infrared radiation (160, 161, 165). Furthermore, transmission flow-through cells with a small and constant path length (around 6 μm) allow direct measurement of biomacromolecules in the aqueous environment and subsequent compensation for interfering water as the small path length reduces the contribution of water to the overall spectrum (160, 165).

In addition to the amide I band, the amide II (1575 – 1480 cm^{-1}) and III (1320 – 1220 cm^{-1}) bands (160) have also been shown to provide useful information

for establishing correlations between spectra and secondary structure (154, 169, 170), although these bands show a markedly lower conformational sensitivity compared to the amide I band. The amide II band mainly corresponds to in-plane N-H bending as well as C-N stretching vibrations (154, 158), while the frequencies within the amide III range mainly derive from C-N stretching as well as N-H bending vibrations with smaller contribution from the C-C stretching and C=O bending vibrations (153). The other bands which correspond to the polypeptide backbone are complex and are of low practical relevance for secondary structure evaluation (159).

1.4.3 Spectral imaging techniques

1.4.3.1 General aspects

Spectroscopic methods are well-established analytical methods for tablet quality control (section 1.4.2). NIR, MIR, and Raman spectra contain valuable information for the determination of physical as well as chemical tablet attributes (46, 109, 111–113). However, these methods detect only a single point of the sample with the spatial information being mathematically integrated resulting in a mean spectrum of the examined point (171). Although the obtained spectral information is often sufficient for adequate sample characterization, no statement can be made about spatial variations within the sample (171). If spatial and spectral information on the sample is desired, Chemical Imaging (CI) is attractive for quality control (172, 173).

Spectral imaging refers to the combination of image and spectral data acquisition. A hyper-dimensional image is obtained by recording spectra from numerous spots or pixels of the sample containing spatial as well as spectral sample information (Fig. 5) (171).

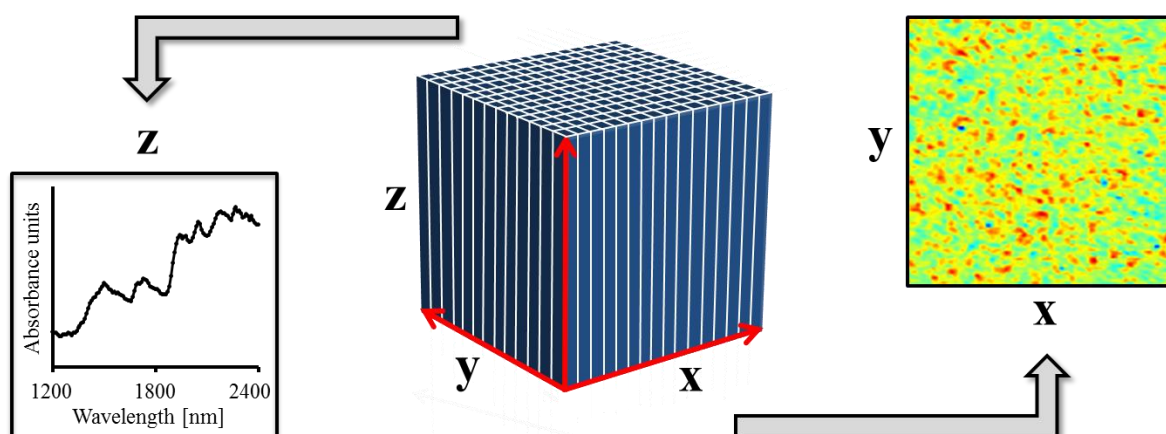


Fig. 5: Three-dimensional spectral data cube obtained by NIR imaging.

The high number of spectra that are usually obtained from the sampled area exhibit a high information content with respect to the physicochemical sample properties, which is a major benefit for pharmaceutical quality control (171, 172, 174). For instance, monitoring of the spatial distribution of tablet ingredients can be achieved to ensure uniformity and a predictable performance of the tablets (175). Dependent on the setup of the imaging instrument and the type of sample, various types of images such as UV, VIS, NIR, MIR, Raman, or terahertz images can be obtained (176). While the term ‘spectral imaging’ covers almost any optical spectroscopic method, ‘Chemical Imaging’ (CI) refers to the vibrational methods such as NIR, MIR, and Raman spectroscopy (171). However, the terminology is ambiguous as both terms are also used synonymously (176). Dependent on the dimensionality of the obtained images, i.e. the number of acquired wavelengths, imaging techniques are further categorized into hyperspectral and multispectral imaging, which cover more or less than 10 wavelengths, respectively (177).

Spectral imaging instruments are widely used for process monitoring in the food (178), paper (179), and polymer (180) industry and have recently gained increasing interest in the pharmaceutical environment (171, 174, 181). Spectral imaging techniques are predestinated for process monitoring in context of the PAT initiative, because of the usually non-destructive sampling and the high information content they provide (171, 174). Among the different imaging techniques, particularly UV, VIS, and NIR imaging are considered attractive for process analysis because they are readily available on the market and are less cost-intensive compared to other techniques (176). However, marked differences exist between these techniques in

terms of the number of performed studies on their applicability for determination of relevant tablet quality attributes and thus process monitoring and control of tablet manufacturing (171, 174, 176, 181). While several studies have been performed to evaluate the suitability of NIR imaging for tablet characterization, the applicability of UV imaging for tablet quality control is widely unexplored.

1.4.3.2 Working principles of spectral imaging techniques

In general, spectral imaging instruments are composed of a light source, an optical image acquisition module, a spectral encoder to select defined wavelengths, as well as a detector and data acquisition system such as a frame grabber board attached to a computer (171). According to the way of recording the hyper-dimensional spectral image, the instruments can be categorized into whiskbroom, pushbroom, and staring imager (Fig. 6) (171, 176, 177), which are described in the following. The interested reader is also referred to detailed descriptions of the instrumental setup in the literature (171, 176, 177).

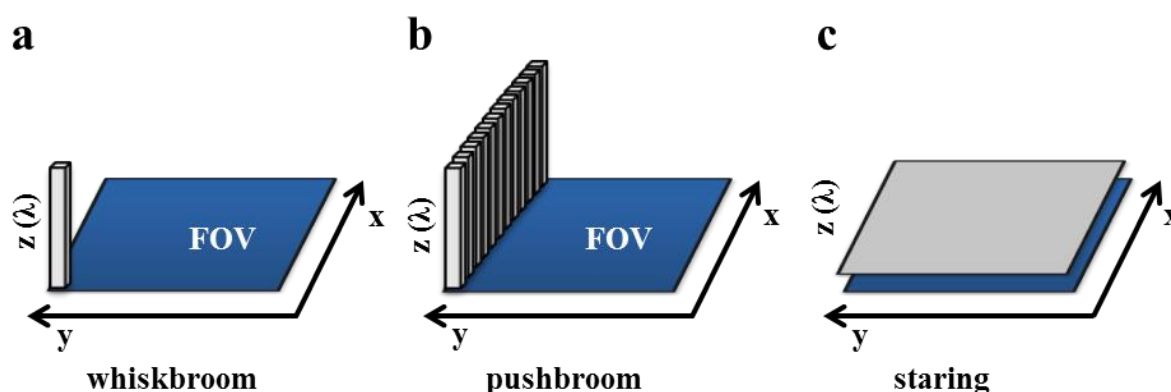


Fig. 6: Visualization of image acquisition methods (FOV: field of view).

During whiskbroom imaging (Fig. 6a), the hyper-dimensional image is incrementally obtained by acquiring full spectra of subsequent points of the sample in the spatial dimension (176). Thus, all wavelengths of a single point or pixel are recorded simultaneously followed by movement of the sample in the x-y direction to bring the subsequent point into the focus of the instrument. This procedure is advantageous in terms of a high quality of the obtained spectra as well as its high flexibility with regard to the size of the investigated area and the raster width (176, 182). However, point mapping is time-consuming and thus may require to find a compromise between a high image acquisition time and a high spatial resolution. Consequently, whiskbroom imager are typically used for off-line quality control (176).

During pushbroom imaging full spectra are simultaneously obtained from all points or pixels in a line (Fig. 6b) (182). After recording of the first line the sample is moved in the y direction to incrementally scan the adjacent lines of pixels until an image of the entire region of interest is obtained (182). In comparison to whiskbroom imaging, pushbroom imaging shows the advantage of a markedly reduced data acquisition time (181). This technique represents a good compromise with respect to spectral and spatial resolution of the obtained images and is well-suited for on-line and in-line quality control (176).

Staring imaging refers to the simultaneous acquisition of the response, i.e. absorbance or reflectance of all pixels at a single wavelength of the sample area (Fig. 6c) (176). Therefore, a powerful source illuminates the entire sample area with light of a defined wavelength which is incrementally selected by application of a tunable moving filter between either the sample and the light source or the sample and the

detector (181). The obtained two-dimensional (x-y direction) images are subsequently stacked (z direction) to obtain a hyper-dimensional image. The major advantage of this setup is the high speed of data acquisition: multi-dimensional images are usually obtained within seconds (181). However, this technique shows a low flexibility with regard to the size of the investigated area and thus the spatial resolution, as these parameters are limited by the detector size of the instrument (181). In addition, the high intensity of the light source may heat up the sample surface which may be disadvantageous for analysis of temperature sensitive samples such as amorphous formulations (181). However, this problem could be circumvented by cooling devices (172). Generally, for analysis by staring imaging the sample has to be stationary, which limits the application of this technique to at-line quality control (176). Nevertheless, NIR imaging instruments are often configured as staring imager and are often applied for quality control of tablets because of the high data acquisition speed and the high information content of the obtained images (171). The instrumental setups of whiskbroom, pushbroom, and staring imaging systems are explained in detail in the literature (171, 176, 177).

1.4.3.3 Application of spectral imaging techniques for non-destructive quality control of tablets

Spectral imaging techniques have been shown to be particularly suited for non-destructive and non-invasive quality control of tablets. Spatially resolved spectral information is obtained by these techniques, which allows to examine additional tablet quality attributes compared to conventional spectroscopic techniques. This additional information allows to thoroughly characterize various physicochemical

tablet properties and may lead to a further understanding of the different tablet manufacturing steps and their related quality relevant parameters. For instance, as mentioned before, determination of the surface density profile is advantageous to guarantee tablets with adequate physical stability (14, 75, 76) and to adjust process parameters such as the tablet lubricant level or the compaction pressure (72–74). Furthermore, the detection and localization of surface defects of either uncoated or coated tablets is necessary to ensure the quality of the prepared tablets and potentially to adjust related parameters such as the compaction pressure or the coating inlet temperature (9, 44, 68). Furthermore, examination of the coating surface texture is required to obtain tablets with the desired appearance and drug release upon ingestion (6). In addition, spectral imaging techniques are generally predestinated to monitor the tablet packing process and to prevent confusion of either the tablets or the packaging material by detection and identification of the packaged tablets and applied blister foils (183). Nowadays, monitoring of tablet packaging is often performed by machine vision systems (71, 184), which are suitable for detection of insufficient physical tablet quality but do not provide chemical information on the samples. In this context, the emerging interest in CI techniques within the pharmaceutical community is demonstrated by the increasing number of related scientific publications in recent years (174, 181).

Among the imaging techniques, NIR imaging has been most widely applied for quality control of tablets (176, 181). Due to the complexity of the obtained hyper-dimensional data cubes, multivariate image analysis is usually applied to the images to obtain the desired physicochemical information on the samples (181). For

instance, the API distribution within tablets has been accurately determined based on analysis of the acquired hyperspectral images by Multivariate Curve Resolution (MCR) or PLS Regression combined with related statistics (175, 185–188). In addition, quantitative information on tablet ingredients has been obtained by NIR imaging combined with multivariate or even univariate analysis applied to the preprocessed spectral image (175, 189, 190). Furthermore, physical tablet attributes such as hardness (60), the surface density distribution (73, 146), as well as the applied force during compaction (191) has been successfully estimated based on NIR images combined with PLS Regression, the intensity of a single peak, and analysis of the spectral slope, respectively. In the context of tablet coating, NIR imaging combined with chemometrical tools such as PCA has been demonstrated to allow evaluation of coating integrity (192, 193). In addition, thickness as well as homogeneity of the applied coat has been successfully determined by PLS Regression or even univariate analysis applied to the NIR images (187, 193). Upon tablet packaging, NIR imaging combined with PCA has been proven to be a powerful technique for tablet identification and determination of the tablet composition within blister packs (183, 194).

Raman imaging combined with univariate analysis as well as multivariate data analysis procedures such as PCA and MCR has been shown to be a suitable technique for determination of the tablet ingredient distribution (195–202) as well as for identification of unknown compounds in tablets (197).

Terahertz pulsed imaging has been successfully applied to evaluate physical attributes of uncoated tablets, for example the tablet surface density profile as well as

the tablet hardness (203). Furthermore, determination of the distribution of the different compounds in tablets has been successful (204). In addition, terahertz imaging has been proven to be particularly suited for quality control of coated tablets. It has been demonstrated that the thickness and homogeneity of the applied tablet coatings (77, 193, 205–210) as well as coating integrity (77, 193, 208) could be accurately determined from terahertz images.

MIR spectroscopic imaging has also been demonstrated to provide valuable information on tablet qualities such as the surface density (211) as well as the ingredient (212) distribution. However, MIR imaging has not been widely applied for non-destructive tablet quality control because of the more complicated sampling compared to NIR or Raman imaging (174, 176, 181).

Comprehensive reviews about the application of spectral imaging techniques for pharmaceutical quality control can be found in literature (171, 174, 181, 213–216).

1.4.3.4 UV imaging for quality control¹

As mentioned before, Raman and particularly NIR imaging are widely investigated spectral imaging techniques that have been demonstrated to be efficient tools for the determination of various tablet quality attributes (171, 174). Such vibrational imaging techniques commonly acquire spectral intensities at many (hundreds to thousands) wavelengths resulting in hyperdimensional spectral data cubes (171, 174). Usually, the information content of the obtained spectra is sufficient for a thorough physicochemical sample characterization. Furthermore, progress with regard to the development of imaging instruments allows analysis of samples

¹Parts of this chapter have been published as shown on page 199 in appendix B.

within minutes or even fractions of seconds dependent on the imaging setup (172, 181, 217). However, for real-time process monitoring remaining challenges are the data acquisition speed (217) as well as handling of the large data sets (171, 176). To obtain spectra with sufficiently high signal to noise ratio, many scans of each sampling point have to be performed which has a negative impact on the sampling time. In this context, the application of imaging techniques that allow to capture spectra of wavelength regions in which the sample exhibits a high molecular absorptivity (absorbance cross section) is generally attractive because it enables acquisition of high quality spectra within a short sensor integration time leading to an increased image acquisition speed (218).

In general, most APIs exhibit chromophores leading to a high molecular absorptivity in the UV range of the electromagnetic spectrum (218). In this regard, single wavelength UV imaging has gained interest for pharmaceutical quality control and has been demonstrated to be an accurate technique to monitor the dissolution profile of APIs (219–221) as the UV images were obtained within milliseconds. These studies indicate the potential of UV imaging for pharmaceutical quality control, although the investigated area of application is limited to single channel measurements, which are accompanied by a low selectivity, and to sampling in the aqueous environment. Thus, it is worthwhile to investigate the suitability of multi-wavelength UV imaging for non-destructive quality control of tablets. So far the potential of non-destructive and non-invasive multispectral UV imaging for quality control of pharmaceuticals is barely explored. Recently, Wu et al. performed the first study investigating the applicability of multispectral UV imaging for evaluation of the API solid state form within tablets

(218). This study demonstrates the advantages of this technique in terms of a non-destructive and non-invasive sampling, a high speed data acquisition, and a sufficiently high selectivity to distinguish different API solid state forms. Although the tablets were imaged at only six wavelengths, the amorphous and crystalline API forms showed distinct UV profiles which allowed to visualize their distribution within the tablets. From this perspective, multispectral UV imaging seems to be a promising technique for control of tablet quality with regard to different manufacturing steps such as compaction, coating, and packaging.

1.5 Analysis of spectral data sets

1.5.1 Spectral data analysis pathway and preprocessing

Spectroscopic techniques such as UV, MIR, NIR, and Raman spectroscopy are widely used for sampling in the pharmaceutical environment (46, 151) as they have been demonstrated to provide a high information content within a minimum of time. However, the obtained spectra are complex and consist of up to thousands of variables, i.e. reflectance or absorbance values at defined wavelengths (115). The objective of the respective data analysis procedures is usually to extract information from the dataset which is highly correlated with the sample attributes of interest and to discard irrelevant information, e.g. noise in the dataset (151). For this purpose, prior to uni- or multivariate analysis, spectral datasets are commonly preprocessed to eliminate undesired variations in the spectra which interfere with the desired information (Fig. 7a) (222, 223).

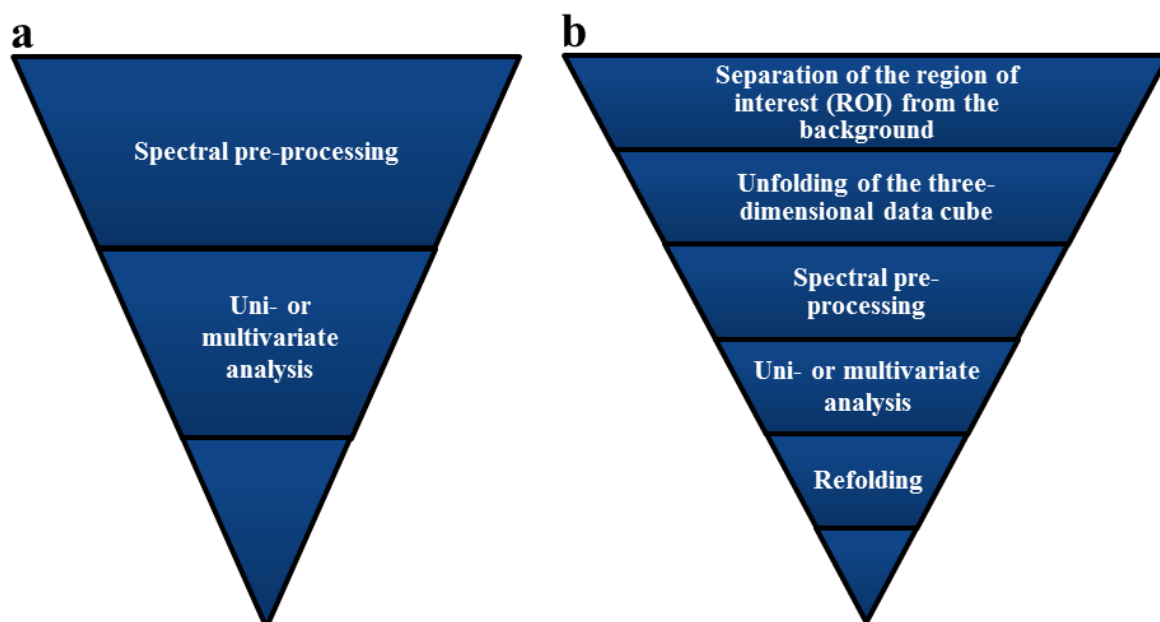


Fig. 7: Data analysis pathway of (a) single-point and (b) imaging spectroscopic datasets.

Such variations are caused by experimental or instrument-based phenomena such as differences in sample morphology, particle size and density, effective path lengths, detector artifacts, or instrumental noise (174, 222–225).

In general, the aim of data preprocessing is to simplify and improve data analysis (226). In this regard, the choice of a proper preprocessing technique is dependent on the desired information obtained from the dataset (181, 226). For instance, variations in light scattering caused by differences in the sample surface texture lead to spectral alterations which interfere with the chemical information on the sample from a spectrum (223, 226), while spectral scattering has been demonstrated to be useful for estimation of physical sample attributes such as tablet hardness (108, 131, 146, 227, 228).

In general, preprocessing techniques should be applied with care and are only needed if undesired variations in the sample properties occur, because such techniques are significantly altering the initial data (151, 222, 223, 229). While the selection of an adequate data pretreatment method increases the robustness of subsequent uni- or multivariate data analysis, inadequate preprocessing reduces relevant spectral information (151). The most frequently used preprocessing methods of spectral datasets can be classified into centering and scaling (230), scatter-correction techniques such as normalization, Standard Normal Variate (SNV), and Multiplicative Scatter Correction, as well as spectral derivatives such as Savitzky-Golay and Norris-Williams transformations (223). In the following sections, the preprocessing techniques applied throughout this thesis will be described.

In general, the preprocessing steps applied to multi- or hyperspectral images are similar compared to single-point spectroscopic datasets (174, 181, 224). However, because of the three-dimensional data cube that is obtained by imaging techniques additional data analysis steps are required as compared to conventional spectroscopy (Fig. 7b). First, the region of interest has to be determined from the images to remove undesired background information (181, 224). Subsequently, the three-dimensional data cubes are usually unfolded to obtain a two-dimensional data matrix for spectral preprocessing and for the following uni- or multivariate data analysis steps (181, 229). To visualize the information obtained from the data analysis procedure, the unfolded two-dimensional data matrix is finally refolded to a three-dimensional image for each wavelength (181, 229).

1.5.1.1 Centering and scaling

Mean centering is one centering method which is commonly applied to spectral datasets prior to multivariate analysis in order to remove spectral offsets (222, 230). Generally, the rank of spectral observations and thus the overall interpretation of the data is remaining unchanged during mean centering (230). The effect of the application of mean centering to UV spectra is illustrated in Fig. 8.

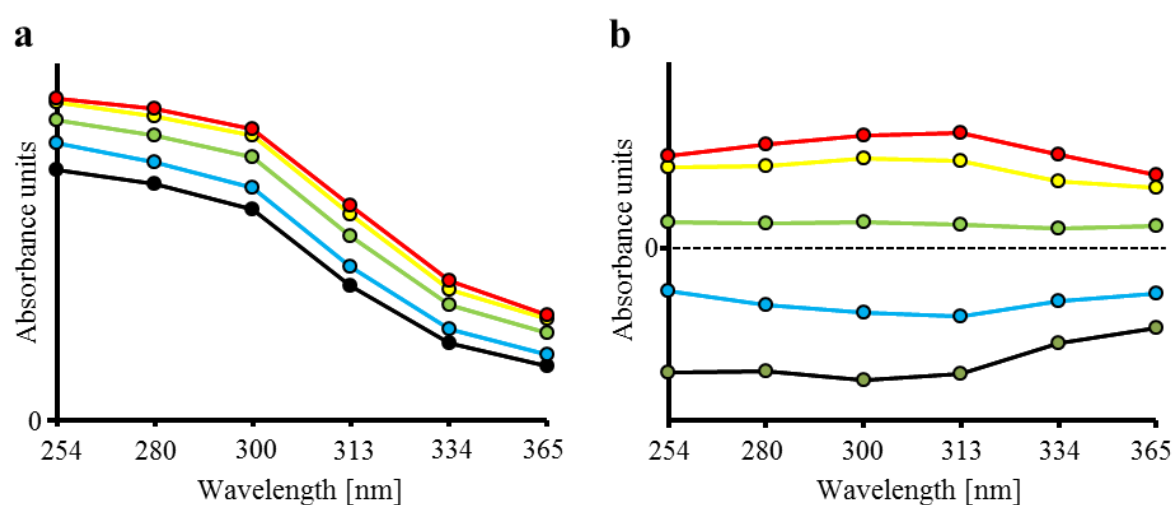


Fig. 8: Unprocessed (a) and mean centered (b) UV spectra of tablets prepared at different compaction pressures.

It has been shown that multivariate models calculated from mean centered datasets often show a significantly increased fit to the data compared to analysis of the unprocessed spectra (230). Mean centered spectral datasets could be accurately modeled with one component less compared to the untreated data e.g. in PCA (230).

By application of PCA to the dataset, each spectrum is represented by a single point in a multivariate space with samples that show similar spectroscopic features forming a cluster in a certain distance from origin of the coordinate system. As described by

Wu et al., the main variance within the dataset, which is explained by the first principal component (PC-1), is the distance of each point to the origin of the multivariate data space (222). After mean centering of the spectral dataset, the center of the cluster of points corresponds to the origin of the multivariate space leading to relevant spectral differences between the points being captured by PC-1 (222, 231).

Mean centering of a data matrix X with the sample spectra I being arranged row-wise and the spectral variables J , i.e. intensities at defined wavelengths, ordered column-wise is performed as follows (222):

$$y_{ij} = x_{ij} - \frac{\sum_{i=1}^I x_{ij}}{I} \quad (\text{Eq. 1})$$

where x_{ij} and y_{ij} are the initial and mean centered elements of the matrix X , respectively. Thus, by mean centering, the mean spectrum of the data matrix X is calculated followed by subtraction of this mean spectrum from each spectrum I of X (230).

Mean centering of the spectral dataset is often followed by a subsequent scaling step before application of multivariate analysis. The reason for data scaling is that the influence of a variable on a multivariate model which is based on least squares data fitting is dependent on the magnitude of its variance (222). In unscaled data matrices, variables with a larger variance have a greater influence on the model compared to variables with a smaller variance (222). However, also variables with a small variance can contain valuable information and thus should be equally weighted. In this context, it has been reported that the performance of multivariate models calculated from spectral datasets can be markedly improved by scaling of the centered data (232).

However, scaling of the data should not be applied uncritically because spectral noise is more pronounced by this procedure which may lead to a reduced model quality (222, 233).

Widely applied scaling techniques are unit variance scaling as well as auto-scaling (222). Scaling to unit variance refers to dividing each variable of a spectrum I of X by the standard deviation of all elements arranged in the respective column resulting in the variance of all variables of X to be unity (234). The term auto-scaling corresponds to the combination of mean centering and unit variance scaling of the dataset (222). Auto-scaling results in a data matrix with a mean of zero and a variance of unity.

1.5.1.2 Baseline correction and normalization

Baseline correction is commonly performed with spectral datasets to remove undesired variations in the spectra such as a spectral offset and variation in the baseline slopes, which are related to physical sample properties or the conditions of the measurement rather than chemical sample information (222, 235). Baseline shifts and slopes in the spectra result from the multiplicative interference of sample density variations, particle size differences, specular reflection, and instrumental drifts (117, 222). In the case of solid samples, scattering of the light emitted from the spectrometer occurs on the sample surface dependent on the density and the particle size of the sample. The light penetrates into the sample and interacts with the sample particles. The spectral path length is changing dependent on the particle size and results in a baseline shift of spectra from samples with different particle sizes (235).

1.5.1.2.1 Offset correction

Offset correction is a straightforward method to remove a parallel baseline shift of spectra (235). Therefore, an arbitrary chosen value a that best defines the baseline of a respective spectrum X is chosen independently for each spectrum. Subsequently, a is subtracted from each variable x_{ij} of a respective spectrum to obtain the transformed spectral elements ($x_{ij,o}$) as follows (235):

$$x_{ij,o} = x_{ij} - a \quad (\text{Eq. 2})$$

1.5.1.2.2 Area normalization

Area normalization is applied to spectral datasets to eliminate variations between spectra which are caused by differences in the effective path lengths or by the sample concentration (117, 174, 236). Area normalization is performed by dividing each variable x_j of a spectrum X by the total sum a of all variables of the respective spectrum as follows (174, 223):

$$x_{norm_j} = \frac{x_j}{a} \quad (\text{Eq. 3})$$

Consequently, the area under the curve is the same for all spectra.

1.5.1.2.3 SNV correction

SNV has been shown to be an effective and widely used algorithm for the elimination of spectral variations which are caused by multiplicative interferences of light scattering and particle size (223, 235, 237). SNV standardization removes baseline shifts and variations in the slope of the spectra while the shape of the spectra is

preserved (222, 226). The effect of the application of SNV correction to NIR spectra is shown in Fig. 9.

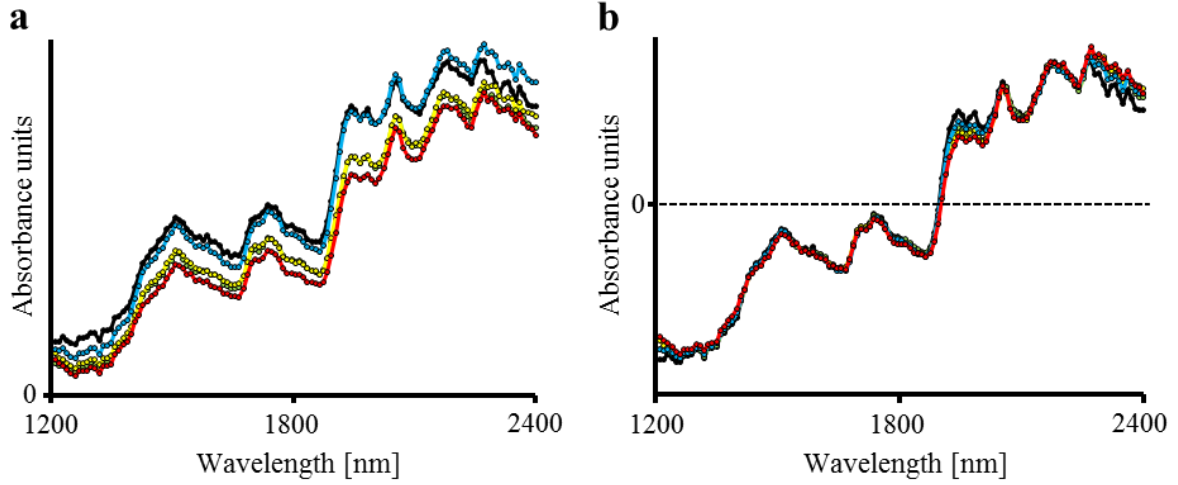


Fig. 9: Unprocessed (a) and SNV corrected (b) NIR absorbance spectra.

SNV correction is applied to each spectrum separately and refers to the calculation of the mean and the standard deviation of the spectral variables followed by subtraction of the mean from the spectral variables and division by the standard deviation according to Eq. 4 (223, 229):

$$x_{SNV} = \frac{x_{org} - a_0}{a_1} \quad (\text{Eq. 4})$$

where x_{SNV} and x_{org} are the SNV corrected and uncorrected spectra, respectively; a_0 is the mean intensity of a spectral vector x_{org} , and a_1 is the standard deviation of all intensities of the spectrum x_{org} . Thus, SNV normalization centers and scales a spectrum to a mean of zero and a standard deviation of unity (229). As with all preprocessing techniques, SNV correction should be applied with care, as it is sensitive to noise in the spectra (223).

1.5.2 Uni- and multivariate analysis

1.5.2.1 General aspects

The choice of the data analysis procedure that is applied to spectral datasets should be driven by the sample information that is desired to be obtained from the dataset as mentioned before, and by the structure or complexity of the data (181, 222). In general, data analysis is based either on uni- or multivariate procedures (Fig. 10). As a basic principle, data analysis routines should be kept as simple as possible and take into account only those spectral variables containing relevant information about the samples (222).

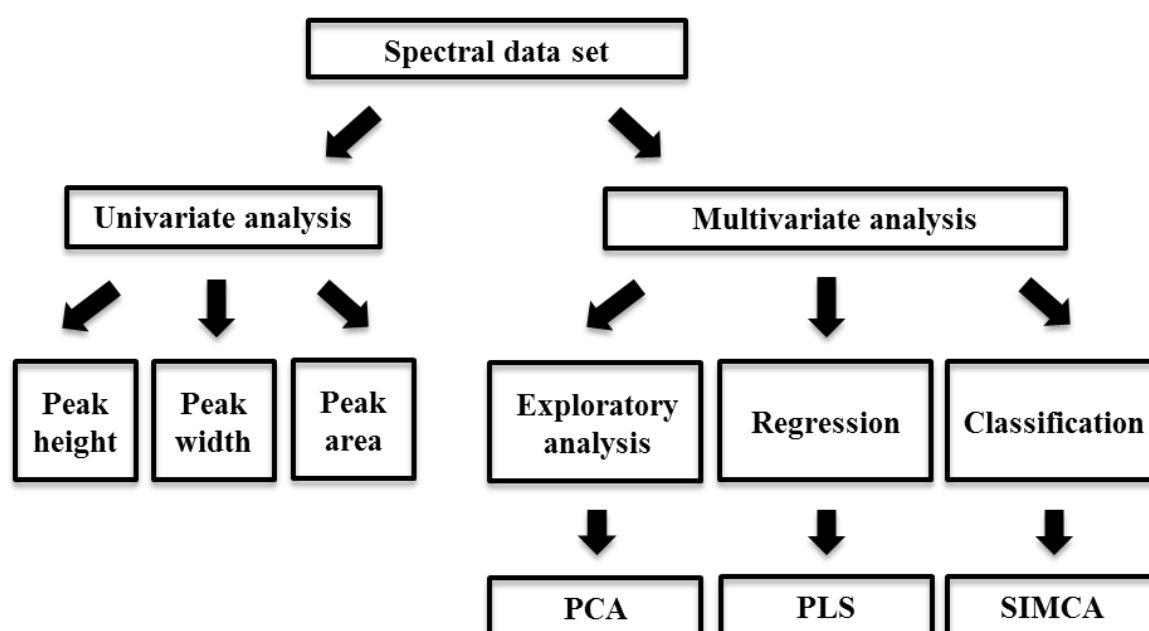


Fig. 10: Overview of uni- and multivariate analysis.

To obtain the desired information about the samples from their spectra, it can be sufficient to analyze a single peak rather than the entire spectrum (181). It has been shown that statistical parameters such as the position of a specific peak, its intensity,

width, and area can be correlated with physicochemical sample properties such as the chemical composition, the concentration of a compound, or the compaction of a powder blend (238–240). However, such an univariate analysis requires prior knowledge on the investigated sample (174): the compound of interest and its spectral pattern has to be known. Furthermore, it has to be ensured that a selected peak is unique for a specific physicochemical parameter without interferences caused by variations in other physicochemical sample properties (174, 181). However, with increasing complexity of the investigated datasets such an overlapping of relevant and irrelevant information as well as correlations between the spectral variables becomes more pronounced leading to unsatisfying results obtained by univariate analysis (128, 181, 222).

To identify relevant relationships in complex datasets and to obtain the desired information, simultaneous examination of a large number of variables instead of one variable at a time is necessary (222, 241). In this regard, multivariate analysis techniques such as PCA and PLS Regression have been shown to be suitable to obtain the required information from complex datasets (21, 128). In contrast to univariate analysis, multivariate analysis takes into account several variables at a time (174). This is beneficial as it allows to detect collinearity in the spectral data and thus to effectively separate the relevant information from noise (241). Consequently, multivariate methods in combination with spectroscopic techniques have become powerful tools to find similarities and differences between samples and play a key role in terms of process monitoring, understanding, and control in context with the FDAs PAT initiative (20, 21, 242).

1.5.2.2 Principal Component Analysis

Principal Component Analysis (PCA) has been described for the first time by Karl Pearson in 1901 (243) and has become a widely used method for multivariate analysis of scientific datasets (174, 241, 244).

PCA has been successfully applied to single-point and imaging spectral datasets for determination of various tablet quality attributes (46, 151, 181) and demonstrated to be a powerful tool for separation of the region of interest from the background within multi- or hyperspectral images (224). Furthermore, PCA has been shown to be a valuable technique to follow changes in the secondary structure of proteins (245).

In general, PCA is an exploratory data analysis technique that allows to detect patterns and trends in the data without prior knowledge about the data (241). PCA is often applied to spectroscopic datasets such as infrared spectra which are regarded as vectors x_{org} composed of a large number of variables $(x_1, x_2, x_3, \dots, x_n)$ that contain useful physicochemical information on the samples but also noise (Eq. 5) (241).

$$x_{org} = (x_1, x_2, x_3, \dots, x_n) \quad (\text{Eq. 5})$$

The overall goal of PCA is to reduce complexity of the data while retaining the relevant information and discarding noise (151, 241). Therefore, collinearity between sample variables is identified and removed by transforming the data from the initial high-dimensional data space to a lower dimensional so-called PC space (Fig. 11) (241, 244).

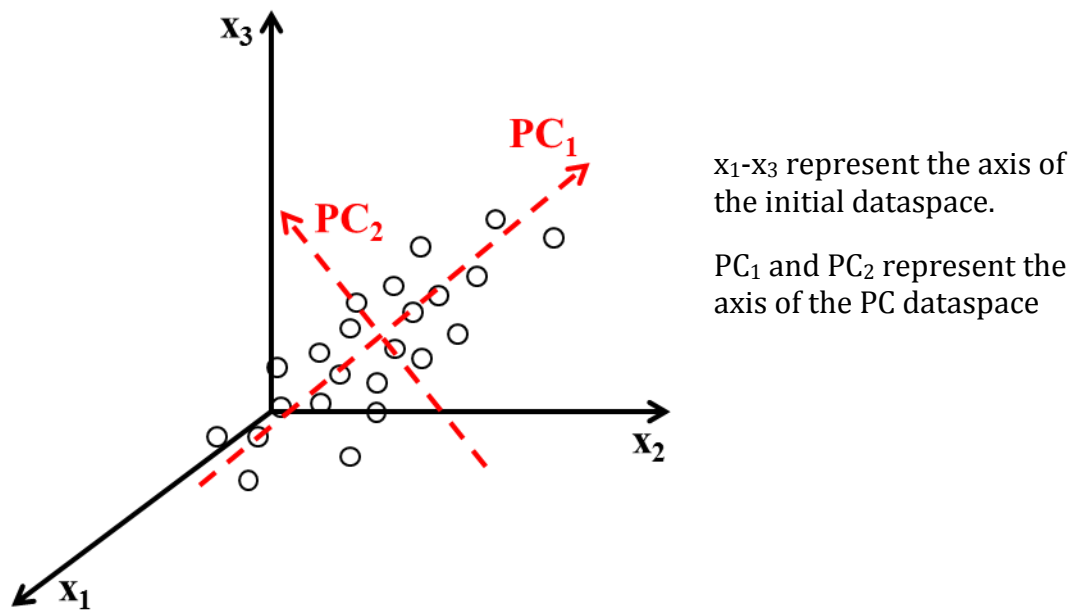


Fig. 11: Illustration of a principal component data space; modified from (246).

The initial data vectors are projected onto a new coordinate system with the direction of the axes or PCs being defined in a least-squares sense to maximize the variance between the different samples (174, 222, 241). The PCs are a linear combination of the initial variables in a mathematical sense under the constraint of orthogonality of the different PCs (241, 244).

The first PC is positioned in a direction that it passes through the center of the initial data and explains the major variance within the dataset (241). PC-2 is also directed through the center of the data and explains as much as possible of the unexplained variance while being uncorrelated to PC-1 (244). As a result of the orthogonality constraint, each PC captures the variance of a different direction in the dataset which is consequently related to a different source of information (241). Thus, a data vector

with a large number of variables is described by only a few uncorrelated PCs which can be mathematically described as follows (231):

$$X = T P' + E \quad (\text{Eq. 6})$$

where X is the initial data matrix of size $N \times M$ with the sample spectra being arranged row-wise (N) and the respective wavelengths column-wise (M); T and P are the scores and transposed loadings matrices of size $N \times A$ and $A \times M$ with A defining the number of PCs, and E being the residual matrix (222). Thus, by application of PCA the data matrix X is decomposed to loadings and scores (Fig. 12) (181). Score values can be interpreted as projections of data vectors onto the PC data space serving as coordinates within the coordinate system (244).

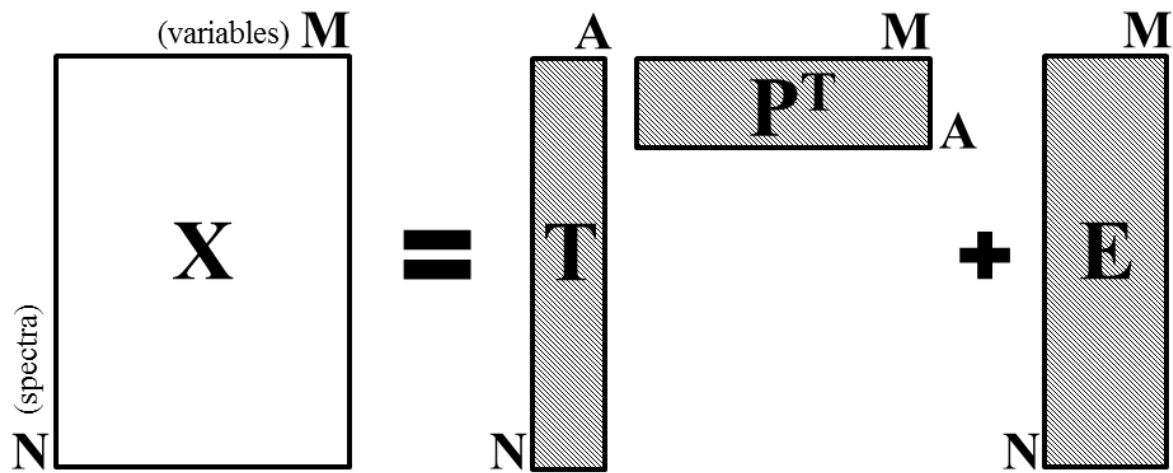


Fig. 12: Data matrices of PCA; adopted from (247).

By visualization of the obtained scores in so-called scores plots, the similarity between samples can be estimated and patterns and trends in the data can be detected (151, 244).

The respective loadings vector represents the weight of each initial variable with

respect to the variance within the dataset and reveals the degree of covariance between the variables (151, 181). Every variable is represented by a single loading value in each PC, i.e. the correlation coefficient between the initial variable and the respective PCs, which is used for understanding and interpretation of the patterns observed in the corresponding scores plot (151, 248).

The variance that is captured by a respective PC is referred to as explained variance and contains a decreasing information content with increasing number of PCs (241). The unexplained variance of each PC is called residual variance E (174, 241). Thus, by including PCs with a high information content in a PCA model and discarding the PCs that mainly capture noise, a significant data reduction is achieved and the extraction of relevant information from even complex datasets is facilitated (174, 241).

1.5.2.3 Partial Least Squares Regression

Partial Least Squares (PLS) is a commonly used algorithm for regression of scientific data and was introduced by Herman and Svante Wold around 1980 (249–251). PLS Regression models based on spectral datasets have been demonstrated to allow accurate prediction of various tablet qualities (46, 151, 181, 228).

The aim of PLS Regression is to find a functional correlation between two datasets X and Y , which both contain measured variables on the same sample (246). Two different PLS approaches can be distinguished: in PLS1 models a correlation between a data matrix X and one target value, represented by the vector Y , is determined, while the aim of PLS2 is to find a correlation between X and several target values Y (247). In general, a regression model is established with the independent variables of

the data matrix X of dimension $N \times M$ serving as predictors for the dependent variables of the response data matrix Y of dimension $N \times K$ (Fig. 13) (246, 247).

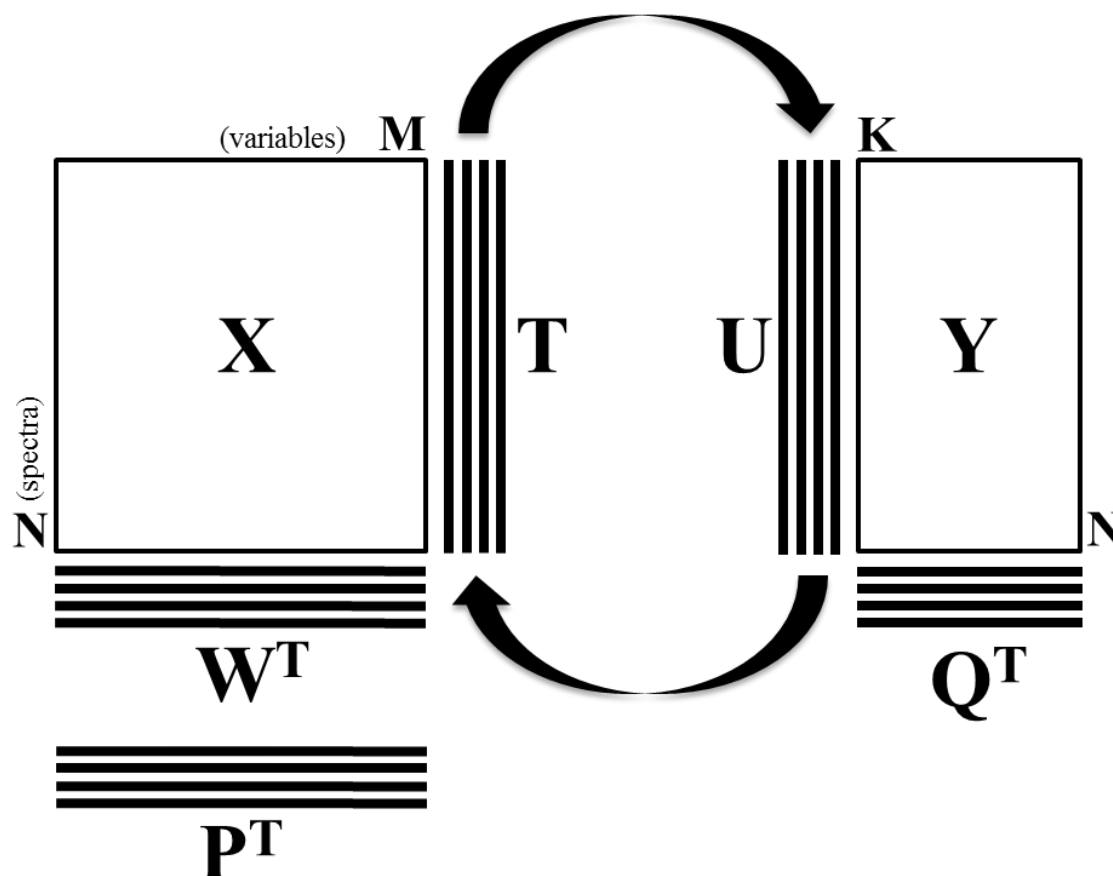


Fig. 13: Underlying structure of a PLS Regression model; adopted from (247).

In the context of spectroscopic techniques for quality control, the PLS calibration model is built between the obtained spectral information which represents the data matrix X composed of N spectra with M spectral intensities at defined wavelengths, and reference values of a certain sample property, such as the API concentration within a tablet that are quoted in the data vector Y (246). Therefore, a simultaneous decomposition of X and Y is performed to find orthogonal factors called latent variables (LVs) that explain as much as possible of the variance of the data matrix X

while being maximally correlated to the response values of matrix Y (248, 252, 253). Therefore, both the X and Y matrix are fitted by PCA models (246). In contrast to PCA, where the direction of the components is defined to explain the maximum variance within a dataset (Fig. 11), in PLS Regression the direction of the factors is defined to explain the maximum covariance between the X and Y matrix (246, 252). Therefore, in PLS Regression the two PCA models are aligned and the information on the structure of the Y data influences the PCA applied to the data matrix X and vice versa (246, 247).

In this context, upon establishment of a PLS calibration model two types of loadings are calculated for the X data matrix and one for the vector Y for each PLS factor (246). As described in the previous section for PCA, the P loadings describe the relationship between the initial data matrix X and the resulting scores (247). However, in contrast to PCA, the P loadings of PLS Regression are usually not orthogonal to each other (247). The obtained weighted loadings (W^T) describe the correlation between the data matrix X and the vector Y under the constraint of orthogonality between the loadings of the different components. Thus, the weighted loadings contain the information on the covariance-based direction of the components and thus vary from the P loadings by the influence of the structure of the Y data (247). In general, those variables of the data matrix X that show a high correlation with variables of vector Y obtain high weights. Similarly, the Q weights (Q^T) explain how the score vector U is formed from the variables of vector Y . The variance in the data matrix X and vector Y that is not taken into account for the construction of the PLS Regression model form the residual matrices E and F , respectively (246).

1.5.3 Pattern recognition techniques

1.5.3.1 General aspects

Unsupervised data analysis techniques such as PCA provide valuable information to assess the variance in multivariate spectral datasets (46, 181, 222). The information obtained from PCA is useful to detect trends and patterns in the data (241). Similarity among the samples can be estimated from the resulting scores plot because samples with similar spectral features form clusters in the scores plot, while those with markedly different spectra are located in discrete regions of the PC space (241). However, the information obtained on the spectral similarity by PCA is not sufficient for a systematic classification of the samples based on their spectral features which is often desired in terms of quality control (241, 245). For instance, samples with insufficient quality, e.g. tablets without the desired API dose, need to be identified as failure and have to be separated from those with the desired quality.

For classification of chemical data, pattern recognition techniques such as k-Nearest Neighbor (KNN) or SIMCA, are well-established (241, 248) and will be discussed in more detail in the following subsections. An overview about the broad range of pattern recognition techniques is given in the literature (248).

1.5.3.2 k-Nearest Neighbor

The k-Nearest Neighbor (KNN) principle is one of the simplest and well-established similarity-based procedures for sample classification (254, 255) and derived from the rules reported by Fix and Hodges in 1951 (256). Similarity-based classifiers such as KNN generally regard multivariate samples, e.g. spectra composed of numerous variables $(x_{i1}, x_{i2}, x_{i3}, \dots, x_{in})$ as vectors x_i (Eq. 5) (241). Such vectors are treated as points in a multidimensional space, where the number of variables n per sample determine the dimensionality of the data space (241). Thus, the position of each point or sample within the n -dimensional space is defined by their respective variables serving as coordinates. From the position of the data points within the data space the similarity of samples is estimated by calculation of the Euclidian distances d between the respective data points as follows (241, 257):

$$d(x_i, x_p) = \sqrt{(x_{i1} - x_{p1})^2 + (x_{i2} - x_{p2})^2 + \dots + (x_{in} - x_{pn})^2} \quad (\text{Eq. 7})$$

where x_i and x_p are input samples with the variables $(x_{i1}, x_{i2}, x_{i3}, \dots, x_{in})$ and $(x_{p1}, x_{p2}, x_{p3}, \dots, x_{pn})$, respectively. In general, the distance between two data points is assumed to be directly related to the sample diversity (241). Thus, while samples with similar variables n form clusters in the n -dimensional data space and are assumed to belong to the same classification group, markedly different samples are found in diverse regions of the data space indicating dissimilar class memberships (258).

Classification of an unknown sample is based on its position and the known class memberships of its nearest neighbors in the data space (241). First, the distances

between the unknown sample and the surrounding data points are calculated followed by arrangement of these distances in an ascending order. Subsequently, the class membership of the unknown sample is determined according to the most common class membership of its KNNs (241, 259). In this regard, the value of k is crucial for classification performance and should be defined individually for each type of dataset based on the error of classification (248, 260).

The simplicity and effectiveness of the classification procedure as well as the easy way of model implementation are considered advantages of KNN as a classification tool (254, 259–261). However, KNN also shows some disadvantages. For instance, if large datasets with many variables are processed, KNN can have a poor run-time performance (248, 260, 261). Furthermore, KNN is a discriminating method and always assigns a sample to one of the predefined classes, which consequently leads to misclassification of unknown samples that do not belong to any of the given classes (248). In addition, poor information on the structure of the given classes and the relevance of each variable with regard to the classification of the samples is provided by KNN (248). In this context, all variables are weighted equally for classification, making KNN sensitive to irrelevant information, which can, however, be avoided by proper selection and defined weighting of the variables (260, 261).

1.5.3.3 Soft Independent Modelling by Class Analogy

Soft Independent Modelling by Class Analogy (SIMCA) (262, 263) is another commonly applied pattern recognition technique for the classification of multivariate datasets such as spectra. In combination with spectroscopic techniques SIMCA has been proven to be a valuable tool for quality control during different tablet manufacturing steps. For instance, SIMCA applied to NIR spectra has been demonstrated to allow a systematic differentiation between powdered bulk materials based on their chemical composition (264, 265). Furthermore, NIR (238) and Raman (266) spectroscopy together with SIMCA analysis have been successfully applied to evaluate powder blend homogeneity. In addition, a SIMCA model based on a NIR dataset has been effectively used to discriminate between uncoated and coated as well as API containing and placebo tablets within blister packs, respectively (138).

SIMCA classification of unknown samples is based on the application of PCA to reference spectra of each class of the data (training set) to model the common spectral variance within the different classes (241). Subsequently, the assignment of an unknown sample to the different classes is determined by projection of the sample onto the disjoint PCA models (267). Therefore, class boundaries are defined for each PCA model prior to classification. In general, there are several ways to define the boundaries of each class which determine if a test sample is assigned to the respective class or rejected (263, 264, 268). Usually, classification is based on the residual distribution of the training set samples obtained upon construction of the PCA models (241). As mentioned before, application of PCA to a spectral dataset involves the built-up of a model based on those PCs that describe the relevant

spectral variance (modeled variance) within the data (231). Spectral variance that results from noise (residual variance) is mainly captured by the higher order PCs which are discarded (241). Upon projection of the sample onto each PCA model, the fit of the model to the unknown sample, which corresponds to the similarity of the unknown sample to the respective training set samples, is determined by comparison of the residual variance of the sample with the residual variance distribution of the respective training set samples using the F-statistics (241, 268). Therefore, prior to classification of the unknown sample, the respective class boundary is defined by application of the F-statistics to the training set of the PCA models (241).

An additional way to determine class boundaries is based on the scores matrix of the respective PCA model. Therefore, after projection of the unknown sample onto the respective PCA model, the probability that the predicted score of the unknown sample differs from the mean of the distribution of the score matrix is determined by application of a multivariate t-test (Hotelling T^2) (268).

In general, to ensure a high classification performance of the SIMCA model, the choice of the number of PCs used to establish the PCA models is crucial (264). The optimum number of PCs is determined individually for each PCA model and usually based on cross-validation of the training dataset (241, 264). On the one hand, the established PCA model is not representative for the respective class if PCs that describe relevant information on the samples are discarded. On the other hand, the inclusion of PCs in the model that mainly describe noise diminishes the information content of the respective PCA model (241).

SIMCA classification shows the advantages of being versatily applicable to datasets with a large as well as small sample number and has no limitation regarding the dimensionality of the dataset (241, 245). Furthermore, the SIMCA model provides diagnostic parameters such as the discriminatory power, which allows to directly assess the influence of each variable on the establishment and performance of the classification model (241). Thus, variables that mainly describe noise and do not significantly contribute to the successful classification of unknown samples can be removed from the model to increase classification performance (241). Furthermore, in contrast to classifiers such as KNN, samples are only assigned to a class if their similarity to the respective class model exceeds the predefined limit. Thus, samples that do not belong to any of the predefined classes can be correctly classified as non-members with respect to all PCA models (248). However, SIMCA also shows some disadvantages. For instance, local PCA models are calculated for each class of the data and are consequently defined by the direction of the largest variance of the data of each class instead of that separating the classes most clearly (268). Furthermore, because of the separate calculation of the PCA models, the spectral differences between the classes that determine the classification of unknown samples are not directly accessible (268).

1.6 Objectives of this work

Because of the increasing interest in tableting as formulation strategy for biomacromolecules, one aim of this thesis was to investigate the impact of tableting on the integrity of trypsin as a model API. In this regard, the influence of compaction on the conformation of trypsin was evaluated by determination of its secondary structure before and after compaction using FTIR spectroscopy. Reversibility of pressure-induced structural changes was examined by application of solid state FITR analysis of the trypsin powder as well as measurements of the reconstituted tablets in the aqueous state. Furthermore, to compare the thermal stability of uncompacted and compacted trypsin, its transition temperature of unfolding as well as its folding reversibility after thermal denaturation were determined by thermal analysis.

Recently, hyperspectral imaging techniques have been demonstrated to be powerful tools for pharmaceutical quality control as they are non-destructive and provide spatially resolved chemical information on the samples. However, the established techniques and related image analysis procedures markedly differ in the ease of application, sensitivity, and speed of data acquisition. In this regard, another aim of this thesis was to investigate the applicability of multispectral UV imaging for non-destructive and fast quality control of tablets. The suitability of UV imaging for determination of relevant chemical as well as physical tablet quality attributes with regard to different tablet manufacturing steps, namely compaction, coating, and packaging was investigated. Therefore, data analysis procedures based on multivariate analysis and pattern recognition techniques were applied to the

obtained UV images to evaluate the potential of UV imaging for automatized quality control within the tablet manufacturing line.

2 Materials and Methods

2.1 Materials

2.1.1 Active Pharmaceutical Ingredients

Acetylsalicylic acid (ASA) was obtained from Fagron (Barsbüttel, Germany). Amylase powder from *Aspergillus oryzae* and lipase powder from *Rhizopus oryzae* were supplied by extrakt chemie (Stadthagen, Germany). Lyophilized bovine trypsin (USP grade, 3330 USP units/mg) powder was obtained from Biozym (Hamburg, Germany).

2.1.2 Tableting excipients

Highly dispersed silicon dioxide (Aerosil® 200), and potato starch were purchased from Fagron (Barsbüttel, Germany). Microcrystalline cellulose (MCC, Avicel® PH-102) was supplied by FMC Biopolymer (Dublin, Ireland) and Kollicoat® IR (polyvinyl alcohol-polyethylene glycol graft copolymer (PVA/PEG)) of two colors (blue and yellow based on aluminum lakes) was kindly supplied by BASF (Ludwigshafen, Germany). Magnesium stearate (MgSt) was donated by Baerlocher (Unterschleissheim, Germany).

2.1.3 Chemical reagents

Benzoyl-L-arginine ethyl ester hydrochloride (BAEE) was obtained from AppliChem (Darmstadt, Germany). Hydrochloric acid, monobasic sodium phosphate, and sodium hydroxide were all purchased from Roth (Karlsruhe, Germany). Deionized water was prepared with a Millipore purification system (Merck Millipore, Schwalbach, Germany).

2.1.4 Bulk tablets

Aspirine® tablets (API: ASA; tablets 'A') were purchased from Sanacorp Pharmahandel GmbH (Planegg, Germany). Bulk tablets of Baytril® (API: enrofloxacin; tablets 'B') and Drontal® Plus (APIs: febantel, praziquantel, pyrantel pamoate; tablets 'D') were provided by Bayer HealthCare, Animal Health (Supply Center Kiel, Germany). Furthermore, bone-shaped tablets resulting from an experimental batch (tablets 'C') were also supplied by Bayer Animal Health to evaluate the suitability of UV imaging for the detection of cracks in tablets.

2.1.5 Packaging material

Aluminum blister cavities and three different blister sealing foils relevant in the pharmaceutical industry (79) (Genotherm® PH 132: polyvinyl chloride (PVC), thickness: 250 µm; Genotherm® PH 154 3A: PVC, thickness: 250 µm; Pentapharm® PA200/02: polychlorotrifluoroethylene (PCTFE)/PVC, thickness: 305 µm) were kindly donated by Bayer HealthCare, Animal Health (Supply Center Kiel, Germany).

2.2 General methods²

2.2.1 Tableting

Tableting was performed either on an instrumented single punch eccentric press (Fette E XI) or on a rotary tablet press (Fette 102i) both from Fette Compacting, Schwarzenbek, Germany. All tableting experiments were performed under controlled conditions (21 °C/45 % RH).

2.2.2 UV imaging

Images of bulk tablets and blister packs were obtained with a VideometerLabUV multispectral imager (VideometerLabUV, Videometer, Hørsholm, Denmark). For tablets with different amylase contents, images of the upper as well as the lower tablet surface were recorded, as differences in the API concentration may occur between the two tablet surfaces because of powder segregation during filling of the die. For all other bulk tablets as well as tablets inside blister packs images of only one surface were acquired, as these UV images contain all required information for evaluation of the applicability of UV imaging and the related analytical procedures for determination of the respective quality attributes of the tablets. The imager was equipped with a Mercury-Xenon UV light source and bandpass filters to illuminate the samples at six wavelengths (254, 280, 300, 313, 334, and 365 nm) as well as a CCD camera to collect the light that is diffusely reflected by the samples. The field of view of the instrument with a size of 11.7 cm × 8.8 cm was imaged within about 18 s and resulted in a raw data array of dimension 960 × 1280 × 6, where the wavelengths are arranged along the third dimension. The spatial resolution was 77.9 μm. The UV

²Parts of this chapter have been published as shown on page 199 in appendix B.

imager and its optical setup is presented in Fig. 14. Control of the instrument was performed with the VideometerLab software (ver. 1.6, Videometer, Hørsholm, Denmark).

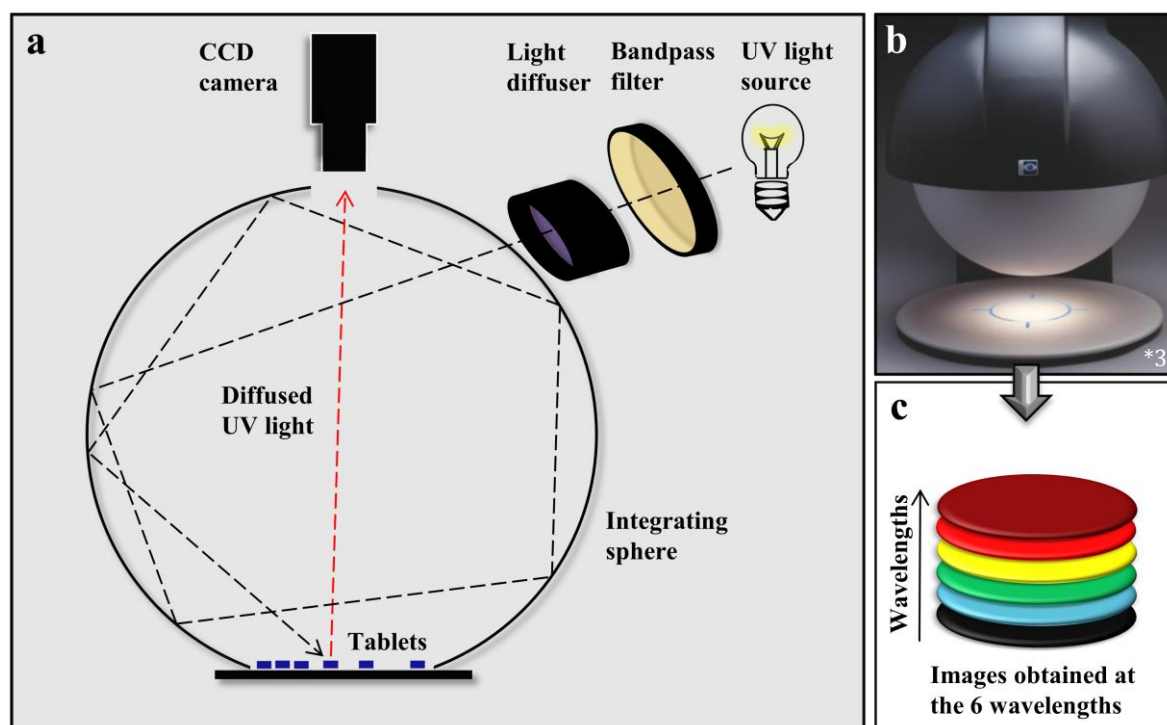


Fig. 14: (a) Working principle of the UV imager, (b) Multispectral UV imager, (c) Resulting three-dimensional data array of a tablet.

2.2.3 Photographic imaging

Photographs of tablets were captured with a Canon EOS 600D-SLR camera (18-megapixel) attached to a Canon EF-S 18-55mm 1:3.5-5.6 IS II objective (both from Canon, Tokyo, Japan). The photographs were processed using Adobe Photoshop® CS2 (ver. 9.0, Adobe Systems, San Jose, USA).

2.2.4 Image analysis and statistics

Analysis of the UV and NIR images was based on PCA, PLS Regression, SIMCA analysis, as well as related statistics and was performed with in-house written Matlab® (ver. 8.1, Mathworks, Natick, USA) scripts using the Image Processing Toolbox (ver. 8.0, Mathworks, Natick, USA) and the PLS_Toolbox (ver. 7.3, Eigenvector Research, Wenatchee, USA) as well as with the Unscrambler X software (Camo, Oslo, Norway).

The number of the LVs that were used to establish the PLS calibration models was determined based on the trend of the root mean square error of calibration (RMSEC) and root mean square error of cross validation (RMSECV) values dependent on the LVs resulting from internal cross validation of the datasets.

Statistical significance of the differences between the reported values in the thesis was assessed by application of single-factor Analysis of Variance using the Excel software (Microsoft Corporation, Redmond, Washington).

2.2.5 Pattern recognition

An often required outcome of quality control and process monitoring is to classify the investigated products based on the determined product attributes. In this context, analytical techniques such as spectroscopy provide complex multivariate datasets that require mathematical procedures to categorize samples based on quality-relevant product characteristics (248). For this purpose, pattern recognition techniques such as KNN, SIMCA, and others have been proven to be useful (241, 248). One advantage of SIMCA compared to KNN is that samples are solely assigned to

given classes if their similarity to the respective class model exceeds the predefined limit, while KNN always assigns a sample to one of the predefined classes (248).

In this thesis, SIMCA analysis was used for quality-based classification of tablets, because a variety of tablet samples, including those which are outside all predefined classes, were investigated. The applied number of PCs used in each PCA model was chosen by examination of the RMSECV as a function of the number of PCs and further minimized to obtain robust classification models.

Classification performance of the SIMCA model was assessed by calculation of the sensitivity and specificity for each PCA model using the following equations (268):

$$\text{Sensitivity} = \frac{tp}{tp+fn} \quad (\text{Eq. 8})$$

$$\text{Specificity} = \frac{tn}{tn+fp} \quad (\text{Eq. 9})$$

where tp is the number of objects that are class members of a respective PCA model and are correctly identified as such, fn is the number of objects with known assignment to a PCA model class that were incorrectly classified as non-members, fp is the number of objects known to be non-members of a respective PCA model class that are incorrectly classified as class members, and tn is the number of objects known to be non-members of a PCA model class which are correctly classified as such.

In general, the sensitivity indicates how well members of a particular class are identified as class members, while the specificity is a measure of how well non-members of a respective class are classified as such (269). The values for specificity

and sensitivity are between 0 and unity with values close to unity indicating a high specificity or sensitivity of the model, respectively (270).

2.3 Specific methods of ‘Influence of tableting on the conformation and thermal stability of trypsin as a model protein’⁴

2.3.1 Preparation of tablets

Plain trypsin powder was gently ground by mortar and pestle, sieved (125 µm mesh), and stored at 21 °C and a relative humidity of 45 % for at least 48 h prior to compaction. Tableting was performed at predefined compaction pressures (40 – 382 MPa) on the Fette E XI eccentric press, equipped with 10 mm flat-faced punches. Tableting was carried out at a compaction speed of 16 rpm in single stroke mode by filling 100 mg of the powder manually into the die.

2.3.2 Assay of trypsin activity

To evaluate the effect of compaction on trypsin, enzymatic activity of unprocessed and compacted enzyme powder was determined by a constant rate UV-photometric assay under steady-state conditions according to the USP monograph ‘Crystallized Trypsin’. Tablets were gently ground by mortar and pestle and the remaining powder was dissolved in 10 mM hydrochloric acid. 200 µL of protein solution were mixed with 3.0 ml of BAEE substrate solution. The absorbance at 253 nm was measured at 30 s intervals for 5 min. Trypsin activity of all samples expressed as a percentage of the mean initial activity of the trypsin powder (activity (%)) was determined from the slope of the absorbance profiles using equations 10 and 11.

$$\text{activity (\%)} = \frac{\text{units}_s}{\text{units}_i} \times 100 \quad (\text{Eq. 10})$$

⁴This chapter has been published as shown on page 199 in appendix B.

$$units_s = \frac{(A_1 - A_2)}{0.003 \times T \times W} \quad (\text{Eq. 11})$$

where $units_s$ is the trypsin activity, in USP units, of the respective samples, $units_i$ is the mean initial trypsin activity of unprocessed trypsin powder, A_1 is the absorbance straight-line final reading, A_2 is the absorbance straight-line initial reading, T is the elapsed time, in minutes, between the initial and final readings, and W is the weight, in mg, of trypsin in the volume of the sample solution.

2.3.3 Fourier transform infrared spectroscopy

Infrared spectra of unprocessed trypsin and ground trypsin tablets were recorded using a Tensor 37 FTIR spectrometer (Bruker, Ettlingen, Germany) equipped with a nitrogen-cooled MCT detector. The instrument was continuously purged with almost dry and carbon dioxide-free air (double column air dryer, SDAT-670/420, DRUMAG GmbH, Bad Saeckingen, Germany) to reduce interfering carbon dioxide and water vapor. Data acquisition and pre-processing of the spectral dataset were performed with the OPUS 7.0 software (Bruker, Ettlingen, Germany). All spectra were corrected for remaining interfering water using the OPUS software algorithm.

Solid state FTIR spectra were recorded using an ATR device (MIRacle, Piketech, Madison, Wisconsin) equipped with a zinc selenide crystal plate. Aqueous state FTIR spectra of the gently ground and reconstituted samples (20 mg trypsin/ml deionized water) were recorded using a calcium fluoride flow-through cell (Aquaspec 1110 M, MicroBiolitics, Esslingen, Germany) with a constant path length of 6.5 μm and connected to a thermostat (Phoenix II P1, Thermo Electron, Karlsruhe, Germany) for

temperature control. For each spectrum 128 and 512 scan interferograms were collected with a spectral resolution of 4 cm^{-1} in the liquid and solid state, respectively. In the liquid state, there was no marked increase in the spectral quality ≥ 128 scans, while in the solid state an acceptable spectral quality was found only ≥ 512 scans. The amide I wavenumber region ($1710\text{--}1600\text{ cm}^{-1}$) of both the solid state and aqueous state spectra was baseline-corrected and area-normalized.

PCA and PLS Regression were applied to the mean centered aqueous state amide I spectra using the Unscrambler X software. The PLS calibration standards were prepared by linking the mean enzymatic activities determined with unprocessed trypsin as well as with trypsin compacted at different pressures (reference dataset) to the amide I spectra of a different set of equally processed (unprocessed or compacted) trypsin samples, which were gently ground and reconstituted in deionized water prior to FTIR analysis (see above). As mentioned before, the optimum number of LVs used to build the PLS calibration model is generally determined by looking at where the RMSECV curve reaches a minimum (in this case at four LVs). To obtain a more robust model and to avoid overfitting of the data the number of LVs was further reduced to three.

To quantify spectral differences that are induced by tableting, a percentage of area overlap (%ao) approach was applied to the baseline-corrected amide I spectra that were area-normalized to 1. To calculate the %ao of two spectra, a new spectrum, composed of the lowest absorption value between the two spectra at each data point is calculated. The area under this new spectrum in relation to the area under the original spectra corresponds to the %ao (271). The %ao was calculated for the solid

state as well as aqueous state spectra of compacted trypsin in relation to a mean spectrum of unprocessed trypsin (n=3) at the respective physical state. For determination of the %ao of the spectra, mathematical integration of the spectra (i.e. determination of the area under the spectra) was performed using the OriginPro 9.0 software (OriginLab Corp., Northampton, Massachusetts).

2.3.4 Liquid-state differential scanning calorimetry

Differential scanning calorimetry (DSC) was performed to determine if the applied pressures during compaction influence the T_m of unfolding of the reconstituted samples as well as the folding reversibility of trypsin after denaturation. Samples were dissolved in 1 mM hydrochloric acid pH 3.0 to obtain a concentration of about 3 mg trypsin/ml. Subsequently, the sample solutions were degassed and analyzed with a Microcal VP differential scanning calorimeter (Microcal Inc., Northampton, Massachusetts).

Unprocessed samples as well as samples compacted at a pressure of either 40 MPa or 382 MPa were heated from 20 to 90 °C at a rate of 1°C per min under a nitrogen atmosphere of 2 bars. Before the experiments, the trypsin concentration was determined photometrically at 280 nm and a baseline run was performed with 1 mM hydrochloric acid in both the sample and reference cell. Calculation of calorimetric enthalpy changes (ΔH , area under the transition peaks) was performed using the Origin DSC data analysis software (OriginLab Corp., Northampton, Massachusetts).

Folding reversibilities after thermal denaturation were determined by performing two consecutive heating scans for each sample. After the first heating scan, sample

and reference cells were cooled down to 20 °C at about 1 K/min followed by a second heating cycle. The folding reversibility results from the ratio (%) between the enthalpy changes of the second (ΔH_2) and the first (ΔH_1) heating scan as follows:

$$\text{folding reversibility (\%)} = \frac{\Delta H_2}{\Delta H_1} \times 100 \quad (\text{Eq. 12})$$

2.4 Specific methods of 'UV Imaging for fast and non-destructive quality control of chemical and physical tablet attributes'⁵

2.4.1 Preparation of tablets

Plain trypsin powder was gently ground by mortar and pestle and sieved using a mesh size of 160 μm . The powder fraction below 160 μm was used for compaction. All other materials (see below) were used as received.

Powder blends (Table 3) containing varying mass fractions of amylase (100 %, 80 %, 60 %, 40 %, 20 %, 0%), 0.5 % MgSt, and MCC as well as a blend containing 50 % trypsin, 49.5 % MCC, and 0.5 % MgSt (trypsin formulation) were prepared using a Turbula blender at 72 rpm (T2F, W.A. Bachofen, Muttensz, Switzerland). First, the respective API was blended with MCC for ten min. After addition of the lubricant (MgSt) to the blends, the mixing process was continued for another three min. The prepared blends were compacted with the rotary tablet press equipped with 10 mm flat-faced punches.

To obtain tablets of different hardness, trypsin formulation tablets were prepared at preselected main compaction pressures in a range between 20 MPa and 305 MPa (Table 3). All amylase tablets (Table 3) were compacted to a constant cylindrical height of 2.60 mm. As the amylase powder mixtures show a different compaction behavior depending on the composition of the tablets, compaction pressures between 30 and 40 MPa had to be applied. The rotary tablet press was operated in single-punch mode at a rotor speed of 10 rpm. For each amylase and trypsin formulation tablet 300 mg of the respective powder blend were manually filled into the die.

⁵This chapter has been published as shown on page 199 in appendix B.

Table 3: Overview of the compaction experimental setup.

Determined tablet quality attribute	Type of tablet	Sample description	Tablet press	Compaction Pressure (MPa)	Total number of prepared tbl.	Analytical characterization of tablets	
						Data analysis procedure	Number of tbl.
API content	Amylase formulation	Intact tablets containing varying mass fractions of amylase (100 %, 80 %, 60 %, 40 %, 20 %, 0%)	Rotary	30 - 40	43	PLS calibration	37
						PLS validation	6
Hardness	Trypsin formulation	Intact tablets of different hardness (0.2 - 5.8 MPa)	Rotary	20 - 305	42	PLS calibration	35
						PLS validation	7
Surface density distribution & Intactness	Plain trypsin powder	Intact tablets with a homogeneous surface density distribution Representative sample: Fig. 23: Tablet C	Eccentric	40	21	Reference dataset - SIMCA class 1	18
						Test dataset for SIMCA	3
	Plain trypsin powder	Intact tablets with an inhomogeneous surface density distribution Representative samples: Fig. 23: Tablet A/B	Eccentric	125 - 410	15	Reference dataset - SIMCA class 2	12
						Test dataset for SIMCA	3
	Plain lipase powder	Intact tablet with a homogeneous surface density distribution Defect/splintered tablets Representative sample: Fig. 23: Tablet D	Eccentric	40	5	Reference dataset - SIMCA class 1	1
						Test dataset for SIMCA	4
	Plain MCC powder	Defect/splintered tablets	Eccentric	40	2	Test dataset for SIMCA	2

Amylase and trypsin formulation tablets were prepared with a rotary tablet press to obtain tablets with a quality comparable to those resulting from a common industrial manufacturing process and are therefore not expected to show quality differences between the upper and lower tablet surface.

Tableting of plain trypsin, plain MCC, and plain lipase powder was performed using the instrumented single punch eccentric press at a compaction speed of 16 rpm (Table 3). Flat-faced tablets with a diameter of 10 mm were obtained in single-stroke mode by filling 350 mg of the respective powder manually into the die.

To obtain intact tablets with a homogeneous (within specification) or an inhomogeneous (out of specification) density distribution, plain trypsin was compacted at preselected compaction pressures (40 MPa - 410 MPa) without addition of lubricant. Whilst unlubricated tablets prepared at low compaction pressures are assumed to show a rather homogeneous density distribution throughout the tablet surface, at high compaction pressures inhomogeneity is expected (72). Trypsin tablets that were prepared at high pressures were expected to show a markedly higher density at the upper edge than in the center of the tablet surface (72). According to the literature, along the edge of the tablet the compaction force is transmitted to a lesser extent to deeper powder layers than in the center of the tablet (73). At higher compaction pressures, the unlubricated powder particles withstand motion caused by a more pronounced die wall pressure and friction and thus localized rather than general compaction occurs (73, 272). Plain trypsin tablets were prepared with an eccentric tablet press because the effect of an increased density at the upper edge of the tablets is generally increasing with the degree of

asymmetrical axial compaction of the powder. Plain trypsin powder has been chosen for preparation of tablets with different surface density profiles because it shows a high die wall friction upon compaction.

To obtain splintered reference tablets, plain MCC and plain lipase powder was compacted at a low pressure (40 MPa). Two different types of splintered tablets (plain MCC and plain lipase tablets) were prepared to demonstrate the applicability of UV imaging and the presented multivariate quality control procedures for evaluation of tablet intactness irrespective of its composition and the type of defect. A high number of plain lipase tablets showed splintering at the tablet edge (Fig. 23, tablet D), while MCC tablets could be prepared with a defect at the center of the tablet surface (image not shown).

2.4.2 Hyperspectral near-infrared spectroscopic imaging

NIR images of the upper surfaces of two representative plain trypsin tablets compacted at a pressure of 40 MPa and 160 MPa, respectively, which were previously analyzed by UV imaging were acquired for reference purposes. As mentioned before, NIR imaging has been previously shown to be a valuable technique for determination of the tablet surface density profile (73). The NIR images were recorded using a Sapphire NIR imager controlled by the ISys software (both from Spectral Dimensions, Olney, USA). NIR images of size 256 pixels \times 320 pixels were obtained in diffuse reflectance mode with a spatial resolution of 40 μm . NIR spectra (121 channels) of each pixel were obtained between 1200 and 2400 nm with a spectral resolution of 10 nm.

2.4.3 Image analysis and related statistics

2.4.3.1 General aspects

Prior to multivariate image analysis, all UV and NIR reflectance profiles were transformed from reflectance (R) to absorbance (A) using the following equation (109):

$$A = \log_{10} \left(\frac{1}{R} \right) \quad (\text{Eq. 13})$$

Pixels belonging to the tablets were separated from the background (Fig. 15: 1) by PCA (224). A hard threshold was set in the first PC-1 scores followed by circular erosion using a circular morphological structuring element with 3 pixels in the radius to remove the edge from the tablet (273).

2.4.3.2 Estimation of the tablet API content

In order to determine the spectral profile of tablets with different amylase contents, mean UV absorbance spectra were calculated from all tablet pixels of the two images for each tablet (Fig. 15: 2a). To eliminate a spectral baseline shift between tablets with different amylase content, the mean spectra of all tablets were centered using the following equation:

$$X = x - a \quad (\text{Eq. 14})$$

where X is the baseline corrected matrix of size $I \times J$, with spectra arranged along the first dimension (I spectra) and wavelengths on the second dimension (J wavelengths), x is a vector of size $1 \times J$ with absorbance values on its elements, and a is the average

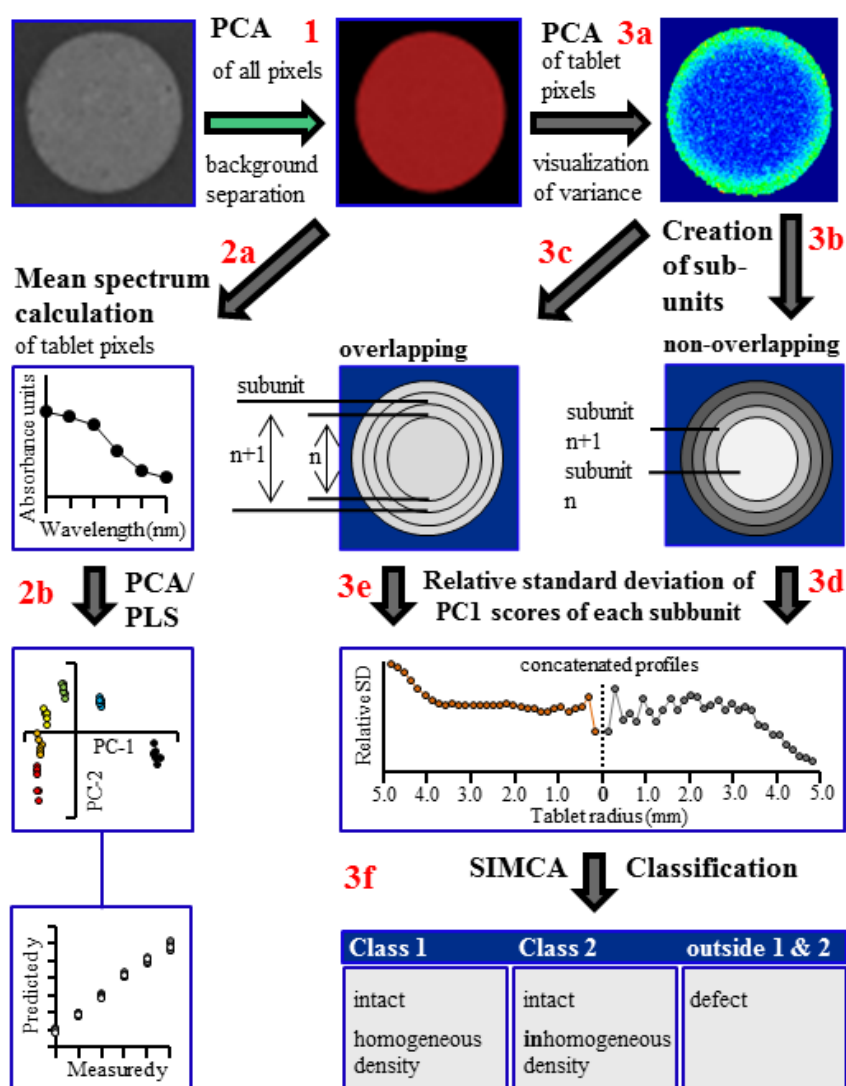


Fig. 15: Imaging data analysis pathway for evaluation of tablet API content, hardness, intactness, and surface density profile.

value of x , respectively. Such a baseline shift may be caused by physical differences between the tablet surfaces due to a different compaction behavior of the powder blends with varying amylase contents fractions (222). PCA and PLS analysis was applied to the mean-centered dataset (Fig. 15: 2b) using the Unscrambler X software.

2.4.3.3 Evaluation of tablet hardness

To evaluate hardness of trypsin formulation tablets from UV images, the UV spectra of all pixels of a respective tablet were averaged to obtain one mean absorbance spectrum for each tablet (Fig. 15: 2a). The mean-centered dataset was further analyzed by PCA and PLS Regression (Fig. 15: 2b).

2.4.3.4 Evaluation of tablet intactness and surface density profile

To evaluate the intactness and the surface density profile of each tablet, the spectral variance throughout the respective compacts (Table 3) was determined by application of an additional local PCA on the segmented pixels belonging to the respective tablet (Fig. 15: 3a). For examination of tablet intactness, the resulting score images were divided into non-overlapping concentric subunits (Fig. 15: 3b). Subsequently, the within-subunit variation was determined by calculating the relative standard deviation (rSD) of the score intensities for each subunit (Fig. 15: 3d). For determination of the surface density profile of the tablets, again subdivision of the PC-1 scores images was performed but with the concentric subunits overlapping in this case (Fig. 15: 3c and e). The data analysis procedure was established with an in-house written Matlab script and is described in detail in the results chapter.

2.4.4 Pattern recognition

SIMCA was applied to the rSD profiles of 43 tablets (Table 3) to systematically classify the tablets according to their intactness and surface density profile (Fig. 15: 3f). Therefore, two different tablet classes were constructed: intact tablets with a rather homogeneous surface density distribution (class 1) and intact tablets with inhomogeneous surface density distribution (class 2). To model the common variance between the rSD profiles within the classes, the profiles from the two approaches of non-overlapping and overlapping concentric subunits were calculated for a large and representative number of tablets known to be member of the respective class (refer to section 2.4.1), i.e. compacted at an either low or high pressure (reference data set; class 1: n=19, class 2: n=12). Subsequently, the resulting rSD profiles of the two approaches for each tablet were truncated for the first (central) subunit and concatenated, followed by application of PCA (mean centered data) on the smoothed (moving average: segment size 3) and mean normalized dataset of each class. To evaluate the classification power of the model, an external prediction set (test set) of tablets with known assignments to the two classes (Table 3; n=12) was subjected to the model. Two PCs were used in each sub-PCA and chosen based on the RMSECV as a function of the PCs. The calculation of the probability of a tablet belonging to a respective sub-PCA model class was based on examination of its Q and T² with regard to the respective sub-PCA model. A strict threshold probability of 0.5 was set for associating the samples with the different classes.

2.4.5 Radial tensile strength of the tablets

Immediately after recording UV images of the trypsin formulation tablets, their diameter, thickness, and crushing strength were determined using an Erweka TBH525 hardness tester (Erweka, Heusenstamm, Germany). As the crushing strength parameter is characteristic for tablet hardness but depends on the dimensions of the tablets, the RTS of each tablet was calculated as dimension-independent hardness parameter. For flat-faced tablets, the RTS is calculated using the following equation (274):

$$\sigma = \frac{2 \cdot F}{\pi \cdot d \cdot t} \quad (\text{Eq. 15})$$

where σ is the tablet tensile strength (MPa), F the crushing strength (N), d the tablet diameter (mm), and t the tablet thickness (mm).

2.5 Specific methods of ‘Non-destructive quality control of tablets and blister packs by UV imaging’⁶

2.5.1 Sample preparation

Various blister packs with the cavities being all empty, partly filled, or all filled with either tablets ‘B’ or tablets ‘D’, as well as blisters that contain both types of tablets in separate cavities were manually prepared and sealed with one of the three blister sealing foils using a stapler.

To obtain bulk tablets with an either intact or defect imprint, tablets ‘A’ were removed from their blister pack and partly damaged with a needle. Tablets ‘C’ were stored at accelerated conditions (40°C/75% RH) for three months and were selected manually with respect to visible cracks.

2.5.2 Photographic imaging

Pictures of tablets ‘A’ and ‘C’ which were previously analyzed by UV imaging were acquired for reference purposes using the Canon EOS 600D single lens reflex camera.

2.5.3 Image analysis and related statistics

2.5.3.1 General aspects

Prior to processing of the multivariate image data, again the UV images were transformed from reflectance (R) into absorbance units (A) using Eq. 13.

⁶This chapter has been published as shown on page 199 in appendix B.

2.5.3.2 Characterization of blister packs

2.5.3.2.1 General aspects

For characterization of blister packs, the pixels belonging to the tablets therein were separated from the background by setting a hard threshold in the sixth wavelength (365 nm) image. To remove the edge from the tablet, circular erosion was applied to the tablet pixels using a circular morphological structuring element with three pixels in the radius (273). To eliminate spectral differences that are solely caused by differences in the tablet surface textures such as a baseline shift (191, 222), SNV correction (Eq. 4) (237) was applied to the spectra of the tablet pixels. Subsequently, mean UV spectra of 1500 pixels were calculated per tablet.

2.5.3.2.2 Pattern recognition

In the present study, PCA-based SIMCA analysis (Unscrambler X software) was applied to the mean spectra of tablets within blister packs to classify the blister packs based on the composition of the tablets therein as well as the used polymer sealing foils. As shown in Table 4, eight different model classes were defined. PCA was applied to the tablet mean spectra ($n=6$) of each class separately to model the common spectral variance between the respective samples of a class. The performance of the classification model was assessed by subjection of the spectra of another 16 tablets (test set) with known class assignments to the eight PCA models of the different classes.

Assignment of the test tablets to the different classes was based on the calculation of the sample to model distances by taking into account the residual variance and

leverage of each sample with respect to the different PCA models.

Table 4: SIMCA classification model.

Class	1	2	3	4	5	6	7	8
Tablets	Tablets 'B'				Tablets 'D'			
Sealing foil	unsealed	PCTFE/ PVC	PVC PH 132	PVC PH 154	unsealed	PCTFE/ PVC	PVC PH 132	PVC PH 154
Number of PCs included in the PCA model	2	1	2	2	2	2	2	2

2.5.3.3 Evaluation of imprint intactness

For the investigation of imprint intactness, PCA was applied to the UV images of beveled edge tablets 'A'. It was expected that the reflectance of the UV light would be markedly changed at the imprinted codes accompanied by spectral changes resulting from a varying surface texture at the characters compared to the smooth regions of the tablet. However, the reflectance of the UV light was also assumed to be markedly altered at the edges of the tablets due to their skew shape causing a different scattering of the UV light. Thus, first of all, the pixels belonging to the tablets were separated from the background by performing PCA on all pixels of each image followed by setting a hard threshold in the PC-1 scores (224). Subsequently, circular erosion of the tablet pixels was performed using a circular morphological structuring element with 20 pixels in the radius (273) to assign pixels of the tablet edge to the background. To visualize the spectral variance throughout the remaining tablet surface, another PCA was applied to the respective pixels of each tablet. The resulting PC-1 scores images were median filtered using a window size of 3x3 pixels to better visualize the tablet surface texture.

2.5.3.4 Detection of cracks

To detect cracks on the surface of tablets 'C', again tablet pixels were separated from the background by PCA followed by erosion of the tablet edge (circular morphological structuring element: shape disk, five pixels in the radius) and application of global PCA to the remaining pixels of the tablets.

2.6 Specific methods of ‘Rapid assessment of tablet film coating quality by multispectral UV imaging’⁷

2.6.1 Preparation of tablets

Tablet compaction was performed on the rotary tablet press equipped with faceted punches of 8 mm diameter. ASA tablets (50.0 % (w/w) ASA, 40.5 % (w/w) MCC, 8.0 % (w/w) starch, 0.5 % (w/w) silicon dioxide, and 1.0 % (w/w) MgSt) with a weight of approximately 250 mg were obtained at main compaction pressures of about 200 MPa and a rotor speed of 20 rpm.

2.6.2 Pan coating

ASA tablets were film coated with a mixture of Kollicoat® IR (blue and yellow, resulting in a green color) using a pan coater (Solidlab 1, Bosch, Schopfheim, Germany) equipped with a nozzle of 1.2 mm diameter. During the coating process the product temperature range was 32 – 46 °C, the air flow rate was varied between 53 and 61 m³ h⁻¹, and the atomizing air pressure and fluid spray rate were set to 0.67 bar and 1.0 g min⁻¹, respectively. Under these intentionally non-ideal process conditions, tablets with intact coating layer that show an either homogeneous or inhomogeneous surface texture, as well as tablets with a defect coating layer (chipped parts or inhomogeneous appearance) were obtained. A small fraction of coated ASA tablets were manually processed with a scalpel to obtain tablets with cracks in the coating layer. Uncoated tablets were prepared by gently scraping of the coating layer.

⁷This chapter has been published as shown on page 199 in appendix B.

2.6.3 Photographic imaging

Photographs of representative ASA tablets which were previously analyzed by UV imaging were captured for reference purposes using the Canon EOS 600D single lens reflex camera.

2.6.4 Photometric stereo

Images of coated ASA tablets with either visually homogeneous or inhomogeneous coating were acquired using a Videometer MultiRay imager (Videometer, Hørsholm, Denmark) combined with the VideometerLab software (ver. 2.8, Videometer, Hørsholm, Denmark) to verify the surface texture analyzed by UV imaging. The instrument consists of a combined darkfield and coaxial brightfield illumination source which illuminates the sample at different angles. As wavelength 465 nm was selected, a silicon range imaging detector was used to collect the reflected light. The obtained images were of size 1280 x 960 pixels with a pixel size of 7.7 μm .

2.6.5 Image Analysis and related statistics

2.6.5.1 General aspects

In-house written Matlab scripts were applied to the images to evaluate intactness as well as the surface texture of coated ASA tablets.

2.6.5.2 Evaluation of tablet coating layer intactness

To evaluate tablet coating layer intactness, ten reference tablets that are either uncoated or homogeneously coated as well as six test tablets that were uncoated or with a homogeneous, inhomogeneous, chipped, or cracked coating were analyzed. Prior to multivariate analysis the UV images were transformed from reflectance (R) to absorbance (A) using Eq. 13. Subsequently, tablet pixels were separated from the background by detection of the circular tablet structures in the 365 nm UV images by Hough transformation (275). After erosion with a circle morphological structuring element with either three pixels (reference tablets) or one pixel (test tablets) in the radius, all remaining pixels within the circles were assigned to the respective tablet (273).

The UV spectra of all pixels of the ten reference tablets which are either uncoated or homogeneously coated were used as an uncoated ASA tablets reference dataset and coating reference dataset, respectively. Global PCA (Table 5: PCA model 1) was applied to both reference datasets to visualize the spectral variance within and between both groups of tablets (Table 5).

Table 5: PCA models applied to the UV images for detection, differentiation, and localization of coating defects. Prior to PCA all spectral datasets were mean-centered.

PCA model		1	2	3
Dataset		All pixels of five uncoated and five intactly coated tablets.	<i>Uncoated ASA tablets reference dataset:</i> all pixels of five uncoated tablets	<i>Coating layer reference dataset:</i> all pixels of five intactly coated tablets
Purpose		Visualization of the spectral variance between uncoated and intactly coated tablets as well as between the respective pixels of tablets with different coating defects	Model for PCA-based SIMCA classification	Model for PCA-based SIMCA classification
Related figure(s)		Fig. 31: b and c; Fig. 32: column III and IV	Fig. 32: column V	Fig. 32: column V
SIMCA	Used for SIMCA	no	yes	yes
	Model class	---	1	2
	Number of PCs included in the model	---	2	1
	Specificity	---	1.0	1.0
	Sensitivity	---	1.0	1.0

To assign all pixels of the six test tablets to either the tablet coating or the uncoated ASA formulation based on their UV spectra, a SIMCA classification model was established based on the following two PCA models (Table 5): one PCA model was applied to the mean centered UV spectra of the uncoated ASA tablet reference dataset (PCA model 2) and another to the mean centered UV spectra of the coating layer reference dataset (PCA model 3). Pixels were assigned to the class to which they were closest considering T^2 and Q combined.

2.6.5.3 Evaluation of tablet coating texture

To distinguish tablets according to their coating texture by UV imaging, intact tablets that showed an either homogeneous (n=8) or an inhomogeneous (n=8) coating in the photographic images were analyzed as follows: in a first step, PCA based background segmentation was applied (224). In the second step, pixels belonging to the facet of the tablets were assigned to the background by circular erosion of the tablet pixels using a circle morphological structuring element with 20 pixels in the radius (273).

From the segmented image, a global PCA was applied to all remaining pixels of the flat region of the 16 investigated tablets to monitor the spectral variance between them. For each tablet, the average score variation (Xa , Eq. 16) was calculated from the respective PC-1 scores as parametric estimator for coating surface texture by modification of the equation for calculation of the average roughness (276) as follows:

$$Xa = \sum_{n=1}^N \frac{|Z_n - \bar{Z}|}{N} \quad (\text{Eq. 16})$$

where Z_n is the individual PC-1 score intensity of each tablet pixel, \bar{Z} is the mean PC-1 score intensity of all pixels of five coated tablets which were considered to show a homogeneous smooth coating (reference set), and N is the total number of pixels of a respective tablet. The way of calculation of \bar{Z} was based on the mean PC-1 score intensity of five homogeneously coated reference tablets instead of that of the respective tablet, because tablets that are widely differing in surface texture could exhibit similar variation values if the scores intensities spread comparably around the arithmetic average of the respective tablet (277). Thus, by calculating the average

distance of the PC-1 scores intensities of the test tablets (Z_n) from the mean score intensity of the reference set (\bar{Z}), solely those test tablets whose score intensities scatter around \bar{Z} show a Xa value comparable to the homogeneously coated reference tablets indicating a surface texture visually considered to be acceptable.

The mean Xa values of the five homogeneously coated reference tablets was calculated and set as 100 %. The Xa values of the remaining 11 tablets (test set) with a visually either homogeneous ($n=3$) or inhomogeneous ($n=8$) coating were calculated as percentage of the mean Xa value of the reference set. The data analysis procedures are explained in detail in the results and discussion section.

3 Results and Discussion

3.1 Results and discussion of 'Influence of tableting on the conformation and thermal stability of trypsin as a model protein'⁸

3.1.1 Influence of tableting on trypsin bioactivity

Pressure-sensitivity of trypsin was evaluated by determination of its enzymatic activity loss dependent on the applied compaction pressure using the USP photometric reference method after tablet reconstitution. Activity of trypsin was shown to be reduced even if the protein was tableted at low pressure (about 1 % decrease in activity at 40 MPa) and further decreased as the compaction pressure increased (Fig. 16a). However, above 190 MPa there is an apparent plateau at an activity loss of about 7 %. It is well-known from previous studies that compaction can successively reduce the activity of proteins, although marked differences were found in the pressure-sensitivity of various proteins (84, 92–94). The observed activity decrease of about 7 % (Fig. 16a) at a pressure of 382 MPa for bovine trypsin is markedly lower compared to the activity loss of about 16 % which has been reported for porcine trypsin by Otsuka and coworkers (84). Thus, the presented data demonstrate the pressure-driven formation of less active species of bovine trypsin and indicate a marked discrepancy of the susceptibility of proteins of similar biological function but different origin towards denaturation.

⁸This chapter has been published as shown on page 199 in appendix B.

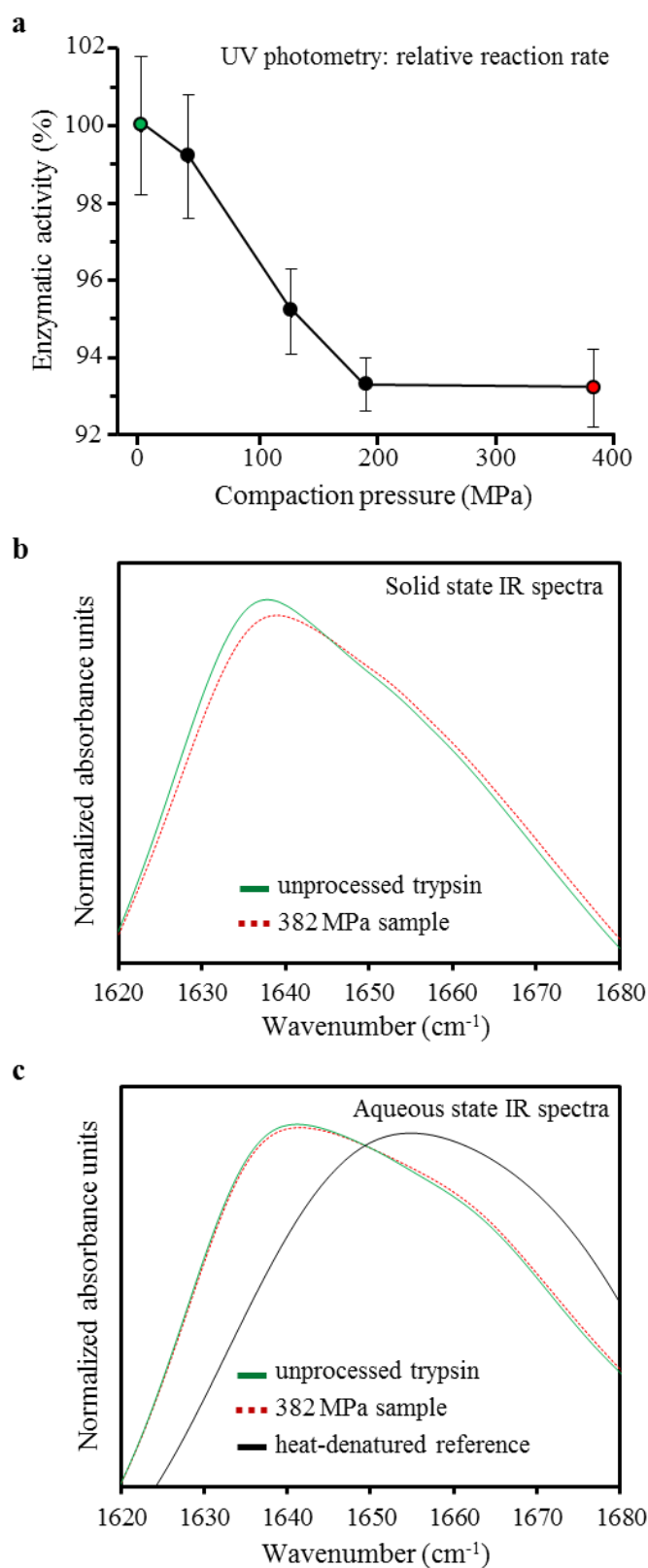


Fig. 16: (a) Enzymatic activity of trypsin as a function of the applied compaction pressure during tableting. Results are calculated as means \pm SD ($n \geq 3$). (b) Solid state and (c) Aqueous state amide I spectra of trypsin. Only representative spectra of unprocessed and 382 MPa samples are shown.

3.1.2 Influence of tableting on the conformation of trypsin

3.1.2.1 Structural characterization by FTIR spectroscopy

To investigate if the changes in enzymatic activity of trypsin that were determined by the USP assay are accompanied by structural alterations, infrared spectra of unprocessed and compacted powder samples were recorded using an ATR device. In Fig. 16b representative amide I spectra of unprocessed and compacted samples are shown. The spectra reveal an increasing spectral change at an increased compaction pressure with a decrease in intensity in the range between 1620 and 1645 cm^{-1} and an increase in intensity in the range between 1645 and 1680 cm^{-1} . Although the minor extent of the observed changes reveal that even compacted trypsin exhibited a predominantly native-like secondary structure, these spectral alterations may be explained by denaturation of β -sheets in favor of other secondary structures (random coil, α -helix, β -turns) to a small extent upon tableting. The exact nature of the alterations should be further investigated using complementary analytical techniques (165). In this context, Otsuka et al. found a correlation between the extent of spectral changes in the solid state and the enzymatic activity in solution (84). However, it is uncertain whether the conformational changes observed in the solid state are partially reversible upon reconstitution, as substrate bonding at the active side of the enzyme can already be hampered by minor structural changes that may remain upon reconstitution and thus accompany a reduced activity. Therefore, to determine the fraction of irreversible structural changes that occurred upon tableting, aqueous state FTIR spectroscopy of the samples was performed after solid state FTIR analysis.

The aqueous state amide I spectra of the samples reveal that there are still spectral differences between unprocessed and compacted trypsin after reconstitution (Fig. 16c). The spectrum of the processed trypsin is very similar to that of the unprocessed trypsin, and very different from that of a heat-denatured sample. However, it is possible that only a small fraction of the protein forms aggregates upon compacting. Therefore, the potential presence of soluble aggregates was determined by size-exclusion chromatography (SEC). However, a comparison between unprocessed and compacted trypsin samples did not reveal peaks from species of higher molecular weight and the total peak areas of the chromatograms were not significantly different (data not shown). Thus, the relatively small spectral changes observed as a result of compaction suggest that minor structural changes occur (Fig. 16c). Pressure as well as thermal denaturation resulted in similar spectral trends of decreasing intensity at 1620-1645 cm^{-1} and increasing intensity at 1660-1680 cm^{-1} , which may be related to decreasing β -sheet structures and concomitantly increasing random coil contents (see below). Thus, the reduced β -sheet content of compacted samples, which was indicated by solid state FTIR analysis, was confirmed to (partially) persist after reconstitution (Fig. 16: b and c). However, the spectral changes in the aqueous are apparently even smaller than those in the solid state.

3.1.2.2 Quantification of the reversibility of pressure-induced conformational changes of trypsin

Solid and aqueous state spectral datasets of unprocessed and compacted trypsin revealed that pressure during tableting induces minor conformational changes and that these are partially reversible after reconstitution of the tablets. However, to make a clear statement regarding the partial reversibility of unfolding, the spectral differences between unprocessed and compacted samples in the solid state as well as in the aqueous state were quantified. For this purpose, the %ao approach (271) was applied to the normalized amide I spectra. An area overlap is displayed in Fig. 17 using a representative spectrum of compacted trypsin and the mean spectrum of unprocessed trypsin ($n=3$).

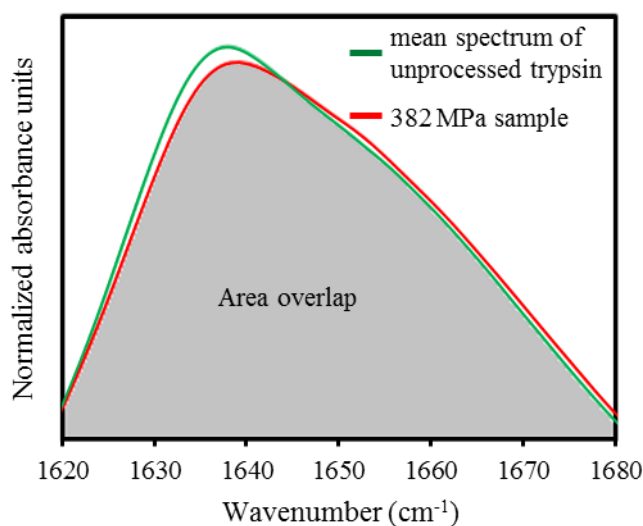


Fig. 17: The area overlap approach applied to a representative compacted trypsin sample and the mean spectrum of unprocessed trypsin ($n=3$). The gray area corresponds to the area overlap of the two solid state spectra.

As shown in Table 6, the %ao of the solid state spectra of unprocessed and compacted trypsin slightly decreases as compaction pressure increases (99.72 ± 0.11 % at 0 MPa vs. 99.09 ± 0.13 % at 382 MPa, $p < 0.01$). Upon reconstitution of the tablets, the differences between the spectra of compacted trypsin and the mean spectrum of the native enzyme were still found to be statistically significant (99.92 ± 0.04 % at 0 MPa vs. 99.61 ± 0.02 % at 382 MPa, $p < 0.01$), but these differences are even smaller than those in the solid state (e.g. 99.61 % vs. 99.09 % at 382 MPa).

Table 6: Area overlap (%) of normalized amide I spectra dependent on the applied compaction pressure. The area overlap is calculated in relation to a mean spectrum of unprocessed trypsin in the solid state and in the aqueous state, respectively. Results are calculated as means \pm SD (n=3).

	0 MPa	190 MPa	382 MPa
Solid state	99.72 ± 0.11	99.38 ± 0.14	99.09 ± 0.13
Aqueous state	99.92 ± 0.04	99.64 ± 0.03	99.61 ± 0.02

Thus, these results demonstrate that the applied pressures during tableting lead to denatured species that are able to partially recover to the native structure upon reconstitution. As shown before, the compaction pressure beyond 190 MPa did not lead to a further decrease in activity (previous section) and to only minor further irreversible structural changes. Consequently, the observed differences in the area overlap between the 190 MPa as well as 382 MPa samples and unprocessed trypsin in the solid state indicate that these observed structural alterations did not contribute to a reduction of the enzymatic activity.

3.1.2.3 Principal Component Analysis of the aqueous state spectral dataset

To gain a more precise insight into the unfolding mechanism of trypsin during tableting, PCA was applied to the aqueous state spectral dataset. PCA is a valuable technique to visualize differences in the extent of conformational changes of proteins and thus facilitates the monitoring of pressure-dependent denaturation (167, 245).

It is obvious from Fig. 18a that PC-1 have the largest negative and positive loading values in the spectral ranges 1620-1645 cm^{-1} and 1660-1680 cm^{-1} , respectively. Thus, the samples are mainly distinguished by PC-1 based on spectral differences between them in these spectral regions. As the PC-1 loadings between 1620 and 1645 cm^{-1} are negative, sample that show a high absorption in that region are found in the negative part of the PCA scores plot, while those showing a comparably lower absorption in the range 1620-1645 cm^{-1} and a higher absorption between 1660 and 1680 cm^{-1} are found in the positive part of PC-1. As discussed above (Fig. 16: b and c), with increasing compaction pressure the peaks that are characteristic for β -sheet structures (1620-1645 cm^{-1}) successively decrease in intensity, while those related to other structures (1660-1680 cm^{-1}) successively increase. Thus, PC-1 captures these spectral changes resulting from secondary structural changes induced by compaction. In agreement, the PC-1 loadings matches with the difference spectra of unprocessed trypsin with a compacted sample as well as with that of a heat-denatured reference, respectively.

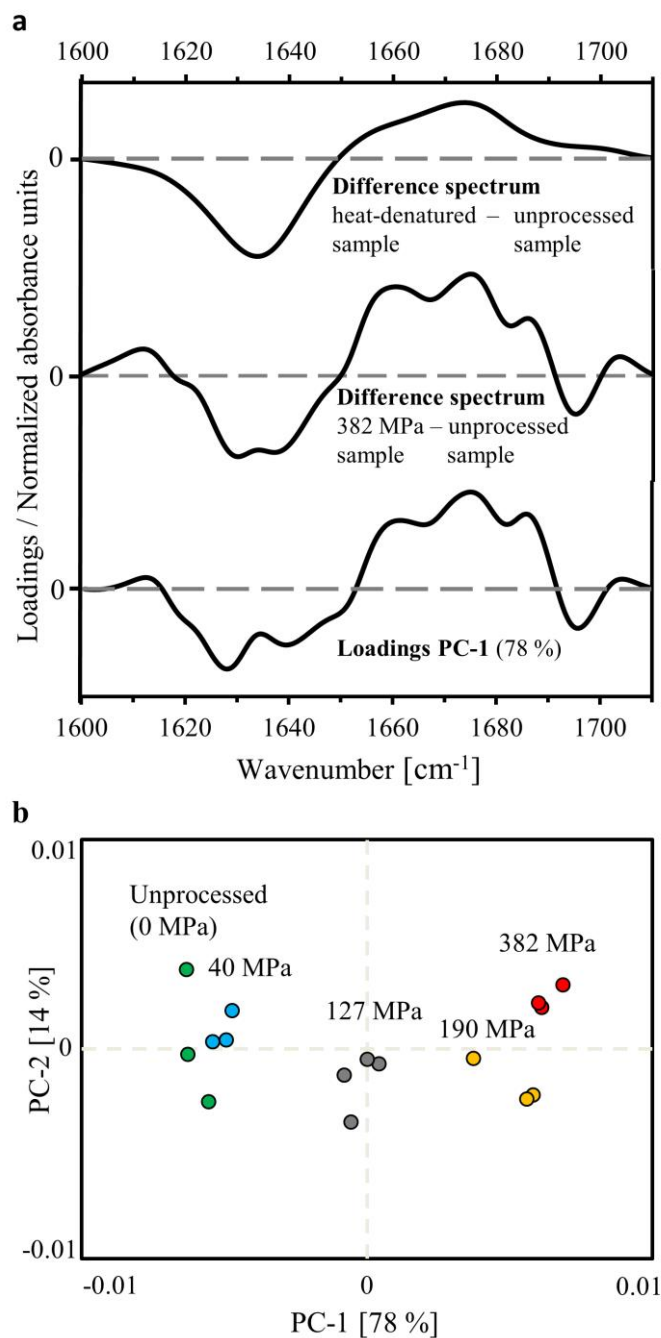


Fig. 18: (a) From top to bottom: difference spectrum of amide I spectra of a heat-denatured sample and unprocessed trypsin; difference spectrum of a sample compacted at 382 MPa and unprocessed trypsin; PCA loadings plot of PC-1. (b) PCA scores plot for trypsin secondary structure changes during tableting.

Consequently, the PCA scores plot illustrates that samples prepared at different compaction pressures are clearly distinguished by PC-1, which explains 78 % of the spectral variance (Fig. 18b). Samples with similar spectroscopic features generally form clusters in the scores plot. With increasing compaction pressure the sample scores move from the cluster of the unprocessed samples in the negative part of PC-1 to the positive part. Furthermore, the scores plot indicates an impact of the compaction pressure on the conformation of trypsin from 40 MPa up to 382 MPa. Pressures exceeding 190 MPa only lead to minor spectral changes as the samples compacted at 382 MPa form a cluster close to the 190 MPa samples. The observed tendency of progressing irreversible spectral changes upon tableting at increasing compaction pressures was therefore in good agreement with the loss of enzymatic activity determined by the USP reference method. The pressure-driven transformation of β -sheet structures might be related to unbound water that remains in the tablet upon pressurization and is thus available for enabling mobility of the protein structure.

3.1.2.4 Partial Least Squares Regression of the aqueous state spectral dataset

It is obvious from the PCA results that the reduced enzymatic activity of trypsin induced upon tableting is associated with a minor conformational change. Because a part of the pressure-induced structural perturbations was shown to be reversible upon dissolution, it is hypothesized that the extent of irreversible changes is correlated to the loss of trypsin activity. To test this hypothesis, aqueous state FTIR spectroscopy in combination with a multivariate calibration model was evaluated in terms of its suitability to predict the functionality of proteins and thus to simplify the

determination of the protein activity compared to time-consuming wet assays.

A PLS calibration model was established using the aqueous state spectral dataset as a predictor for the activity of trypsin which was determined by the photometric assay. Three LVs were used to build the model. As shown in Fig. 19, a clear correlation between the FTIR spectra and the enzymatic activity could be confirmed.

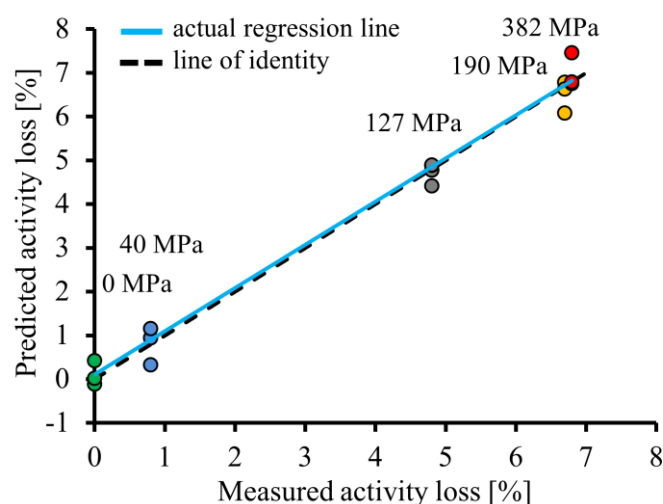


Fig. 19: PLS Regression plot (R^2 of calibration: 0.988, slope: 0.988, RMSECV: 0.47 %) of predicted activity according to the aqueous state FTIR spectral dataset (predicted activity loss) vs. activity loss according to the USP photometric reference method (measured activity loss).

A RMSECV of 0.47 % reveals that PLS Regression applied to the aqueous state spectral dataset is a valuable tool for accurate determination of changes in the enzymatic activity even if these changes are accompanied by only minor perturbances in the three-dimensional structure of the enzymes. However, the present PLS Regression model has been established based on the infrared spectral dataset and enzymatic activity values of only a single protein, trypsin. Thus, this

model is limited to this particular protein. The correlation between infrared spectral changes and the biological functionality of the respective biomolecule has to be determined individually for each investigated protein or biotherapeutic. Nevertheless, the present results clearly show the potential of liquid state infrared spectroscopy in combination with PLS Regression for estimation of the integrity of biomolecules.

3.1.3 Influence of tableting on the transition temperature of unfolding and folding reversibilities of trypsin

Spectroscopic and thermodynamic protein characterization is crucial for understanding protein product quality and stability. If stress-induced denaturation has occurred during the life-cycle of proteins due to a change of the environmental conditions, the proteins must be able to subsequently regain their native three-dimensional structure to guarantee the desired biological activity. In addition to the spectroscopic characterization of compaction effects on protein structure, the effects on the T_m of unfolding and folding reversibility were assessed. For this purpose, liquid state DSC was performed.

The thermograms of unprocessed trypsin as well as those of samples compacted at an either low (40 MPa) or high (382 MPa) compaction pressure show two endothermic transitions at about 56 °C (main transition peak) and 65 °C (secondary transition peak), respectively (Fig. 20). According to previous reports, at pH 2.8 - 3.0 and a protein concentration of 1-3 mg/ml, thermal denaturation of unprocessed trypsin manifests itself in a two-state transition between the native and denatured state, resulting in a single-peak thermogram with a T_m of about 54 °C (278, 279). Thus, the main transition peak at about 56 °C (peak 1, Fig. 20) can be assigned to thermally induced unfolding of native trypsin molecules and served for determination of the T_m dependent on the compaction pressure. The transition at higher temperature (peak 2, Fig. 20) may be related to the lower molecular weight species of trypsin observed in SEC. Unprocessed powder showed a T_m of 55.7 ± 0.2 °C compared to 55.5 ± 0.1 °C for 40 MPa samples and 55.6 ± 0.2 °C for 382 MPa samples (Table 7).

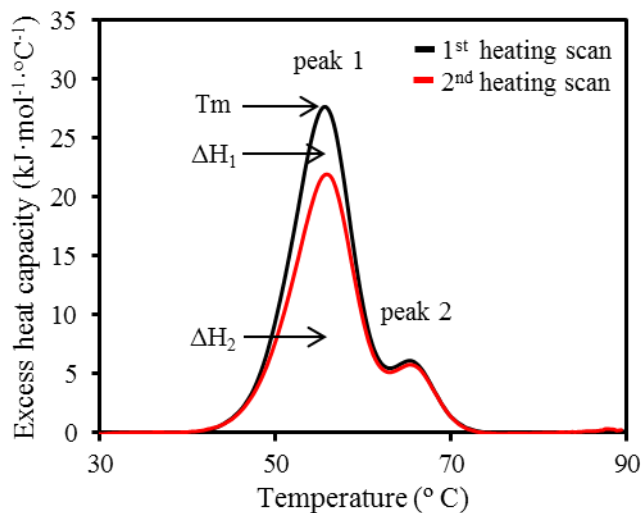


Fig. 20: Representative example of consecutive calorimetric heating scans for unprocessed trypsin. Thermograms were recorded at a heating rate of 1 K/min and subsequently concentration normalized. ΔH : calorimetric enthalpy; T_m : transition temperature of unfolding.

Table 7: Transition temperature (T_m) of unfolding and folding reversibility after thermal denaturation of trypsin samples in dependence of the applied compaction pressure. Results are calculated as means \pm SD ($n=3$).

	0 MPa	40 MPa	382 MPa
T_m (°C)	55.7 ± 0.2	55.5 ± 0.1	55.6 ± 0.2
Folding Reversibility (%)	84.8 ± 2.4	82.0 – 87.0*	77.2 ± 1.8

*range of two samples

Thus, the results showed that tableting did not significantly alter the T_m of trypsin. To determine the influence of compaction on the folding reversibility of all trypsin species after thermal denaturation, two consecutive heating scans were performed for each of the unprocessed and processed samples (Fig. 20). The thermograms reveal that the enthalpy change in the second heating scan of all samples decreased compared to the first heating scan. This reduction in the enthalpy is more pronounced at the main transition peak than at the secondary transition peak. These results indicate that thermally induced denaturation of all trypsin samples is partially irreversible, because non-native protein molecules require less enthalpy to denature during the second heating cycle dependent on the extent of ordered secondary structure (82). Unprocessed trypsin showed a folding reversibility of $84.8 \pm 2.4 \%$ calculated from the ratio of the areas under the two transition peaks (Fig. 20) of the second heating scan over that of the first heating scan. Compaction of trypsin at increasing pressures was associated with a decreasing ability to refold after denaturation (Table 7). Samples compacted at a pressure of 382 MPa showed a significantly ($p < 0.05$, $n=3$) lower folding reversibility after denaturation compared to unprocessed trypsin. Thus, structural perturbances that are induced during tableting are accompanied by a lower folding reversibility of trypsin.

3.1.4 Conclusion

Tableting was shown to induce transformation of native trypsin to misfolded species. The protein exhibits a slightly altered conformation in the solid state dependent on the applied compaction pressure but is able to partially refold upon reconstitution. After reconstitution of the trypsin tablets in water, the protein exhibits reduced functionality but a near-native secondary structure. Aqueous state infrared spectroscopy in combination with chemometrics was found to be a powerful tool to follow these pressure-dependent structural changes and to determine the extent of their reversibility. Application of PLS on the aqueous state spectral dataset allows accurate evaluation of the protein's activity in a minimum of time and thus simplifies time-consuming activity determinations.

Besides the impact of tableting on the conformation of trypsin, tableting also reduces the folding reversibility of trypsin after thermal unfolding. In contrast, no significant changes in the transition temperature of unfolding were detected as a result of the applied compaction pressure.

In conclusion, this study reveals that tableting can have a negative impact on the quality of protein APIs because stress applied during compaction may irreversibly alter the conformation as well as the stability of the proteins during further handling and administration. However, in the present study the influence of compaction on the conformation and thermal stability has been only investigated for one model protein, trypsin. According to the literature, there is a marked variation in the sensitivity of different biomolecules in terms of denaturation upon tableting. In turn, there may also be a marked difference in the influence of the compaction pressure on the

thermal stability of biomolecules after reconstitution of the tablets, which has to be investigated in further studies on an individual base for such biomolecules which have the potential to be formulated as tablets.

3.2 Results and discussion of 'UV Imaging for fast and non-destructive quality control of chemical and physical tablet attributes'⁹

3.2.1 Estimation of the tablet API content

An important chemical tablet attribute that is routinely determined to ensure product quality is the content of the API within the tablets. For quality control during manufacturing, tablet specifications have to be determined with high accuracy within a minimum of time. To investigate if UV imaging is a suitable technique to estimate the tablet API content, UV images of the upper and lower surfaces of tablets consisting of different fractions of amylase were analyzed (see methods section). UV imaging was shown to be a fast analyzing technique, as it allows to obtain an image of dimension 11.7 cm × 8.8 cm, which covers multiple tablets with a spatial resolution of 77 μm within about 18 s. As shown in Fig. 21a, tablets with varying amylase contents show distinct mean UV spectra that were calculated from all pixels of a respective tablet. With increasing amylase content there is an increase in the spectral slope caused by a markedly higher UV absorption of amylase in the region of 254 to 300 nm compared to MCC. This can be explained by the chemical structure of amylase, as amino acids such as tryptophan and tyrosine exhibit chromophores leading to a high UV absorbance at these lower wavelengths. In contrast, MCC shows a featureless UV spectrum due to the lack of distinct chromophores, which confirms the findings by Wu et al. (218). In order to investigate whether the variations observed in Fig. 21a can be separated in a multivariate space, PCA was applied to the mean spectra of the images of all tablets. The resulting PCA loadings plots from PC-1 and PC-2 (Fig. 21b) reveal that the first component explains the differences in the spectral slope caused by the varying amylase contents of the tablets. According to the loadings,

⁹This chapter has been published as shown on page 199 in appendix B.

PC-2 describes the unexplained systematic variation that remains after PC-1, which mainly manifests itself at 254, 300 and 313 nm.

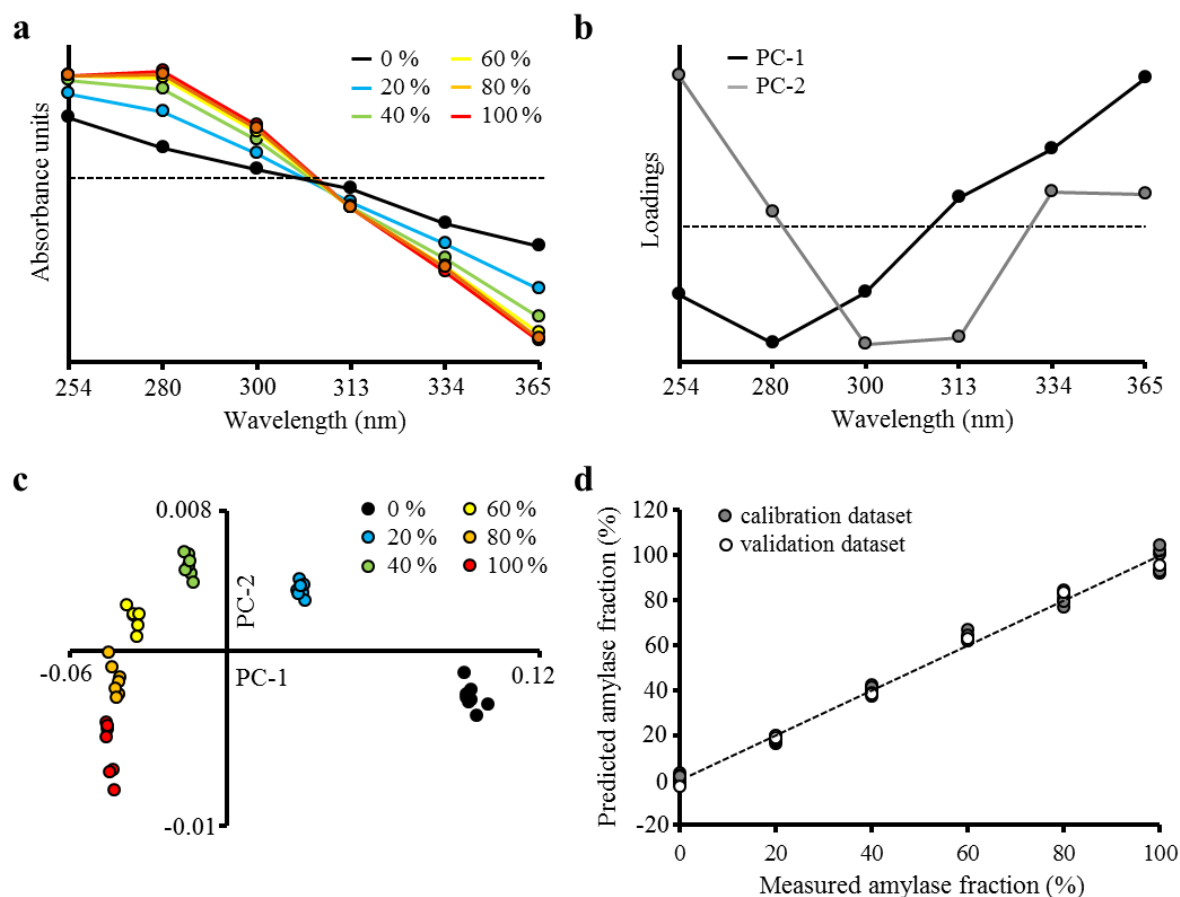


Fig. 21: (a) Representative mean UV absorbance spectra of tablets with different amylase contents (b) PCA loadings plots (c) PCA scatter plot for tablets with different amylase contents (d) PLS Regression plot (R^2 of calibration: 0.991, slope: 0.991) of the predicted amylase content of the tablets based on the mean UV absorbance spectra as a function of the tablet amylase content (RMSEP: 3.1 %).

The PCA scores plot is presented in Fig. 21c and illustrates that tablets with different amylase content are clearly differentiated by the first and the second PC (PC-1: 99.4 %; PC-2: 0.5 %) and form separated clusters in the plot. With increasing amylase content the sample scores move from the positive to the negative part of PC-1. To investigate if the spectral information of the UV images systematically

correlates with the true amylase content in the tablets, a PLS calibration model was established. As mentioned above, PLS Regression is a commonly used linear calibration model for regression of spectral imaging data (280). The model was built based on the mean spectra of 37 tablets (Table 3) that were used as predictors for the amylase content of the respective tablets. The resulting least-squares fit calibration curve (Fig. 21d, black dots) indicates a clear linear relation (2 LVs, slope: 0.991, R^2 : 0.991) between the amylase content that was predicted from the tablet images and that present in the respective tablets. This observation is in agreement with a previous study, where NIR spectral imaging was used for determination of the API content in tablets (190). Validation of the PLS model was performed by subjecting the mean spectra of another six amylase tablets that were randomly chosen from the tablet types with different amylase contents to the regression model (Fig. 21d: white dots). A root mean square error of prediction (RMSEP) of 3.1 % reveals that the content of amylase in the tablets could be estimated based on the spectral information obtained from the UV images. Thus, multispectral UV imaging combined with PLS Regression is a useful technique for non-destructive and fast control of the API content in tablets.

3.2.2 Estimation of the radial tensile strength of tablets

Tablet hardness is an important physical quality attribute because it influences product performance during further processing or handling (16). To investigate if multispectral UV imaging can be used as a surrogate method for tablet hardness, trypsin formulation tablets that were compacted at various compaction pressures and thus exhibit a wide range of RTS values (0.2 - 5.8 MPa) were analyzed. The calculated mean UV spectra of five representative trypsin tablets of identical composition but with different RTS reveal that there are no significant differences in the shape of the spectra (Fig. 22a). However, a significant shift in the baseline of the spectra occurs with increasing RTS of the tablets. According to the literature, this baseline shift can result from differences in the powder porosity of the tablet surface giving rise to variations in scattering phenomena (107, 129).

To examine if a systematic variation exists in the UV images of the tablets with different RTS, PCA was applied to the mean spectra of the 42 investigated tablets. The respective loadings plots are presented in Fig. 22b and reveal that PC-1 explains the variance within the dataset resulting from an increasing baseline shift with increasing tablet hardness. PC-2 explains the variation in the baseline slope, which can be caused by phenomena related to fluorescence. The resulting scores scatter plot (Fig. 22c) illustrates that tablets of different RTS are clearly distinguished from each other by the first PC that explains 99.6 % of the variance within the dataset.

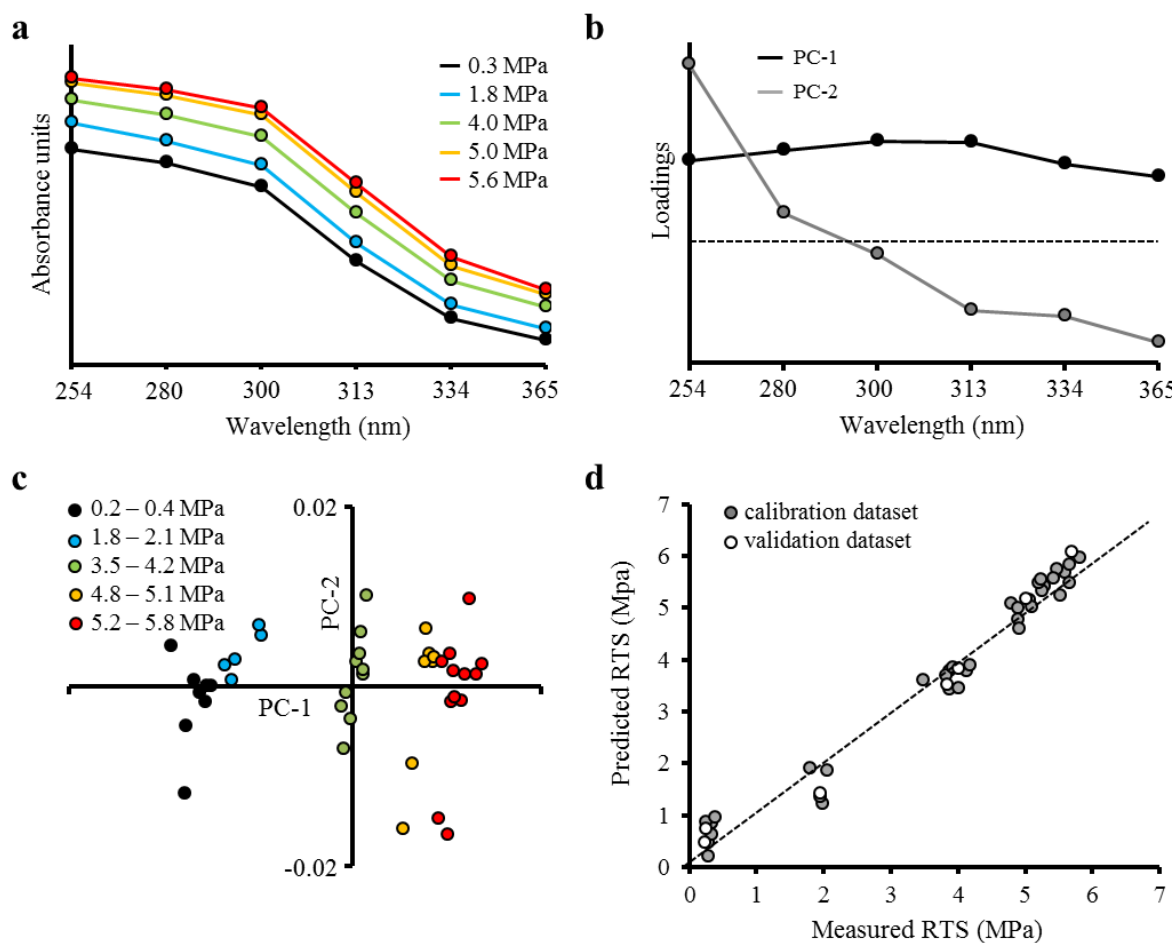


Fig. 22: (a) Representative mean UV absorbance spectra of tablets with a different RTS as determined by a hardness tester (b) PCA loadings plots (c) PCA scatter plot for tablets with a different RTS (d) PLS Regression plot (R^2 of calibration: 0.972, slope: 0.972) of the predicted RTS of trypsin tablets based on the mean UV absorbance spectra as a function of the measured RTS (RMSEP: 0.36 MPa).

To correlate this spectral baseline shift with the actual RTS of the tablets, a PLS calibration model was established using one LV. The calibration model was built using 35 out of the 42 spectra from the investigated tablets (Table 3) that were used as predictors for their RTS, which was determined by a hardness tester (Fig. 22d: gray dots). Accuracy of the model was proven by an external validation set consisting of the mean UV spectra of another seven tablets (Table 3; Fig. 22d: white dots) that were randomly chosen from the different groups of tablets with

different RTS (colored clusters in the PCA scores plot). As illustrated in Fig. 22d, a linear correlation was found between the predicted RTS based on the mean UV spectra of the tablets and their measured RTS. Overall, a RMSEP of 0.36 MPa reveals the potential of UV imaging to be used as a surrogate method for the RTS of the tablets. It has to be mentioned that the correlation between the actual RTS of tablets and the smoothness of the surface that causes the observed spectral baseline shift is dependent on the tablet formulation and dimension and thus has to be determined individually for each type of tablet. However, for routine control the presented data indicate that UV imaging in combination with PLS regression appears to have the potential for estimation of the tablet RTS.

3.2.3 Evaluation of tablet intactness and surface density profiles

Multispectral UV imaging was investigated in terms of its suitability to determine further relevant physical tablet attributes, namely to detect tablet defects and to monitor tablet surface density profiles. To evaluate the spectral variance within the images of tablets that were compacted at different pressures (Table 3), PCA was applied to the segmented spectra of each tablet separately (Fig. 15: 3a). The resulting PC-1 score image of representative plain trypsin tablets compacted at either 160 MPa (tablet A) or 125 MPa (tablet B) indicate increased intensity of the scores at the edge of the tablets (Fig. 23: column I). In contrast, the score image of a plain trypsin tablet prepared at a low compaction pressure (tablet C) does not show a trend in the distribution of the intensity values. In the image of a lipase tablet (tablet D), an irregular shaped region of increased intensity at the edge of the tablet as well as a small high intensity spot in the lower left part of the score image can be detected. Representative mean UV spectra of the center region in comparison to either the edge (tablets A-C) or the regions of high-intensity pixels (tablet D) of the investigated tablets are shown in Fig. 23 (column II). It is obvious from the plots that all spectra of a respective tablet are of the same shape. However, a marked baseline shift is observed between the spectra of the center and the edge of the tablets that were compacted at high pressures (tablets A and B) as well as between tablet center and high intensity pixels of tablet D. As described in the literature, a loading that describes such a baseline offset reflects the shape of the spectra (246). Thus, the PCA loadings plots reveal that this offset in the baseline of the UV spectra is explained by PC-1.

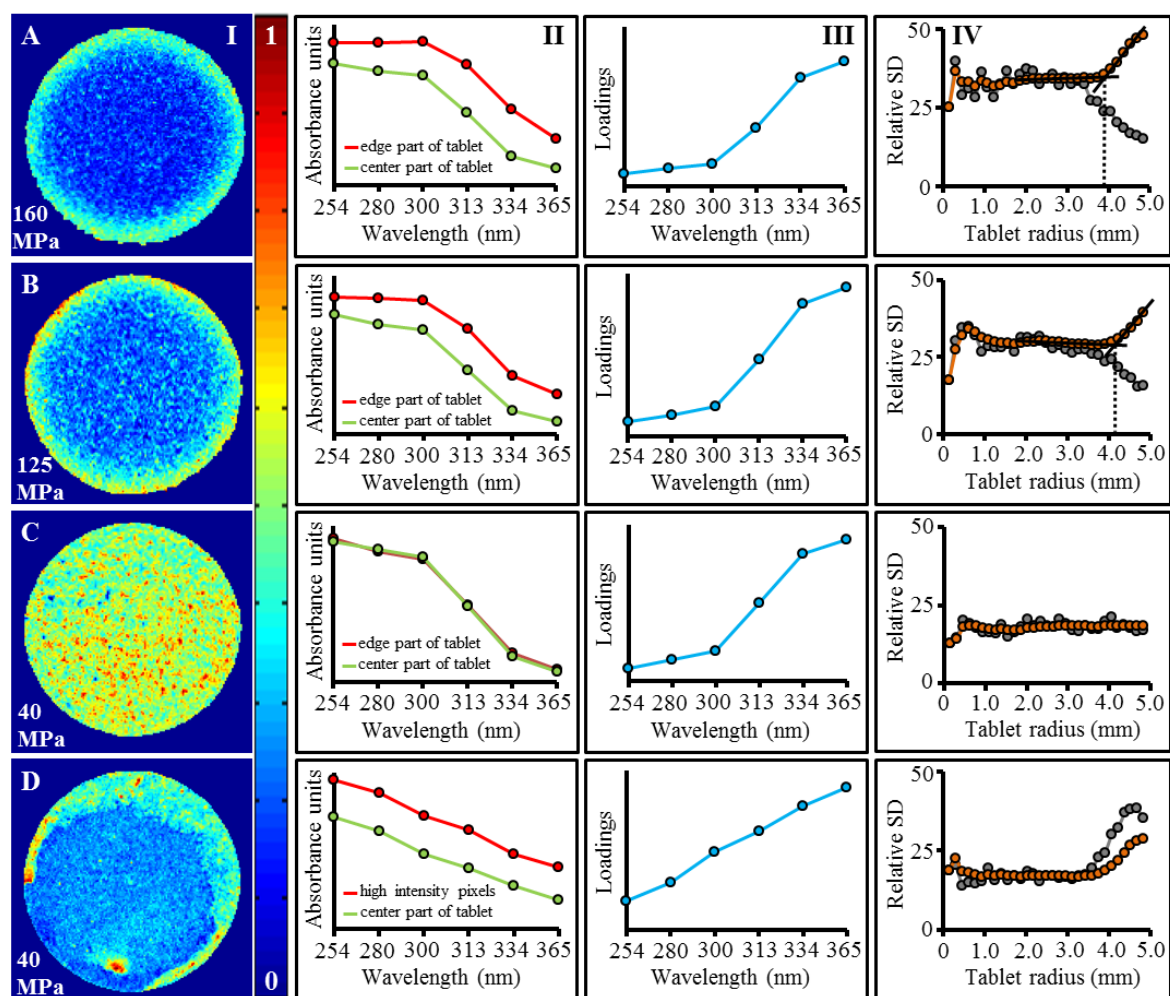


Fig. 23: Analysis of UV images of tablets prepared at different compaction pressures. Columns from left to right correspond to the PCA score images of PC-1, mean UV spectra of representative tablet regions, loadings plots of PC-1, and relative SD of PC-1 scores of the concentric subunits as a function of the tablet radius (thickness of subunits: 2 pixels).

As discussed in the previous section, it is well known that spectroscopic techniques working in reflectance mode are sensitive to various phenomena related to light scattering, which is caused by material physical characteristics such as surface texture (174, 281). Thus, the incident light is absorbed to a different extent at parts of increased roughness, e.g. at splintered parts of tablets, compared to flat surface parts. Furthermore, tablets are reported to have a smoother surface in regions of higher

density of the compact, which also results in less diffuse reflectance and therefore higher absorbance of the incoming light (73, 146). Thus, on the one hand the observed baseline shifts may be explained by a localized increased surface roughness due to splintered parts of the tablet (tablet D). On the other hand differences in the packing density between the center and the edge of the tablet surface (tablets A and B), which results from die wall friction and is therefore more pronounced at high compaction pressures, may lead to baseline shifts.

Generally, it is favorable to control the previously defined product specifications of a large number of tablets by timely measurements in direct vicinity of the production process compared to laboratory-based testing random samples after the process, because it allows to establish a feedback control system and readjustment of tableting parameters to obtain tablets 'within specification' during further processing (20, 171). Therefore, implementation of the analytical technique in the production line as well as automation of the quality control procedure is required. However, visual inspection of the obtained data, e.g. PCA scores images, is a too slow analytical routine to monitor the high speed tableting process. Thus, to assess the suitability of the implementation of quality control based on UV images, an image analysis approach was performed using the PC-1 scores images of the tablets (see below).

Tablet intactness evaluation was based on the calculation of the rSD of all scores within non-overlapping subunits of the PCA scores image (Fig. 15: 3d). The plots of the rSDs of the corresponding subunits as a function of their radius reveal that the within-subunit variation is nearly constant or even decreases from the center to the edge of the tablet surface for intact compacts (Fig. 23: tablets A-C, column IV,

gray profiles) while splintered parts on the tablet surface are clearly detected because they result in a markedly increased rSD of the enclosing subunits (tablet D). To determine the tablet surface density profile, the rSDs of overlapping concentric subunits with increasing radius (Fig. 15: 3e) were analyzed. By the overlapping subunit approach, the rSD of the score intensities is also calculated for pixels that are horizontally arranged. Thus, for tablets that show a nearly homogeneous density distribution at the center and a region of increased density (roiD) at the edge, the rSD significantly increases as the radius of the concentric subunit exceeds a certain value (Fig. 23: tablets A and B, column IV, orange curve) because more high-intensity pixels are entrapped by subunits with a large radius. In contrast, the plot of the rSDs as a function of the tablet radius shows an almost flat baseline for the tablet with a rather homogeneous density profile (Fig. 23: tablet C, column IV, orange curve).

For reference purposes, the results obtained from the UV images were compared with the information that was achieved by NIR imaging of selected tablets because NIR imaging has previously been shown to be a suitable imaging technique to non-destructively assess density profiles of tablets (73). In Fig. 24 the results of analyzing NIR images of tablet A and C obtained by the above mentioned image analysis procedure are shown. It is obvious, that the PCA score images resulting from the NIR data reveal a similar pattern compared to the scores images obtained from the respective UV images. Again, the loadings plots reveal that PC-1 describes the spectral variance, which results from differences in the density throughout the surface of the tablets as the main variance within the spectral dataset is due to a baseline shift (Fig. 24: columns II and III). Thus, UV imaging provides information about the

physical intactness of the tablets comparable to NIR imaging.

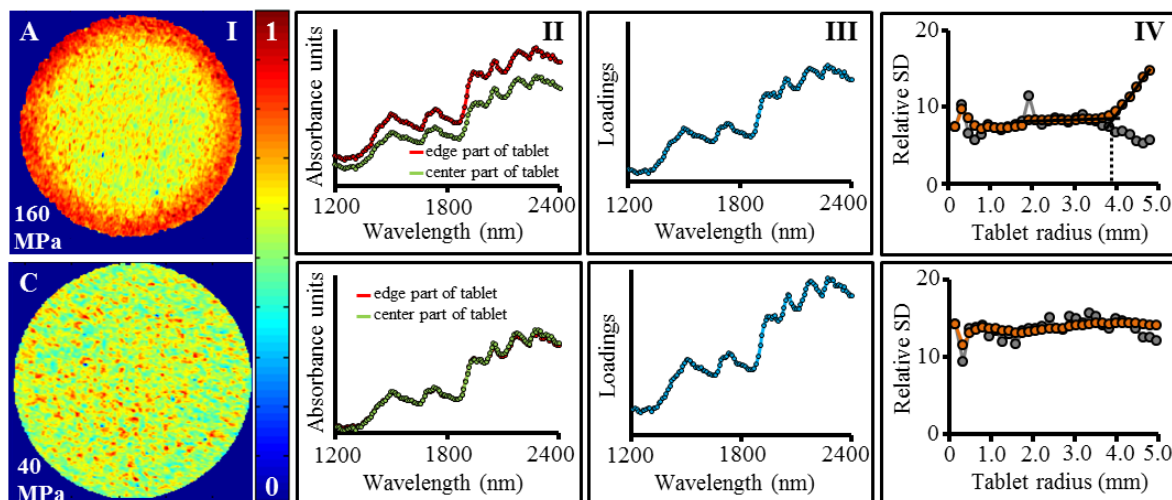


Fig. 24: Analysis of NIR images of tablets prepared at different compaction pressures. Columns from left to right correspond to the PCA score images of PC-1, mean NIR absorbance spectra of representative image regions, loadings plots of PC-1, and relative SD of PC-1 scores of the concentric subunits as a function of the tablet radius (thickness of subunits: 4 pixels).

So far, it could be shown that tablets ‘within specification’ can be distinguished from those that are either splintered or that exhibit a trend in their surface density profile (out of specification) because their corresponding rSD plots are markedly different. However, also the rSD plots of various tablets ‘within specification’ differ from each other. Thus, to discriminate tablets that were ‘within specification’ from tablets ‘out of specification’ in an automatized manner, in a first step a SIMCA model was established based on the rSD plots obtained from the multivariate analysis of the UV images. As described in section 2.4.4 and shown in Table 8, the SIMCA classification model was based on two classes, which were constructed by application of PCA to the rSD plots obtained from the UV images of a set of reference tablets with an either homogeneous (class 1) or inhomogeneous (class 2) surface density distribution.

These reference tablets were obtained by compaction of plain trypsin and lipase powder at either low or high compaction pressures (see above; Table 3).

Table 8: Classification according to the SIMCA model. Tablets were assigned to class 1 and class 2 based on their intactness and surface density profiles.

Known tablet specifications			Class 1: Intact tablet – homogeneous density profile	Class 2: Intact tablet – inhomogeneous density profile
Intact tablet – homogeneous density profile	Plain trypsin tablets	1	*	-
		2	*	-
		3	*	-
Intact tablet – inhomogeneous density profile		4	-	*
		5	-	*
		6	-	*
Defect/ splintered tablet	Plain trypsin tablets	7	-	-
		8	-	-
		9	-	-
		10	-	-
	Plain MCC tablets	11	-	-
		12	-	-

*) assignment of the tablet to the respective class

-) no assignment of the tablet to the respective class

In a next step, it was investigated if the two concatenated rSD profiles of a set of test tablets (see above) with previously known assignment to one of the two model classes based on the applied compaction pressure, are assigned to class 1 or 2 (Fig. 15: 3f). The resulting classification table (Table 8) shows that the test tablets with a rather homogeneous surface density profile (samples 1-3) were correctly classified as members of class 1 based on their rSD profiles resulting from analysis of the respective UV images. Moreover, the intact tablets with inhomogeneous surface density profile (samples 4-6) were correctly assigned to class 2. It is furthermore obvious from Table 8 that all splintered tablets (samples 7-12) neither correspond to class 1 nor to class 2. Hence, the misclassification rate is low and considered

acceptable. The tablets were correctly differentiated based on their intactness as well as their surface density profile (sensitivity and specificity of the SIMCA model: 1.0 based on the present external validation data set). Therefore, UV imaging in combination with the described image analysis routine allows automatized control of the mentioned physical tablet attributes in a minimum of time and therefore might be an attractive approach for real-time or near real-time monitoring of the tablet compaction process.

3.2.3.1 Quantification of surface density inhomogeneity

For process control and formulation optimization purposes it may be advantageous to gain knowledge on the extent of the region of increased density (roiD) at the edge of the tablet surface to estimate the necessity and the extent of modification of the lubricant level or adjustment of the tableting parameters. To obtain this information from UV imaging, again the rSD plots resulting from the approach of dividing the PCA scores images of the tablets A-C in overlapping concentric subunits were used (Fig. 15: 3e; Fig. 23: column IV, orange curve). The results obtained from the UV images were compared to those found by NIR imaging (Fig. 24: column IV, orange curve).

First, tangents were applied to the plateau part as well as to the slope of the linear part of the rSD curves followed by determination of the intersection of the tangents (Fig. 23: tablets A and B, column IV; Fig. 24: tablet A). The point of intersection of the tangents is indicative for the particular circular subunit where a distinct change of the density begins. The diameter of the roiD at the edge of the tablet surface was then calculated from the tablet diameter and the diameter of the plateau region of the rSD

curve using the following equation:

$$roiD \varnothing = \frac{tablet \varnothing - plateau \ region \ of \ the \ rSD \ curve \ \varnothing}{2} \quad (Eq. 17)$$

where \varnothing is the diameter and *roiD* is the region of increased density.

Calculation of the *roiD* diameters from the UV data of the tablets (Fig. 23) resulted in a markedly larger *roiD* diameter for tablet A (1100 μm) than for tablet B (870 μm). As expected, to obtain tablets with a homogeneous surface density profile, the manufacturing conditions of the tablets that were compacted at a higher pressure (such as tablet A) have to be readjusted to a greater extent than those of the tablets prepared at a lower pressure (such as tablet B). According to Figs. 23 and 24, the diameter of the *roiD* that was obtained from the UV image of tablet A (1100 μm) was in agreement with that calculated from the corresponding NIR image (1100 μm). The results indicate that UV imaging is a valuable technique to obtain qualitative information on the physical tablet attributes and quantitative information on the surface density profiles of the tablets both being useful for further process optimization. Accuracy of the quantification of the *roiD* has to be further verified by analysis of a larger sample population.

3.2.4 Conclusion

Multispectral UV imaging has been demonstrated to be a rapid and effective technique to non-destructively monitor chemical and physical quality attributes of tablets. UV images were found to provide reliable information on the tablet API content. However, it is worth to mention that for obtaining reliable information on the total tablet API content from surface imaging techniques such as UV imaging, the distribution of the API at the upper surface has to be representative of the API distribution within the entire tablet. Furthermore, UV imaging could be successfully used as a surrogate marker for a relevant tablet bulk property, i.e. the RTS. In addition, a quality control procedure based on multivariate analysis of the UV images and related statistics was presented, which provides not only qualitative information on the intactness of the tablets and their surface density profiles but also quantitative information on the density variations throughout the tablet surfaces. Automation of tablet characterization was achieved by SIMCA modeling of the UV imaging data.

Considering the short data acquisition time and the amount and relevance of the provided information, UV imaging is already nowadays an attractive approach for formulation optimization purposes and, with limitations, for quality control in the production process of tablets. Nevertheless, further improvement in the instrumental setup is required to further reduce the data acquisition time thus allowing true real-time adjustment of the tableting process parameters. In this context, UV imaging shows a high potential for shortening of the data acquisition time because most of the APIs on the market exhibit a higher absorptivity (absorption cross section) in the UV than in the NIR range (218, 282). Thus, UV spectroscopy shows a higher sensitivity

and has a lower limit of quantification compared to NIR spectroscopy (282). Consequently, UV imaging potentially allows data acquisition at a higher speed and at lower API concentrations, which has to be confirmed in further studies.

As previously mentioned, physical tablet attributes such as hardness, surface density profile, and intactness, were previously successfully evaluated by other imaging techniques such as NIR imaging or terahertz pulsed imaging. However, as described by Kessler (282), UV spectroscopy generally shows a higher scattering coefficient compared to NIR spectroscopy, making this technique particularly sensitive for alterations in the sample surface texture. This texture sensitivity may be accompanied by a higher accuracy of UV imaging compared to NIR imaging in terms of evaluation of tablet hardness and surface density profile.

The relevance of UV imaging as technique for chemical and physical characterization of tablets of varying composition, shape and category, such as beveled, convex, as well as coated tablets has to be confirmed in further studies.

3.3 Results and discussion of ‘Non-destructive quality control of tablets and blister packs by UV imaging’¹⁰

3.3.1 Verification of blister pack filling

Individual packaging of tablets in blister packs is a common manufacturing procedure within the pharmaceutical industry. Thus, to ensure the required quality of the finished dosage form it is essential to verify correct filling of the blister cavities. From that perspective, the suitability of UV imaging to control the content of the blister packs was determined. Therefore, UV images of all blister packs (empty, partly, or completely filled cavities) that contained two different kind of tablets (tablets ‘B’ and ‘D’) were recorded. The blister packs were imaged unsealed as well as sealed with one of the three different blister sealing foils: two different monolayer PVC foils (Genotherm® PH132 and PH 154 3A) and a PCTFE/PVC multilayer foil (Pentapharm® PA200/02). As illustrated by the representative UV images in Fig. 25a, tablets within the blister cavities can be clearly distinguished from the aluminum blister background. Pixels belonging to the tablets showed a markedly higher absorbance than the pixels related to the background, because of various ingredients within the tablets that exhibit chromophores leading to a higher absorbance in the emitted spectral range (254 – 365 nm). Even tablets below the sealing foils are clearly detectable, which reveals translucency of the different polymer foils for the emitted UV light (Fig. 25a: II, III, IV). To count the tablets within the cavities, pixels belonging to the tablets were separated from those of the background by setting a hard threshold in the sixth wavelength (365 nm) of the UV images. Thus, binary images were obtained with tablet pixels being highlighted (Fig. 25b). Subsequently, tablet counting was achieved by a routine searching for connected parts of pixels with the

¹⁰This chapter has been published as shown on page 199 in appendix B.

binary value unity (red) in the binary images (283). As presented in Fig. 25, the tablets inside the cavities of the blister packs are clearly detected and correctly counted based on the UV images.

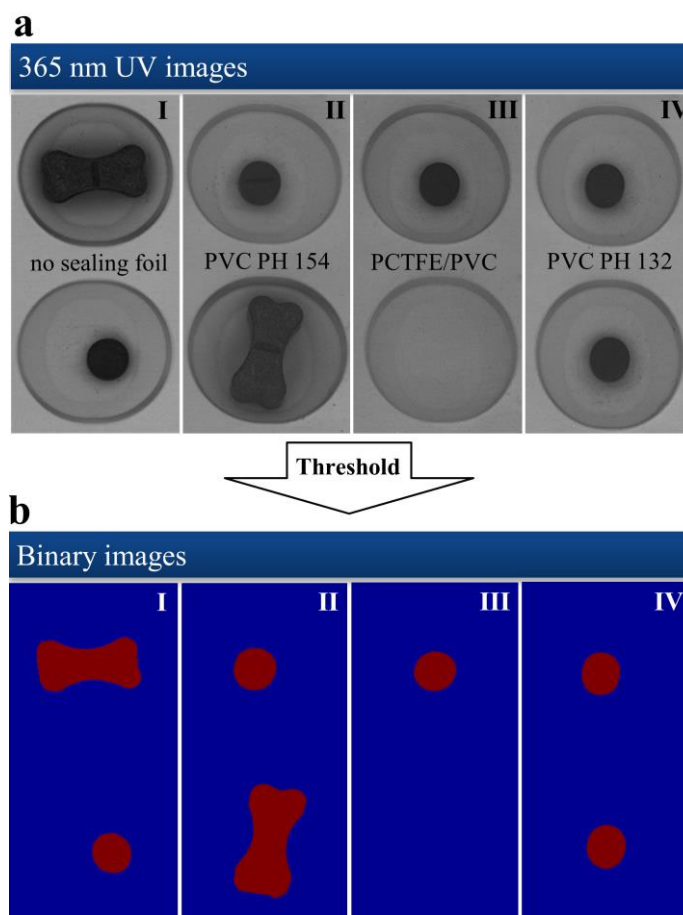


Fig. 25: (a) Representative UV images of partly or completely filled blister packs that contain tablets 'B' and/or tablets 'D'. The blister packs were either unsealed (I) or sealed with PVC PH 154 foil (II), PCTFE/PVC foil (III), or PVC PH 132 foil (IV). (b) Binary images of the blister packs with tablets being highlighted (red).

3.3.2 Characterization of blister packs

3.3.2.1 General aspects

Besides a correct filling of the blister packs, another relevant quality issue during manufacturing of tablets is cross-contamination within the packaging line. For instance it is essential to ensure that the correct tablets are packed into the blister packs and that the designated polymer foils are used for sealing. From that perspective, UV imaging was evaluated in terms of its suitability to distinguish between blister packs based on the composition of the tablets therein as well as on the used blister sealing foil. Therefore, the UV images of various prepared blister packs were analyzed. The obtained mean spectra of tablets 'B' and tablets 'D' (Fig. 26a: blue curves) that were measured within unsealed blister packs reveal that the tablets of different composition show distinct absorbance profiles. Furthermore, it is obvious from the absorbance profiles in Fig. 26a that tablets 'B' and 'D' still show distinct spectra even if measured within blisters that were sealed with either PVC (green and red curves) or PCTFE/PVC foil (black curves). The sealing foils did not hamper differentiation of the blister packs based on the composition of the tablets therein, although it is apparent that the differences between tablets of different composition become smaller. It is furthermore obvious from Fig. 26a that the spectra of both tablet formulations vary depending on the covering sealing foil, as the respective polymers differ in their interaction with the emitted UV light. However, the two different types of PVC foil (PH 132 and PH 154) that are of equal chemical composition but differ in the way of production lead to comparable UV spectra of the blistered tablets.

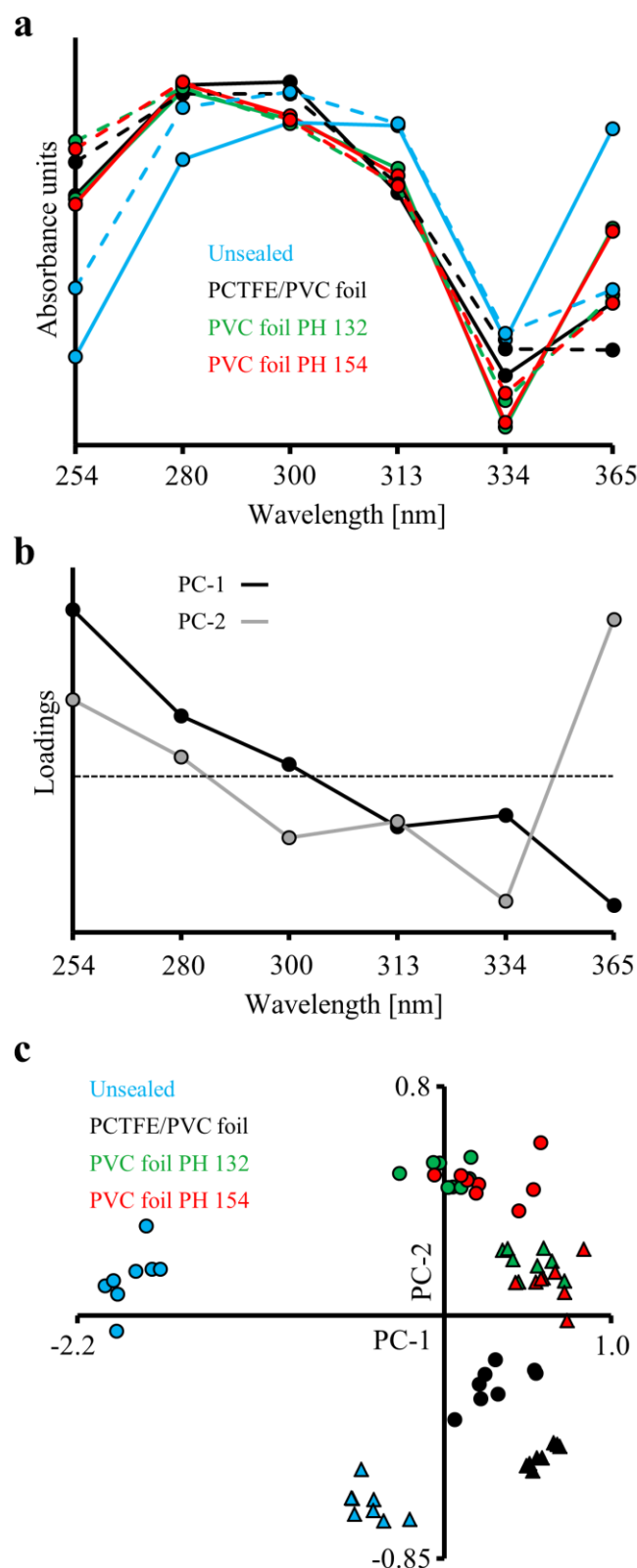


Fig. 26:(a) Representative mean UV spectra of tablets 'B' (—) and 'D' (---) within blister packs.(b) PCA loadings plots of PC-1 and PC-2. (c) PCA scores plot of mean UV spectra of tablets 'B' (●) and 'D' (▲) within blister packs.

Thus, to investigate if these spectral differences between the tablets in the blister cavities allow a differentiation of the blister packs based on the tablet composition and the used sealing foil, PCA was applied to the mean spectra of the tablets inside the cavities. It is obvious from the resulting PCA loadings plots that PC-1 and PC-2, which explain 77 % and 20 % of the variance within the dataset, respectively, describe the relevant spectral differences between the samples that are caused by the different tablet formulations as well as the applied sealing foils (Fig. 26: a and b). The PCA scores plot (Fig. 26c) reveals that blister packs filled with tablets of different composition and sealed with varying polymer foils form clusters in the plot. Blister packs containing different types of tablets are distinguished from each other by PC-1 and PC-2, as blister packs filled with tablets 'D' are generally found at higher PC-1 and lower PC-2 scores compared to blisters with tablets 'B'. Furthermore, unsealed tablets 'B' and 'D' are located in the negative part of PC-1, while the sealed tablets are mainly found in the positive part of PC-1 and are further distinguished according to the type of the polymer foil by PC-2. However, in agreement with the spectral observations in Fig. 26a, a differentiation between the filled blister packs sealed with either PVC foil PH 132 or PH 154 is not achieved by PCA, as the respective samples are superimposed in the scores plot.

3.3.2.2 Pattern recognition

To be suitable as a real-time or near real-time quality control tool within the high-speed production process of tablets, automation of the quality control procedure is required. Thus, it was investigated if UV imaging allows routine classification of the blister packs. For this purpose, a PCA-based SIMCA classification model was built

based on the mean UV spectra of the tablets within the blister cavities with the aim to assign the blister packs to eight different classes (Table 4 and 9) dependent on the type of tablets and the sealing foil.

Table 9: Classification table of blister packs according to the tablet composition and sealing foil.

Model class	1	2	3	4	5	6	7	8
Tablets	Tablets 'B'				Tablets 'D'			
Sealing foil	unsealed	PCTFE/ PVC	PVC PH 132	PVC PH 154	unsealed	PCTFE/ PVC	PVC PH 132	PVC PH 154
Test set								
1 'B' – unsealed	*							
2 'B' – unsealed	*							
3 'B' – PCTFE/PVC		*						
4 'B' – PCTFE/PVC		*						
5 'B' – PVC PH 132			*	*				
6 'B' – PVC PH 132				*				
7 'B' – PVC PH 154				*				
8 'B' – PVC PH 154			*	*				
9 'D' – unsealed					*			
10 'D' – unsealed					*			
11 'D' – PCTFE/PVC						*		
12 'D' – PCTFE/PVC						*		
13 'D' – PVC PH 132							*	*
14 'D' – PVC PH 132								*
15 'D' – PVC PH 154							*	*
16 'D' – PVC PH 154							*	*
Model parameters								
Specificity	1.00	1.00	0.50	1.00	1.00	1.00	0.50	1.00
Sensitivity	1.00	1.00	0.93	0.86	1.00	1.00	0.86	0.86

It is obvious from the obtained classification table (Table 9) that blister packs containing tablets 'B' or 'D' that were either unsealed (samples 1,2 and 9,10) or sealed with PCTFE/PVC multilayer foil (samples 3,4 and 11,12) were correctly assigned to the respective class. Moreover, no further samples of the test set were incorrectly assigned to these classes resulting in a specificity and sensitivity of the respective PCA models of 1. In addition, the blister packs sealed with one of the two different monolayer PVC foils could be distinguished from those that are either unsealed or

sealed with PCTFE/PVC foil, as they were correctly assigned to the classes of that polymer (samples 5-8 and 13-16). However, a systematic differentiation of the blister packs based on the two different types of PVC foil (PH 132 and PH 154) could not be achieved resulting in specificity and sensitivity values below 1. Again, this is in agreement with the obtained mean spectra of such blister packs (Fig. 26a: green and red curves), which are of comparable shape with only minor differences to one another.

In general it could be shown that UV Imaging is a sensitive technique to distinguish between blister packs based on the composition of the tablets therein even through PVC and PCTFE/PVC blister sealing foils as these foils are mostly transparent for the emitted UV light. However, the two polymers differ in their interaction with the incoming UV light and thus lead to different UV spectra of the blister packs. Hence, the UV images of the blister packs contain valuable information on the formulation of the tablets therein as well as on the blister sealing foil which can be used for classification of the tablets according to these blister pack specifications.

3.3.3 Visual inspection of unblistered tablets

3.3.3.1 Imprint intactness

Defects of the imprinted codes of tablets can reduce customer acceptance as well as patient compliance, and may affect drug safety due to a loss of identifiers (13, 71). Thus, imprint intactness has to be examined after the compaction cycle. Therefore, as manual quality control procedures are time-consuming and costly, machine vision systems are preferable. Although machine vision systems are available that allow accurate examination of imprinted codes (71), in this study the suitability of UV imaging for evaluation of the integrity of the imprint of tablets 'A' was investigated.

In Fig. 27 column I, photographic images of tablets with intact 'ASPIRIN 0,5' imprint (Fig. 27: Ia) as well as tablets with pronounced defects of the characters 'R' (Fig. 27: Ib) and 'PIR' (Fig. 27: Ic) are presented. An inspection routine based on the UV images of these tablets (Fig. 27: column II) was applied as described in section 2.5.3.3. It is obvious from the resulting PC-1 scores images (Fig. 27: column III) obtained from application of PCA to the tablet pixels after background separation that the imprint is clearly highlighted compared to the smooth regions of the tablets, because the pixels enclosing the imprinted characters show a high score intensity. In contrast, in regions of defect imprints (circles) most pixels are markedly lower in intensity and only small unconnected high-intensity pixel clusters are detectable.

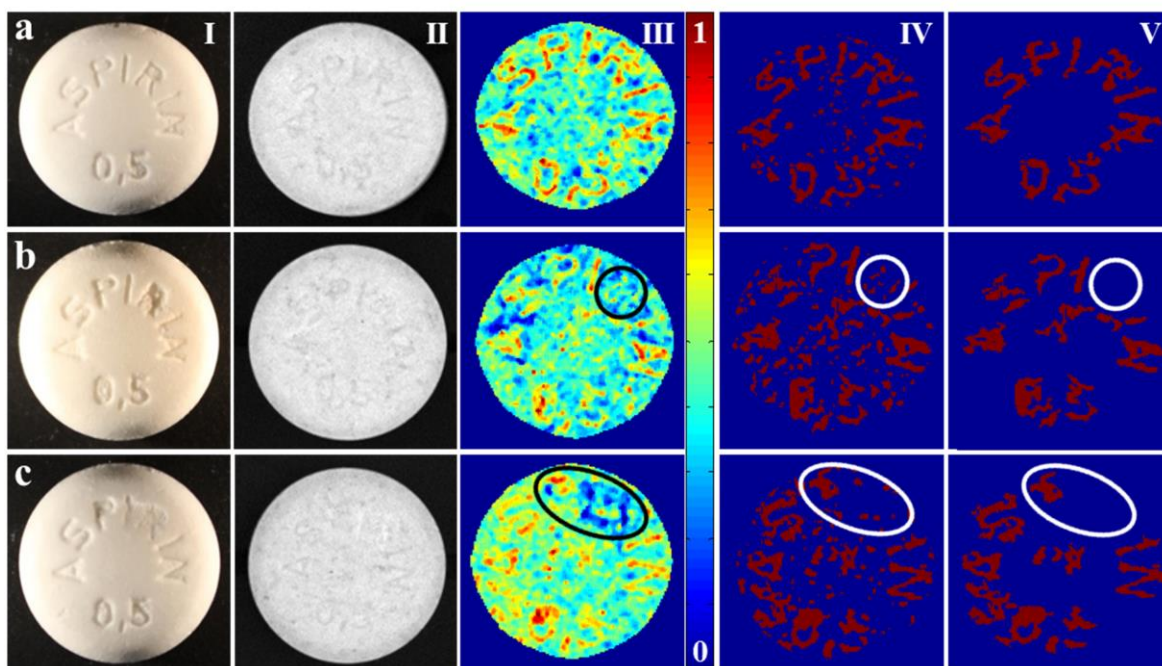


Fig. 27: Image analysis of tablets 'A' with either intact (a) or defect (b and c) imprint. Columns from left to right correspond to photographic images (I), 365 nm gray scaled UV images (II), PC-1 scores images resulting from application of PCA to the UV images (III), binary images obtained by setting a hard threshold in the scores images (IV), processed binary images (V).

The mean UV spectra of high- and low-intensity pixels of the tablets reveal that the main spectral variance results from a baseline shift rather than from differences in the shape of the spectra (Fig. 28a). As described in section 2.5, it is well-known that such shifts in the spectral baseline correspond to physical alterations of the samples (191, 222). PC-1 explains the spectral variance caused by this baseline shift, because the loadings plot of PC-1 reflects the shape of the UV profiles (Fig. 28b) (246). Thus, PC-1 gathered the differences in the reflectance of the emitted UV light resulting from surface texture variations at the imprinted codes.

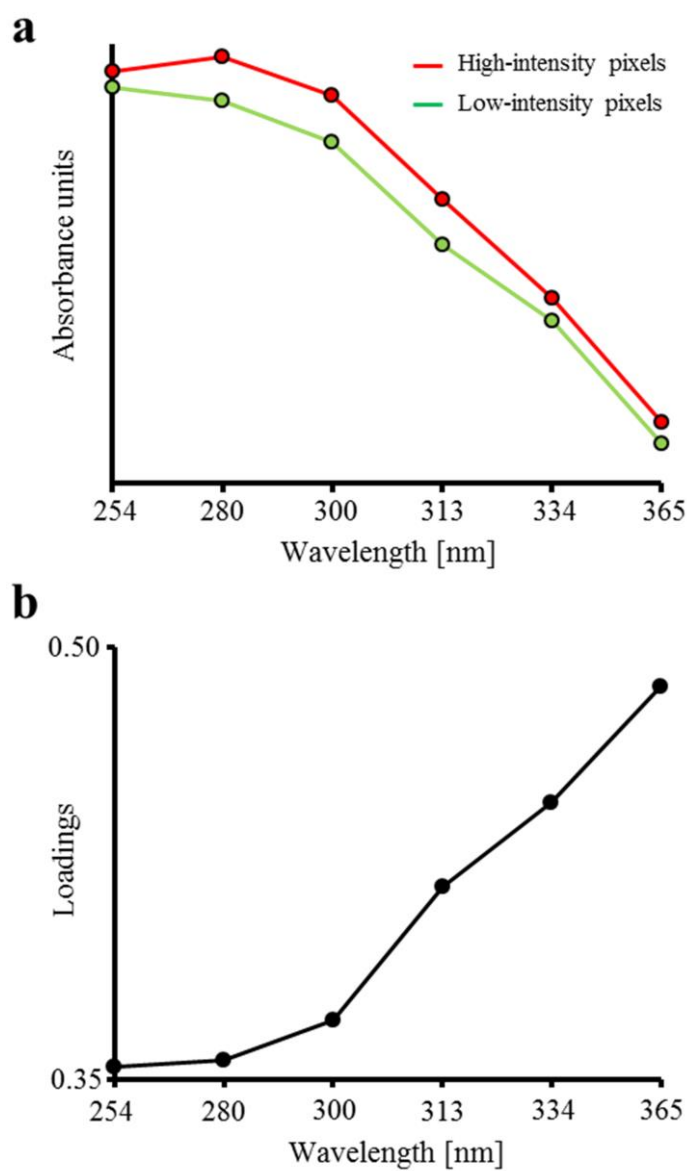


Fig. 28: (a) Representative mean UV absorbance spectra of high- and low-intensity pixels (refer to Fig. 27: column III) of tablet 'A' with intact imprint. (b) Loadings plot of PC-1.

For detailed evaluation of the imprint intactness based on PCA of the UV images, a hard threshold was set in the PC-1 scores to extract the high-intensity pixels that enclose the imprinted characters. As shown in Fig. 27, column IV, the imprint becomes highlighted in the obtained binary images, as most of these pixels are attributable to the imprinted code. To eliminate those pixels that are highlighted but do not enclose the characters, another threshold was set on the binary images defined as the pixel-quantity of the smallest imprinted character. Thus, the resulting binary images (Fig. 27: column V) mainly contain those connected pixels that correspond to the different characters. It is obvious from Fig. 27 that the characters of the intact imprint are clearly readable. Furthermore, imprint defects are reliably detected, as the damage at the imprinted characters which simulates e.g. sticking during compaction, is accompanied by an irregular surface texture that leads to pronounced changes in the reflectance of the emitted UV light resulting in various smaller clusters of high score intensity pixels that are removed by application of the above mentioned threshold to the scores (Fig. 27: columns III, IV, and V; rows b and c; circles).

3.3.3.2 Tablet surface cracks

During tablet manufacturing it is essential to verify physical integrity of the prepared compacts to guarantee final product quality. Cracks within tablets may lead to a reduced patient compliance as well as a changed tablet disintegration and dissolution behavior. From that perspective, UV imaging was evaluated in terms of detection of tablet surface cracks. Photographical images of representative examples of tablets 'C' with different extents of cracks on the surface are shown in Fig. 29, row a.

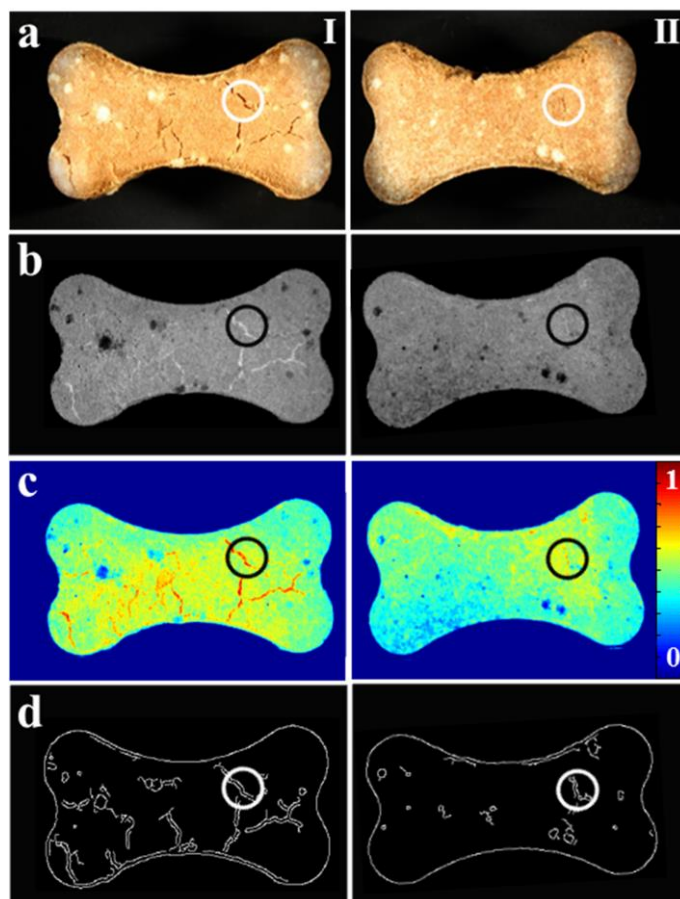


Fig. 29: Image analysis of tablets 'C' with cracks on the surface. Rows from top to bottom correspond to photographic images (a), 365 nm UV images (b), PC-1 scores images obtained from application of PCA to the UV images (c), and binary images resulted from application of an edge detection algorithm to the scores images (d).

Several major cracks are obvious on the surface of the tablet shown in the left column (I), while that in the right column (II) only shows minor defects (examples for cracks are highlighted by circles). To detect such cracks based on the obtained UV images (Fig. 29: row b), again PCA was applied to the tablet pixels after background separation (section 2.5) to visualize the spectral variance throughout the tablet surfaces. The resulting scores images reveal that surface cracks are highlighted because the surrounding pixels are of higher intensity compared to those of intact surface regions (Fig. 29: row c). According to Fig. 30a, the respective mean UV profiles of low- and high-intensity pixels mainly differ in the baseline offset and slope rather than in the shape of the spectra. The emitted UV light is scattered to a higher extent at the surface cracks compared to smoother regions of the tablet surface resulting in a reduced reflectance and thus higher absorbance of the radiation. As shown in Fig. 30b, this spectral variance is explained by PC-1, as the corresponding loadings plot is of comparable shape to the UV spectra of the tablet pixels (Fig. 30a). Thus, the PC-1 scores images reflect the texture of the tablet surfaces. However, minor cracks (Fig. 29: column II; circles) are hardly detectable from the images.

To further highlight such cracks and to simplify tablet inspection, an algorithm was applied to the PCA scores images that identifies edges in the images (284). It is obvious from Fig. 29d that major (column I; circles) as well as smaller cracks (column II; circles) are clearly detectable in the obtained binary images and thus allow an accurate examination of the tablet surface properties. Thus, it could be shown that UV imaging in combination with a multivariate image analysis approach is a suitable tool to detect tablet surface cracks.

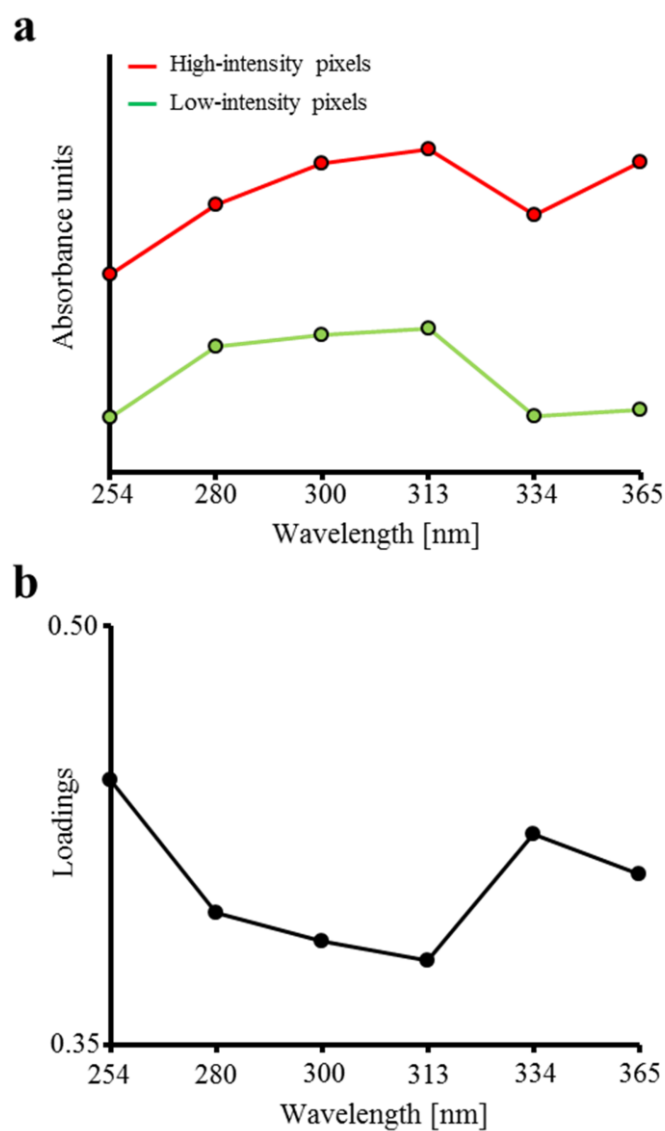


Fig. 30: (a) Representative mean UV absorbance spectra of high- and low intensity pixels (refer to Fig. 29c) of tablet 'C' with cracks on the surface. (b) Loadings plot of PC-1.

3.3.4 Conclusion

Multispectral UV imaging was shown to be a fast, non-destructive, and reliable method for quality control within the tablet manufacturing line. An analytical procedure based on UV imaging was presented for counting of tablets and distinguishing of tablets dependent on their composition within blister packs. UV images of tablets within sealed blister packs combined with SIMCA analysis allowed classification of the blister packs according to the composition of the tablets therein as well as the type of polymer sealing foil. Sealing foils that are of similar chemical composition but result from different production procedures lead to comparable UV profiles of the respective filled blister packs. Thus, batch-to-batch variations of the polymer foils did not hinder a correct classification of the blister packs based on the respective polymer. Furthermore, visual inspection of the physical intactness of unblistered tablets, namely evaluation of the imprint integrity and detection of surface cracks, was successfully achieved. Therefore, UV imaging is considered an attractive approach to routinely verify blister pack filling, detection of cross-contamination of the tablets therein as well as of the primary packing material, and evaluation of physical tablet integrity.

The presented technique is promising for simultaneous monitoring of various product parameters and, considering the high-speed of data acquisition, for implementation into the tablet manufacturing process. The applicability of UV imaging to provide relevant product specifications for accumulating bulk tablets as well as further improvement of the imprint intactness evaluation procedure by an optical character recognition approach has to be investigated in further studies.

3.4 Results and discussion of 'Rapid assessment of tablet film coating quality by multispectral UV imaging'¹¹

3.4.1 Detection, differentiation, and localization of coating defects

To investigate the suitability of multispectral UV imaging to evaluate the integrity of the tablet coating layer, first of all it was investigated if uncoated and coated ASA tablets can be distinguished from each other based on their solid state UV absorbance spectra. Therefore, mean UV spectra (Fig. 31a) of all pixels of an uncoated ASA tablet (Fig. 32: row A) as well as of a tablet with an intact coating and homogeneous smooth texture (Fig. 32: row B) were calculated from the respective UV images. It is obvious from Fig. 31a that the two types of tablets exhibit markedly different absorbance profiles that vary considerably with regard to the overall extent of UV absorbance as well as in the shape of the spectra. The tablet with the green-colored PVA/PEG coating layer (green curve) shows a markedly higher absorbance at all six wavelengths compared to the uncoated ASA tablet (blue curve) resulting in a baseline shift between the two spectra. Based on the chemical composition of the coating material, the coated ASA tablet shows a comparably featureless UV profile characteristic of the spectral response of the lakes in the coating formulation, while the uncoated tablet shows an increasing UV absorbance with decreasing wavelength due to the presence of ASA. To visualize the spectral variance of all pixels of a total of ten uncoated and intactly coated tablets (five tablets each), as well as to investigate if a systematic differentiation of the pixels of the two different tablet types is possible based on their UV spectra, PCA was applied to a reference dataset composed of all pixels of both tablet types (Table 5: PCA model 1).

¹¹This chapter has been published as shown on page 199 in appendix B.

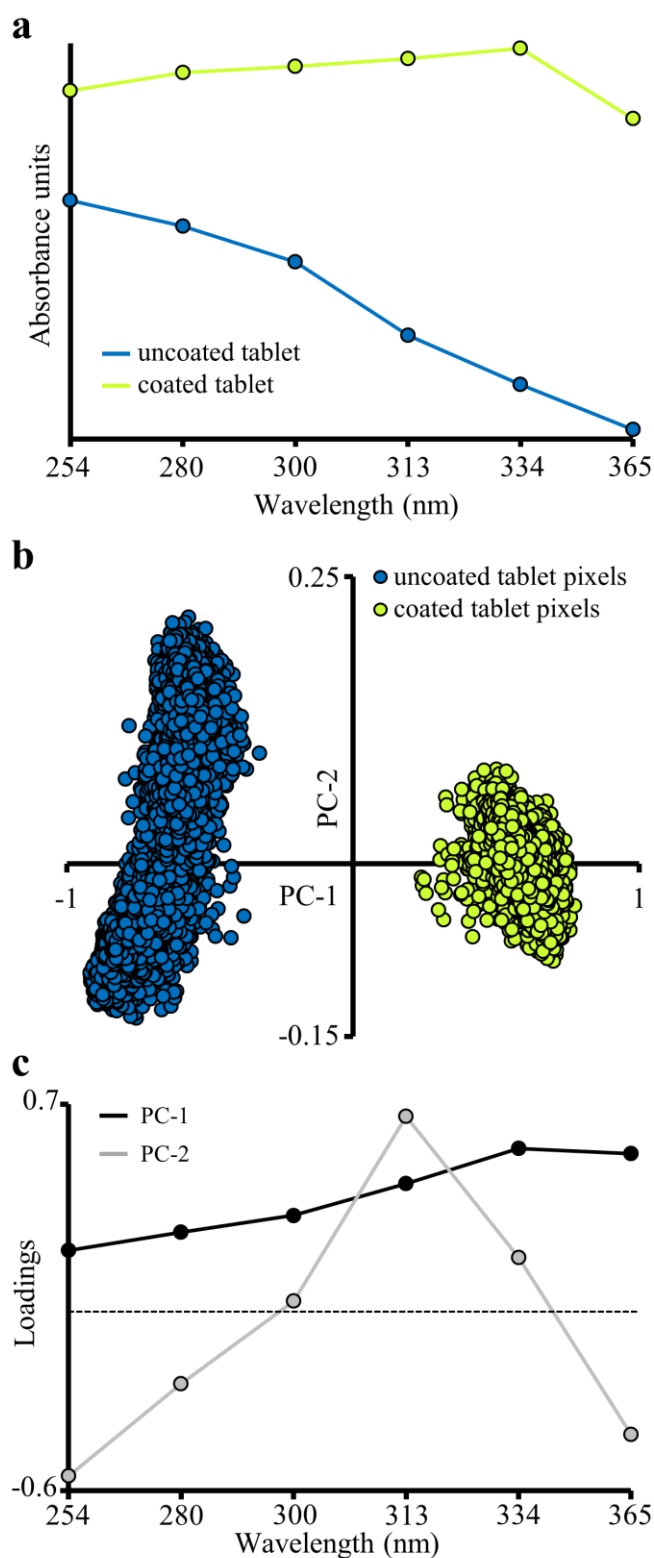


Fig. 31: (a) Mean UV absorbance spectra of an uncoated and a coated ASA tablet, respectively (b) PCA (Table 5: model 1) scatter plot applied to all pixels of uncoated and coated ASA tablets (c) Loadings plot of PC-1 and PC-2.

As shown in Fig. 31b, all pixels of both, the uncoated (blue dots) as well as the intactly coated ASA tablets (green dots) form clusters in the scores plot which are clearly differentiated by PC-1 that explains 98.6 % of the spectral variance. All pixels of the coated tablets show a positive PC-1 score intensity, while pixels belonging to the uncoated ASA tablets form a cluster at negative PC-1 scores. In contrast, the pixels of both tablet types are not distinguished by PC-2 which captures only 1.1 % of the spectral variance. Consequently, as shown in the corresponding loadings plot in Fig. 31c, PC-1 differentiates the pixels based on the observed differences in the shape of the pixel spectra of coated and uncoated ASA tablets, while PC-2 does not explain relevant spectral differences between uncoated and coated tablets. Thus, pixels belonging to the coated ASA tablets can be distinguished from those of uncoated tablets based on the UV spectra.

In a next step, the coating integrity of ASA tablets that are chipped at either the center or the edge of the tablet surface (Fig. 32: row C and D), of a tablet with a inhomogeneous coating (row E), as well as of a tablet with a crack in the coating layer (row F) was analyzed based on the respective UV images (Fig. 32: column II). Therefore, the spectral features of each pixel of the test tablets were extracted from the UV images and projected onto the PCA model which was previously built based on all pixels of the reference dataset composed of five uncoated and five intactly coated ASA tablets (PCA model 1). As shown in the resulting PCA scores plot (Fig. 32: column III, row A), all pixels of the uncoated ASA test tablet are plotted next to the cluster or are even superimposed on the cluster related to the uncoated ASA reference tablets, which confirms complete absence of the coating layer. Furthermore, all pixels of the

ASA tablet with an intact coating serving as test (Fig. 32: row B) form a cluster in direct vicinity of coating pixels (column III), which verifies tablet coating intactness.

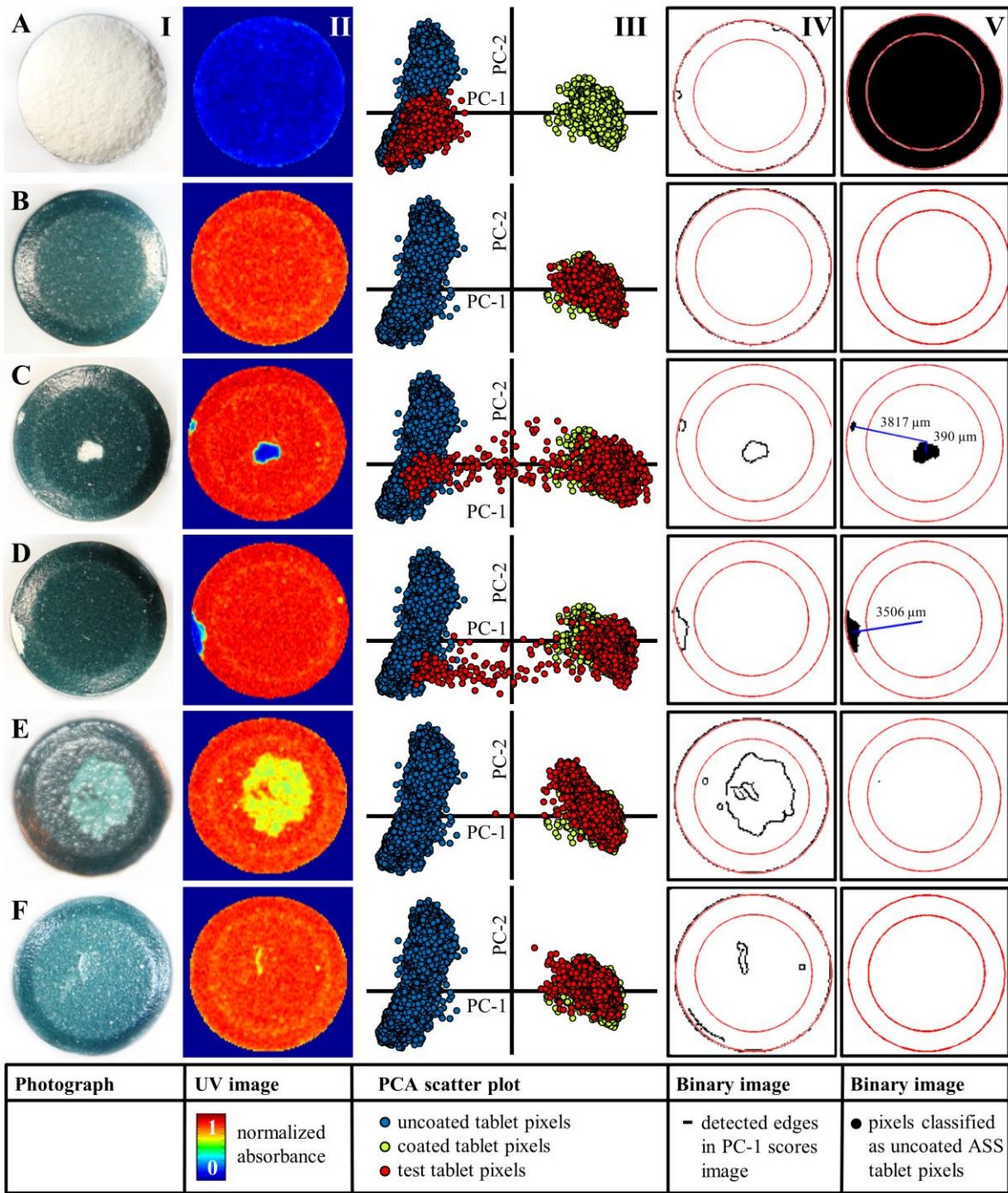


Fig. 32: Image analysis of representative ASA tablets with either homogeneous or inhomogeneous coatings. Columns from left to right correspond to photographic images (I), UV images at 365 nm (II), PCA (Table 5: model 1) scatter plots (III), binary images obtained from application of an edge detection algorithm on PC-1 (Table 5: PCA model 1) scores images (IV) binary images with pixels assigned to the class of uncoated ASA tablet pixels (Table 5: PCA model 2) being highlighted (V).

In contrast, the scores plots of tablets with a partially chipped coating (column III, rows C and D) reveal that the majority of the tablet pixels are superimposed on the reference cluster of coating pixels, but there are also a number of non-clustered pixels with scores in-between the two reference clusters and even pixels that are superimposed onto the uncoated ASA tablets reference cluster. These observations show that a considerable number of the pixels of the test tablet show spectral characteristics of both, the coating layer as well as the uncoated ASA tablet or even spectra similar to the uncoated tablet. Thus, the PCA results correctly indicate that regions of the coating layer are chipped, which is accompanied by the appearance of the uncoated ASA tablet and thus leads to a decreased intensity of the PC-1 scores of the enclosing pixels. However, not all coating defects are accompanied by the appearance of the subjacent ASA tablet as shown by photographic images of tablets with an inhomogeneous coating caused by twinning of tablets during the coating process (Fig. 32: row E) or with a crack in the coating (Fig. 32: row F). The scores plots resulting from subjecting the pixels of these tablets to the PCA model reveal that most of the pixels are superimposed on the coating pixel cluster with a small number of pixels showing lower PC-1 and higher PC-2 score intensities compared to the pixels of the intactly coated test tablet (Fig. 32: row B). It is hypothesized that these pixels surround the defect regions of the coating and show a slightly reduced absorbance compared to the smooth regions of the coat because of a partial discoloration of the coating layer in the regions of the defects.

Consequently, pixels enclosing chipped coating regions are clearly separated from pixels of an intact coating by PCA, while pixels surrounding defects that are not

accompanied by appearance of the subjacent ASA tablet can be hardly differentiated from pixels of an intact coating by analysis of the PCA scores plots.

To achieve automatized detection, differentiation, and localization of the coating defects based on the UV images, a two-step image analysis routine was applied to the tablets shown in Fig. 32. First, to visualize all tablet coating defects, an edge detection algorithm (284) was applied to the scores images (data not shown) of each tablet obtained from subjecting the test tablet pixels to the PCA model 1 (Table 5). In agreement with the UV images (Fig. 32: column II) as well as the previously obtained results from scores plots of the tablets, pixels corresponding to the coating defects show a more or less altered UV spectrum compared to pixels enclosing an intact coating. Thus, the regions of such defects are being highlighted in the scores images. The algorithm detects such structures caused by the difference in intensity of the PC-1 scores between adjacent pixels at the edges of the defects. The resulting binary images with the detected edges being highlighted are shown in Fig. 32, column IV. It is obvious, that the detected edges which neither correspond to the entire tablet nor to the tablet facet can either be assigned to minor inhomogeneities of the coatings (rows E and F) or to the respective defects of the tablet coatings (rows C - F).

In a second step, to automatically distinguish between chipped coatings and coating defects that are not accompanied by appearance of the subjacent ASA tablet, a PCA-based SIMCA classification model was built with the purpose to assign each pixel of the test tablets that are shown in Fig. 32 to either the class of uncoated ASA tablet pixels (class 1) or the class of intact coating pixels (class 2). The SIMCA model was based on two PCA models (Table 5: PCA models 2 and 3) calculated from the

reference pixel datasets of either class 1 or 2. Pixels that were assigned to the class of uncoated ASA tablet pixels (class 1) were automatically highlighted in binary images (Fig. 32: column V). It is obvious that, in agreement with the photographs and the UV images, no single pixel of the tablet with a uniform coating (row B) and of the tablet with cracked coating (row F) were assigned to class 1. In contrast, all pixels of the uncoated ASA tablet (row A) as well as the pixels surrounding the pronounced coating defects at the center and edge of the tablets in rows C and D are correctly assigned to the class of uncoated ASA tablet pixels (class 1) and are thus highlighted in the binary images. As shown in the binary image of the tablet with an inhomogeneous coating (row E), all pixels except one, which could be removed by setting a threshold in the binary images based on the pixel quantity of highlighted pixel clusters, were correctly assigned to class 2. Specificity and sensitivity (Eqs. 8 and 9) of the classification model, which were calculated based on all pixels of the homogeneously coated and uncoated test tablets (rows A and B) are both 1.0 for both class 1 as well as class 2 indicating an adequate model quality. Thus, the defects of the investigated coated tablets that are accompanied by appearance of the subjacent ASA formulation could be clearly detected by a SIMCA classification model based on their UV images.

Subsequently, localization of these defects was achieved by calculation of the distance from the center of the tablet to the center of the defects, which gives valuable information for readjustment of the coating process parameters. By comparing the defects found by application of either the edge detection algorithm or of the SIMCA model, a differentiation of coating defects that are not accompanied by appearance of

the subjacent ASA tablet and defects resulting from chipped coatings parts could be achieved.

It has to be mentioned that the detection of coating defects which are accompanied by the appearance of the subjacent tablet formulation are routinely performed by machine vision systems working in the VIS range. However, for a reliable detection of coating defects with VIS instruments, usually a high contrast in coloration between the coating layer and the tablet formulation is required. In contrast to VIS imaging, UV imaging is able to distinguish between different compounds based on their chemical nature irrespective of the contrast in coloration between them (218). As different chemical compounds show distinct UV profiles, this fact is considered to be a major benefit of UV imaging compared to systems working in the VIS range and it indicates the potential of UV imaging for the detection of defects even if the applied coating is of similar color (such as a moisture barrier coating) as the tablet formulation.

3.4.2 Evaluation of tablet coating texture

A homogeneous surface texture accompanied by adequate appearance and gloss of the coating layer is usually a desired endpoint of the tablet coating process as the surface characteristics markedly affect product quality and performance (6). To investigate if UV images are suitable to distinguish between coated ASA tablets with the desired homogeneous surface texture (Fig. 33: row A) and those with an unacceptably inhomogeneous coating (Fig. 33: row B), representative coated tablets of both groups were chosen based on their visual appearance (Fig. 33: column I) and subsequently analyzed by UV imaging.

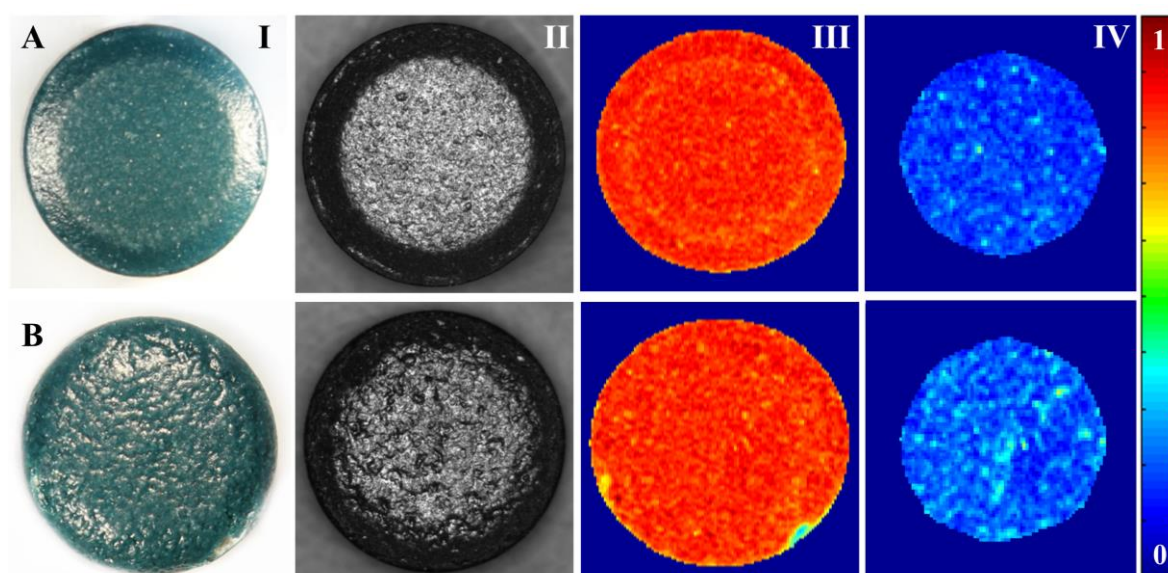


Fig. 33: Image analysis of representative ASA tablets with an acceptably homogeneous (a) or an inhomogeneous (b) coating texture. Columns from left to right correspond to photographic images (I), photometric stereo darkfield images (II), UV images at 365 nm (III), and PC-1 scores images (IV).

It is well-known from the literature that spectral techniques working in diffuse reflectance mode are sensitive to variations in the surface texture of the samples (174, 281). Surface texture variations accompany spectral differences that manifest

themselves in a spectral baseline offset rather than in a specific absorbance at a given wavelength (191, 222, 223). To confirm the different surface textures of tablets that visually appear either homogeneous or inhomogeneous (Fig. 33: column I), in a first step darkfield images of the coated ASA tablets were captured by a photometric stereo imager to obtain a detailed surface map. It is obvious from the resulting images that the tablet visually considered to be smooth exhibits a rather homogeneous surface texture throughout the entire surface with small valleys and peaks on a micro scale (Fig. 33: column II, row A). In contrast, the surface of the tablet considered to be unacceptably inhomogeneous clearly shows irregularities on a larger scale (Fig. 33: column II, row B), which is in agreement with the photographs. In Fig. 33, column III, the 365 nm channel UV images of the respective tablets are shown. To monitor the UV spectral variance throughout the coated ASA tablets in relation to each other in all six wavelengths of the UV images, PCA was applied to the UV image pixels of the central regions of 16 homogeneously ($n=8$) and inhomogeneously ($n=8$) coated tablets simultaneously. It is assumed that the variations in surface texture of the coated tablets cause major spectral differences that are consequently captured by PC-1 and are visualized in the scores images. As shown in Fig. 33, column IV, the PC-1 score intensity varies less throughout the surface of the tablet with a homogeneous coating (Fig. 33: row A) compared to the tablet with an inhomogeneous coating (Fig. 33: row B) and thus indicates a more even surface texture. As expected, the mean UV spectra of representative pixels with a low and high PC-1 score intensity mainly differ in the spectral baseline (Fig. 34a). Accordingly, the loadings plot of PC-1 (Fig. 34b) that explains 99.9 % of the spectral variance mainly reflects the shape of

the UV spectra and thus verifies that PC-1 captures spectral differences resulting from physical irregularities in the coating surface (246).

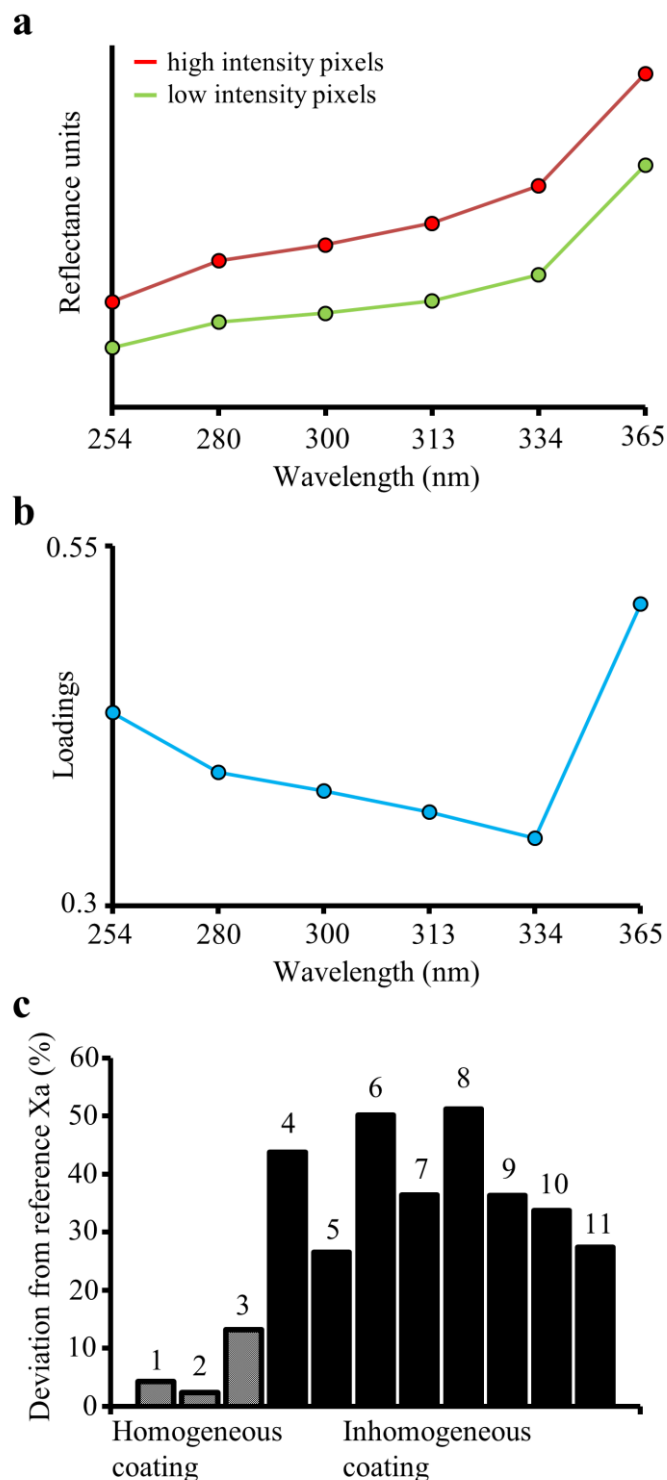


Fig. 34: (a) Mean UV spectra of high and low PC-1 score intensity pixels (b) Loadings plot of PC-1 (c) Deviation of the average score variation (X_a) of 11 test tablets from the mean reference X_a of tablets with the desired coating texture.

To systematically compare the coating texture of the investigated tablets and to identify tablets that do not exhibit the desired homogeneous coating, the average score variation (X_a , Eq. 16) was calculated for each of 16 coated tablets from the respective PC-1 scores images as estimate for the coating surface texture. A reference dataset composed of the PC-1 scores images of five tablets with a homogeneous coating was used to calculate a mean X_a value which is representative for tablets with the desired coating profile. Subsequently, the PC-1 scores images of another 11 tablets of the entire dataset with visually acceptable appearance (Fig. 34c: samples 1-3) and with an unacceptably inhomogeneous coating (Fig. 34c: samples 4-11) were analyzed by calculation of the deviation of the respective X_a from the mean X_a of the reference tablets (= 100%). It is obvious from Fig. 34c that tablets with a visually homogeneous coating show X_a values that are only about 3-13 % higher than the mean X_a value of the reference set (samples 1-3), while tablets with a visually inhomogeneous coating differ from the reference X_a by values between 27 % and 51 %. Thus, tablets that exhibit an unacceptably inhomogeneous coating can be distinguished from those with a homogeneous coating by defining a limit of acceptable deviation from the mean X_a of tablets with desired coating texture. Thus, the estimation of the degree of coating surface homogeneity and thus the detection of insufficient coating quality was successfully based on six-wavelengths UV images. It is worth to mention that because there is a systematic variation, i.e. a baseline shift, between the spectra in terms of texture analysis, a further reduction of the number of wavelengths, which would be accompanied by an increased sample throughput, might be possible to facilitate the measurement in the process environment. Such a reduction of the number of

wavelengths can be justified if the analysis is started out with a higher number of wavelengths to establish a robust model and subsequently reduced in the number of wavelengths until the robustness and reliability of the model significantly decreases. However, such a reduction of the number of wavelengths has to be applied with caution, because the loading plot in Fig. 34 clearly suggests that all wavelengths are used to describe the underlying variation of the data (all wavelengths show a loading value being different from 0).

It is worth to mention that in this study analysis of the coating intactness and texture by UV imaging is based on different PCA models and texture analysis has only been applied to tablets that have previously shown to be intactly coated. Thus, the PCA model for texture analysis is trained particularly on intactly coated tablets and consequently provides reliable results only with regard to the coating texture of these tablets. To avoid misleading conclusions, it is essential that the two PCA models for evaluation of tablet coating intactness and for texture analysis are applied to the test tablets one after another.

3.4.3 Conclusion

Multispectral UV imaging allowed accurate and fast characterization of tablet coating layer intactness. Coating defects such as chipped parts, cracks, and inhomogeneities could be detected and analyzed by image analysis routines applied to the UV images of the coated ASA tablets. Tablets with intact coating and either homogeneous or inhomogeneous coating texture were successfully differentiated based on the UV images. The amount and relevance of the obtained data combined with a high speed image acquisition makes UV imaging an attractive technique for at-line quality control of the coating process. In this context, the implementation of multispectral UV imaging in the manufacturing line of coated tablets has to be further investigated. Furthermore, although neither warming of the samples nor any visual changes of the tablet coating were observed after exposure of the samples to UV radiation during the measurements, the potential influence of UV radiation on curing of the tablet coating should be investigated in a further study.

4 References

-
- [1] Celik, M.
Pharmaceutical powder compaction technology.
2nd ed., Informa Healthcare, London (2011)
- [2] Silva, C.O., Sarmento, B., Reis, C.P.
Oral Delivery of Biopharmaceuticals.
In: Mucosal Delivery of Biopharmaceuticals
(das Neves, J., Sarmento, B., eds.): 125–47, Springer US, Boston (2014)
- [3] Pavlou, F., Sutton, S.
Tabletting: the issues facing today's manufacturers.
Pharm. Technol. Eur. 22 (2010)
- [4] Jivraj, M., Martini, L.G., Thomson, C.M.
An overview of the different excipients useful for the direct compression of tablets.
Pharm. Sci. Technol. Today 3(2): 58–63 (2000)
- [5] Plumb, K.
Continuous Processing in the Pharmaceutical Industry.
Chem. Eng. Res. Des. 83(6): 730–738 (2005)
- [6] Rohera, B.D., Parikh, N.H.
Influence of plasticizer type and coat level on Surelease film properties.
Pharm. Dev. Technol. 7(4): 407–420 (2002)
- [7] Pearnchob, N., Siepmann, J., Bodmeier, R.
Pharmaceutical applications of shellac: moisture-protective and taste-masking coatings and extended-release matrix tablets.
Drug Dev. Ind. Pharm. 29(8): 925–938 (2003)
- [8] Siepmann, F., Hoffmann, A., Leclercq, B., Carlin, B., Siepmann, J.
How to adjust desired drug release patterns from ethylcellulose-coated dosage forms.
J. Control. Release 119(2): 182–189 (2007)
- [9] Levina, M., Cunningham, C.R.
The effect of core design and formulation on the quality of film coated tablets.
Pharm. Technol. Eur. 17(4): 29–37 (2005)
- [10] Sohi, H., Sultana, Y., Khar, R.K.
Taste masking technologies in oral pharmaceuticals: recent developments and approaches.
Drug Dev. Ind. Pharm. 30(5): 429–448 (2004)
-

-
- [11] Možina, M., Tomaževič, D., Pernuš, F., Likar, B.
Real-time image segmentation for visual inspection of pharmaceutical tablets.
Mach. Vis. Appl. 22(1): 145–156 (2011)
- [12] Kesselheim, A.S. et al.
Variations in pill appearance of antiepileptic drugs and the risk of nonadherence.
JAMA Intern. Med. 173(3): 202–208 (2013)
- [13] Food and Drug Administration
Code of Federal Regulations Title 21. Part 206. Imprinting of solid oral dosage form drug products for human use (2014 revised).
<http://www.ecfr.gov/cgi-bin/text-idx?SID=5b934d170fd3e069135ed47883b4261b&mc=true&node=pt21.4.206&rgn=div5>.
Accessed 21 September 2015.
- [14] Sinka, I.C., Cunningham, J.C., Zavaliangos, A.
Analysis of tablet compaction. II. Finite element analysis of density distributions in convex tablets.
J. Pharm. Sci. 93(8): 2040–2053 (2004)
- [15] Sinka, I., Cunningham, J., Zavaliangos, A.
The effect of wall friction in the compaction of pharmaceutical tablets with curved faces: a validation study of the Drucker–Prager Cap model.
Powder Technol. 133(1-3): 33–43 (2003)
- [16] Higuchi, T., Narsimha Rao, A., Busse, J.W., Swintosky, J.V.
The physics of tablet compression. II. The influence of degree of compression on properties of tablets.
J. Pharm. Sci. 42(4): 194–200 (1953)
- [17] Hiestand, E.N., Wells, J.E., Peot, C.B., Ochs, J.F.
Physical processes of tableting.
J. Pharm. Sci. 66(4): 510–519 (1977)
- [18] Wray, P.E.
The Physics of Tablet Compaction Revisited.
Drug Dev. Ind. Pharm. 18(6-7): 627–658 (1992)
-

-
- [19] Food and Drug Administration
Pharmaceutical CGMPs for the 21st Century: a risk-based approach (2004).
<http://www.fda.gov/downloads/Drugs/DevelopmentApprovalProcess/Manufacturing/QuestionsandAnswersonCurrentGoodManufacturingPractices/cGMPforDrugs/UCM176374>.
Accessed 15 May 2015.
- [20] Food and Drug Administration
Guidance for Industry: PAT - a framework for innovative pharmaceutical development, manufacturing, and quality assurance (2004).
<http://www.fda.gov/downloads/Drugs/Guidances/ucm070305>.
Accessed 15 May 2015.
- [21] Tho, I., Bauer-Brandl, A.
Chemometrics (PCA) in Pharmaceuticals: Tablet Development, Manufacturing and Quality Assurance.
In: Principal Component Analysis - Multidisciplinary Applications (Sanguansat, P., ed.): 43–58, InTech, Rijeka (2012)
- [22] Bruno, B.J., Miller, G.D., Lim, C.S.
Basics and recent advances in peptide and protein drug delivery.
Ther. Deliv. 4(11): 1443–1467 (2013)
- [23] Leonard, T.W., Lynch, J., McKenna, M.J., Brayden, D.J.
Promoting absorption of drugs in humans using medium-chain fatty acid-based solid dosage forms: GIPET.
Expert Opin. Drug Deliv. 3(5): 685–692 (2006)
- [24] Lax, R., Meenan, C.
Challenges for Therapeutic Peptides Part 2: Delivery Systems.
Innov. Pharm. Technol. (43): 42–44 (2012)
- [25] Choonara, B.F., Choonara, Y.E., Kumar, P., Bijukumar, D., Du Toit, L.C., Pillay, V.
A review of advanced oral drug delivery technologies facilitating the protection and absorption of protein and peptide molecules.
Biotechnol. Adv. 32(7): 1269–1282 (2014)
- [26] Arakawa, T., Prestrelski, S.J., Kenney, W.C., Carpenter, J.F.
Factors affecting short-term and long-term stabilities of proteins.
Adv. Drug Deliv. Rev. 46(1-3): 307–326 (2001)
-

-
- [27] Pinto Reis, C., Silva, C., Martinho, N., Rosado, C.
Drug carriers for oral delivery of peptides and proteins: accomplishments and future perspectives.
Ther. Deliv. 4(2): 251–265 (2013)
- [28] Carl, S.M., Mehta, N., Stern, W.
Oral delivery of peptides by Peptelligence technology.
Drug Dev. Deliv. 27: 12–15 (2013)
- [29] Lewis, A.L., Richard, J.
Challenges in the delivery of peptide drugs: an industry perspective.
Ther. Deliv. 6(2): 149–163 (2015)
- [30] Binkley, N. et al.
A phase 3 trial of the efficacy and safety of oral recombinant calcitonin: the Oral Calcitonin in Postmenopausal Osteoporosis (ORACAL) trial.
J. Bone Miner. Res. 27(8): 1821–1829 (2012)
- [31] Aungst, B.J.
Absorption enhancers: applications and advances.
AAPS J. 14(1): 10–18 (2012)
- [32] Maher, S., Leonard, T.W., Jacobsen, J., Brayden, D.J.
Safety and efficacy of sodium caprate in promoting oral drug absorption: from in vitro to the clinic.
Adv. Drug Deliv. Rev. 61(15): 1427–1449 (2009)
- [33] Mullard, A.
Oral GLP1 analogue rounds Phase II corner.
Nat. Rev. Drug Discov. 14(4): 227 (2015)
- [34] Tscheik, C., Blasig, I.E., Winkler, L.
Trends in drug delivery through tissue barriers containing tight junctions.
Tissue Barriers 1(2): 1–8 (2013)
- [35] Kotla, N.G., Shivapooja, A.
Recent Developments in Colon Specific Drug Delivery Systems: Approaches Promising in Targeting Colon.
Int. J. Pharm. Clin. Res. 6(1): 101–106 (2014)
- [36] Brayden, D.J., Mrsny, R.J.
Oral peptide delivery: prioritizing the leading technologies.
Ther. Deliv. 2(12): 1567–1573 (2011)
-

-
- [37] Geoffroy, J.M., Rivkees, D.
Pharmaceutical Manufacturing: Changes in Paradigms.
In: Pharmaceutical Dosage Forms - Tablets: Manufacture and Process Control, 3rd ed. (Augsburger, L.L., Hoag, S.W., eds.): 85–119, Informa Healthcare, New York (2008)
- [38] European Medicines Agency
Directive 2003/94/EC for medicines and investigational medicines for human use (2003).
<http://eur-lex.europa.eu/legal-content/EN/TXT/?uri=celex:32003L0094>.
Accessed 21 September 2015.
- [39] Food and Drug Administration
Code of federal regulations title 21. Part 211. Current Good Manufacturing Practice for finished pharmaceuticals (2014).
<http://www.accessdata.fda.gov/scripts/cdrh/cfdocs/cfcfr/CFRSearch.cfm?CFRPart=211&showFR=1>.
Accessed 15 May 2015.
- [40] Food and Drug Administration
Code of federal regulations title 21. Part 210. Current Good Manufacturing Practice in manufacturing, processing, packing, or holding of drugs (2014).
<http://www.accessdata.fda.gov/scripts/cdrh/cfdocs/cfcfr/CFRSearch.cfm?CFRPart=210&showFR=1>.
Accessed 15 May 2015.
- [41] ICH
Good manufacturing practice guide for active pharmaceutical ingredients Q7 (2000).
http://www.ich.org/fileadmin/Public_Web_Site/ICH_Products/Guidelines/Quality/Q7/Step4/Q7_Guideline.
Accessed 8 January 2015.
- [42] Nally, J.D.
Status and Applicability of U.S. Regulations: Current Good Manufacturing Practices in Manufacturing, Processing, Packaging, and Holding of Drugs.
In: Good manufacturing practices for pharmaceuticals, 6th ed. (Nally, J.D., ed.): 1–12, CRC Press, Boca Raton (2007)
- [43] Food and Drug Administration
Guidance for Industry: Changes to an approved NDA or ANDA (2004).
<http://www.fda.gov/downloads/drugs/guidancecomplianceregulatoryinformation/guidances/ucm077097>.
Accessed 15 May 2015.
-

-
- [44] Yu, L.X.
Pharmaceutical quality by design: product and process development, understanding, and control.
Pharm. Res. 25(4): 781–791 (2008)
- [45] Clark, G.
FDA's PAT initiative.
Pharm. Technol. Eur. (10) (2004)
- [46] De Beer, T., Burggraeve, A., Fonteyne, M., Saerens, L., Remon, J.P., Vervaet, C.
Near infrared and Raman spectroscopy for the in-process monitoring of pharmaceutical production processes.
Int. J. Pharm. 417(1-2): 32–47 (2011)
- [47] ICH
Guideline on pharmaceutical development Q8 (2R) (2009).
http://www.ich.org/fileadmin/Public_Web_Site/ICH_Products/Guidelines/Quality/Q8_R1/Step4/Q8_R2_Guideline.
Accessed 15 May 2015.
- [48] Lionberger, R.A., Lee, S.L., Lee, L., Raw, A., Yu, L.X.
Quality by design: concepts for ANDAs.
AAPS J. 10(2): 268–276 (2008)
- [49] Bakeev, K.A., Menezes, J.C.
Future Trends for PAT for Increased Process Understanding and Growing Applications in Biomanufacturing.
In: Process Analytical Technology, 2nd ed. (Bakeev, K.A., ed.): 521–43, John Wiley & Sons, Chichester (2010)
- [50] Buchholz, S.
Future manufacturing approaches in the chemical and pharmaceutical industry.
Chem. Eng. Process. 49(10): 993–995 (2010)
- [51] Poechlauer, P., Manley, J., Broxterman, R., Gregertsen, B., Ridemark, M.
Continuous Processing in the Manufacture of Active Pharmaceutical Ingredients and Finished Dosage Forms: An Industry Perspective.
Org. Process Res. Dev. 16(10): 1586–1590 (2012)
-

-
- [52] Chatterjee, S.
FDA Perspective on Continuous Manufacturing: IFPAC Annual Meeting, Baltimore (2012).
<http://www.fda.gov/downloads/AboutFDA/CentersOffices/OfficeofMedicalProductsandTobacco/CDER/UCM341197>.
Accessed 17 August 2015.
- [53] Schaber, S.D., Gerogiorgis, D.I., Ramachandran, R., Evans, J.M., Barton, P.I., Trout, B.L.
Economic Analysis of Integrated Continuous and Batch Pharmaceutical Manufacturing: A Case Study.
Ind. Eng. Chem. Res. 50(17): 10083–10092 (2011)
- [54] Leuenberger, H.
New trends in the production of pharmaceutical granules: batch versus continuous processing.
Eur. J. Pharm. Biopharm. 52(3): 289–296 (2001)
- [55] Robert, J.-L.
Q8(R2): Pharmaceutical Development: ICH-GCG ASEAN, Kuala Lumpur (2010).
http://www.ich.org/fileadmin/Public_Web_Site/Training/ICH_Endorsed_Training_Events/ASEAN_training_on_Q8_Q9_Q10_Guidelines/Q8_Pharmaceutical_development_JL.Robert.
Accessed 12 July 2015.
- [56] Fahmy, R., Kona, R., Dandu, R., Xie, W., Claycamp, G., Hoag, S.W.
Quality by design I: Application of failure mode effect analysis (FMEA) and Plackett-Burman design of experiments in the identification of "main factors" in the formulation and process design space for roller-compacted ciprofloxacin hydrochloride immediate-release tablets.
AAPS PharmSciTech 13(4): 1243–1254 (2012)
- [57] Funke, A.
QbD in der Praxis – systematisches Vorgehen bei der Entwicklung pharmazeutischer Herstellprozesse: Symposium der Fachgruppe Arzneimittelkontrolle / Pharmazeutische Analytik der DPhG, Braunschweig (2013).
https://www.tu-braunschweig.de/Medien-DB/pharmchem/funke_dphg_2013.
Accessed 13 April 2015.
-

-
- [58] Lawrence, X.Y., Lionberger, R., Olson, M.C., Johnston, G., Buehler, G., Winkle, H.
Quality by design for generic drugs.
Pharm. Technol. 33(10): 122–127 (2009)
- [59] Nosal, R., Schultz, T.
PQLI Definition of Criticality.
J. Pharm. Innov. 3(2): 69–78 (2008)
- [60] Igne, B., Anderson, C.A., Drennen, J.K.
Radial tensile strength prediction of relaxing and relaxed compacts by near-infrared chemical imaging.
Int. J. Pharm. 418(2): 297–303 (2011)
- [61] Venables, H.J., Wells, J.I.
Powder Mixing.
Drug Dev. Ind. Pharm. 27(7): 599–612 (2001)
- [62] Wahl, P.R., Fruhmann, G., Sacher, S., Straka, G., Sowinski, S., Khinast, J.G.
PAT for tableting: inline monitoring of API and excipients via NIR spectroscopy.
Eur. J. Pharm. Biopharm. 87(2): 271–278 (2014)
- [63] Mateo-Ortiz, D., Muzzio, F.J., Méndez, R.
Particle size segregation promoted by powder flow in confined space: the die filling process case.
Powder Technol. 262: 215–222 (2014)
- [64] European Directorate for the Quality of Medicines and HealthCare
European pharmacopoeia.
8th ed., Council of Europe, Strasbourg (2013)
- [65] Narang, A.S., Rao, V.M., Guo, H., Lu, J., Desai, D.S.
Effect of force feeder on tablet strength during compression.
Int. J. Pharm. 401(1-2): 7–15 (2010)
- [66] Mendez, R., Muzzio, F.J., Velazquez, C.
Powder hydrophobicity and flow properties: effect of feed frame design and operating parameters.
AIChE J. 58(3): 697–706 (2012)
- [67] Mehrotra, A., Llusa, M., Faqih, A., Levin, M., Muzzio, F.J.
Influence of shear intensity and total shear on properties of blends and tablets of lactose and cellulose lubricated with magnesium stearate.
Int. J. Pharm. 336(2): 284–291 (2007)
-

-
- [68] Kakimi, K., Niwa, T., Danjo, K.
Influence of compression pressure and velocity on tablet sticking.
Chem. Pharm. Bull. 58(12): 1565–1568 (2010)
- [69] Tousey, M.D.
Sticking and picking: some causes and remedies.
Tablets and capsules (10) (2003)
- [70] Waimer, F., Krumme, M., Danz, P., Tenter, U., Schmidt, P.C.
The influence of engravings on the sticking of tablets. Investigations with an instrumented upper punch.
Pharm. Dev. Technol. 4(3): 369–375 (1999)
- [71] Možina, M., Tomaževič, D., Pernuš, F., Likar, B.
Automated visual inspection of imprint quality of pharmaceutical tablets.
Mach. Vis. Appl. 24(1): 63–73 (2013)
- [72] Eiliazadeh, B., Briscoe, B.J., Sheng, Y., Pitt, K.
Investigating density distributions for tablets of different geometry during the compaction of pharmaceuticals.
Part. Sci. Technol. 21(4): 303–316 (2003)
- [73] Ellison, C.D., Ennis, B.J., Hamad, M.L., Lyon, R.C.
Measuring the distribution of density and tableting force in pharmaceutical tablets by chemical imaging.
J. Pharm. Biomed. Anal. 48(1): 1–7 (2008)
- [74] Michrafy, A., Kadiri, M.S., Dodds, J.A.
Wall friction and its effects on the density distribution in the compaction of pharmaceutical excipients.
Chem. Eng. Res. Des. 81(8): 946–952 (2003)
- [75] Han, L.H., Elliott, J.A., Bentham, A.C., Mills, A., Amidon, G.E., Hancock, B.C.
A modified Drucker-Prager Cap model for die compaction simulation of pharmaceutical powders.
Int. J. Solids Struct. 45(10): 3088–3106 (2008)
- [76] Sixsmith, D., McCluskey, D.
The effect of punch tip geometry on powder movement during the tableting process.
J. Pharm. Pharmacol. 33(1): 79–81 (1981)
- [77] Ho, L. et al.
Analysis of sustained-release tablet film coats using terahertz pulsed imaging.
J. Control. Release 119(3): 253–261 (2007)
-

-
- [78] Food and Drug Administration
Guidance for Industry: Container closure systems for packaging human drugs and biologics (1999).
<http://www.fda.gov/downloads/Drugs/Guidances/ucm070551>.
Accessed 15 May 2015.
- [79] Waterman, K.C., MacDonald, B.C.
Package selection for moisture protection for solid, oral drug products.
J. Pharm. Sci. 99(11): 4437–4452 (2010)
- [80] Nelson, E., Busse, L.W., Higuchi, T.
The physics of tablet compression. VII. Determination of energy expenditure in the tablet compression process.
J. Pharm. Sci. 44(4): 223–225 (1955)
- [81] Frokjaer, S., Otzen, D.E.
Protein drug stability: a formulation challenge.
Nat. Rev. Drug Discov. 4(4): 298–306 (2005)
- [82] Forbes, R.T., Barry, B.W., Elkordy, A.A.
Preparation and characterisation of spray-dried and crystallised trypsin: FT-Raman study to detect protein denaturation after thermal stress.
Eur. J. Pharm. Sci. 30(3–4): 315–323 (2007)
- [83] Henzler-Wildman, K.A., Lee, D.K., Ramamoorthy, A.
Determination of alpha-helix and beta-sheet stability in the solid state: a solid-state NMR investigation of poly(L-alanine).
Biopolymers 64(5): 246–254 (2002)
- [84] Otsuka, M., Fukui, Y., Otsuka, K., Ozaki, Y.
Comparative evaluation of bioactivity change of crystalline trypsin during compression by chemoinformatics and 2-D Fourier-transform infrared spectroscopy.
Analyst 131(10): 1116–1121 (2006)
- [85] Jorgensen, L., Hostrup, S., Moeller, E.H., Grohgan, H.
Recent trends in stabilising peptides and proteins in pharmaceutical formulation - considerations in the choice of excipients.
Expert Opin. Drug Deliv. 6(11): 1219–1230 (2009)
- [86] Rosenberg, A.S.
Effects of protein aggregates: an immunologic perspective.
AAPS J. 8(3): E501–7 (2006)
-

-
- [87] Costantino, H.R., Griebenow, K., Mishra, P., Langer, R., Klibanov, A.M.
Fourier-transform infrared spectroscopic investigation of protein stability
in the lyophilized form.
Biochim. Biophys. Acta, Protein Struct. Mol. Enzymol. 1253(1): 69–74
(1995)
- [88] Griebenow, K., Klibanov, A.M.
Lyophilization-induced reversible changes in the secondary structure of
proteins.
Proc. Natl. Acad. Sci. U. S. A. 92(24): 10969–10976 (1995)
- [89] Maltesen, M.J., Bjerregaard, S., Hovgaard, L., Havelund, S., van de Weert, M.
Analysis of insulin allostery in solution and solid state with FTIR.
J. Pharm. Sci. 98(9): 3265–3277 (2009)
- [90] Dong, A., Prestrelski, S.J., Allison, S.D., Carpenter, J.F.
Infrared spectroscopic studies of lyophilization- and temperature-induced
protein aggregation.
J. Pharm. Sci. 84(4): 415–424 (1995)
- [91] Prestrelski, S.J., Tedeschi, N., Arakawa, T., Carpenter, J.F.
Dehydration-induced conformational transitions in proteins and their
inhibition by stabilizers.
Biophys. J. 65(2): 661–671 (1993)
- [92] Picker, K.M.
Influence of tableting on the enzymatic activity of different α -amylases
using various excipients.
Eur. J. Pharm. Biopharm. 53(2): 181–185 (2002)
- [93] Wurster, D.E., Ternik, R.L.
Pressure-induced activity loss in solid state catalase.
J. Pharm. Sci. 84(2): 190–194 (1995)
- [94] Chan, H., Ongpipattanakul, B., Au-Yeung, J.
Aggregation of rhDNase occurred during the compression of KBr pellets
used for FTIR spectroscopy.
Pharm. Res. 13(2): 238–242 (1996)
- [95] Wolkers, W.F., Oldenhof, H.
In situ FTIR assessment of dried *Lactobacillus bulgaricus*: KBr disk
formation affects physical properties.
Spectrosc. 19(2): 89–99 (2005)
-

-
- [96] Meyer, J.D., Manning, M.C., Carpenter, J.F.
Effects of potassium bromide disk formation on the infrared spectra of dried model proteins.
J. Pharm. Sci. 93(2): 496–506 (2004)
- [97] Zacour, B.M., Drennen, J.K., Anderson, C.A.
Development of a fluid bed granulation design space using critical quality attribute weighted tolerance intervals.
J. Pharm. Sci. 101(8): 2917–2929 (2012)
- [98] Guenard, R., Thureau, G.
Implementation of Process Analytical Technologies.
In: *Process Analytical Technology*, 2nd ed. (Bakeev, K.A., ed.): 17–36, John Wiley & Sons, Chichester (2010)
- [99] United States Pharmacopeia Convention
United States Pharmacopeia and National Formulary.
30th ed., Port City Press, Baltimore (2007)
- [100] Dickens, J.E.
Overview of Process Analysis and PAT.
In: *Process Analytical Technology*, 2nd ed. (Bakeev, K.A., ed.): 1–15, John Wiley & Sons, Chichester (2010)
- [101] Popp, J., Tuchin, V.V., Chiou, A., Heinemann, S.H.
Handbook of biophotonics: Photonics in pharmaceuticals, bioanalysis and environmental research.
1st ed., Wiley-VCH, Weinheim (2012)
- [102] Tabasi, S.H., Fahmy, R., Bensley, D., O'Brien, C., Hoag, S.W.
Quality by design, part I: application of NIR spectroscopy to monitor tablet manufacturing process.
J. Pharm. Sci. 97(9): 4040–4051 (2008)
- [103] Romero-Torres, S., Pérez-Ramos, J.D., Morris, K.R., Grant, E.R.
Raman spectroscopic measurement of tablet-to-tablet coating variability.
J. Pharm. Biomed. Anal. 38(2): 270–274 (2005)
- [104] Romero-Torres, S., Pérez-Ramos, J.D., Morris, K.R., Grant, E.R.
Raman spectroscopy for tablet coating thickness quantification and coating characterization in the presence of strong fluorescent interference.
J. Pharm. Biomed. Anal. 41(3): 811–819 (2006)
-

-
- [105] Andersson, M., Folestad, S., Gottfries, J., Johansson, M.O., Josefson, M., Wahlund, K.-G.
Quantitative analysis of film coating in a fluidized bed process by in-line NIR spectrometry and multivariate batch calibration.
Anal. Chem. 72(9): 2099–2108 (2000)
- [106] Andersson, M., Josefson, M., Langkilde, F.W., Wahlund, K.G.
Monitoring of a film coating process for tablets using near infrared reflectance spectrometry.
J. Pharm. Biomed. Anal. 20(1-2): 27–37 (1999)
- [107] Kirsch, J.D., Drennen, J.K.
Near-infrared spectroscopy: applications in the analysis of tablets and solid pharmaceutical dosage forms.
Appl. Spectrosc. Rev. 30(3): 139–174 (1995)
- [108] Kirsch, J.D., Drennen, J.K.
Nondestructive tablet hardness testing by near-infrared spectroscopy: a new and robust spectral best-fit algorithm.
J. Pharm. Biomed. Anal. 19(3-4): 351–362 (1999)
- [109] Reich, G.
Near-infrared spectroscopy and imaging: basic principles and pharmaceutical applications.
Adv. Drug Deliv. Rev. 57(8): 1109–1143 (2005)
- [110] Möltgen, C.-V., Herdling, T., Reich, G.
A novel multivariate approach using science-based calibration for direct coating thickness determination in real-time NIR process monitoring.
Eur. J. Pharm. Biopharm. 85(3 Pt B): 1056–1063 (2013)
- [111] Rantanen, J.
Process analytical applications of Raman spectroscopy.
J. Pharm. Pharmacol. 59(2): 171–177 (2007)
- [112] Ryan, J.A., Compton, S.V., Brooks, M.A., Compton, D.A.
Rapid verification of identity and content of drug formulations using mid-infrared spectroscopy.
J. Pharm. Biomed. Anal. 9(4): 303–310 (1991)
- [113] Gustafsson, C., Nyström, C., Lennholm, H., Bonferoni, M.C., Caramella, C.M.
Characteristics of hydroxypropyl methylcellulose influencing compactibility and prediction of particle and tablet properties by infrared spectroscopy.
J. Pharm. Sci. 92(3): 494–504 (2003)
-

-
- [114] Lewis, I.R., Edwards, H.
Handbook of Raman spectroscopy: from the research laboratory to the process line.
28th ed., CRC Press, New York (2001)
- [115] Chalmers, J.M., Griffiths, P.R., eds.
Handbook of Vibrational Spectroscopy.
1st ed., John Wiley & Sons, Chichester (2002)
- [116] Siesler, H.W., Ozaki, Y., Kawata, S., Heise, H.M.
Near-infrared spectroscopy: principles, instruments, applications.
1st ed., Wiley-VCH, Weinheim (2002)
- [117] Smith, B.C.
Fundamentals of Fourier transform infrared spectroscopy.
2nd ed., CRC Press, Boca Raton (2011)
- [118] Workman Jr, J., Weyer, L.
Practical Guide and Spectral Atlas for Interpretive Near-infrared Spectroscopy.
2nd ed., CRC Press, Boca Raton (2012)
- [119] Blanco, M., Alcalá, M.
Content uniformity and tablet hardness testing of intact pharmaceutical tablets by near infrared spectroscopy.
Anal. Chim. Acta 557(1-2): 353–359 (2006)
- [120] Blanco, M., Alcalá, M., González, J.M., Torras, E.
A process analytical technology approach based on near infrared spectroscopy: tablet hardness, content uniformity, and dissolution test measurements of intact tablets.
J. Pharm. Sci. 95(10): 2137–2144 (2006)
- [121] Strachan, C.J., Rades, T., Gordon, K.C., Rantanen, J.
Raman spectroscopy for quantitative analysis of pharmaceutical solids.
J. Pharm. Pharmacol. 59(2): 179–192 (2007)
- [122] De Beer, T.R.M. et al.
In-line and real-time process monitoring of a freeze drying process using Raman and NIR spectroscopy as complementary process analytical technology (PAT) tools.
J. Pharm. Sci. 98(9): 3430–3446 (2009)
- [123] Smith, B.C.
Infrared spectral interpretation: a systematic approach.
2nd ed., CRC Press, Boca Raton (1998)
-

-
- [124] Larkin, P.
Infrared and Raman spectroscopy; principles and spectral interpretation.
1st ed., Elsevier, Waltham (2011)
- [125] Steele, D.
Infrared Spectroscopy: Theory.
In: Handbook of Vibrational Spectroscopy, 1st ed. (Chalmers, J.M., Griffiths, P.R., eds.): 44–70, John Wiley & Sons, Chichester (2002)
- [126] Munson, J., Stanfield, C.F., Gujral, B.
A Review of Process Analytical Technology (PAT) in the U.S. Pharmaceutical Industry.
Curr. Pharm. Anal. 2(4): 405–414 (2006)
- [127] Lewis, E.N., Schoppelrei, J.W., Makein, L., Kidder, L.H., Lee, E.
Near-Infrared Chemical Imaging for Product and Process Understanding.
In: Process Analytical Technology, 2nd ed. (Bakeev, K.A., ed.): 245–79, John Wiley & Sons, Chichester (2010)
- [128] Sašić, S., Blackwood, D., Liu, A., Ward, H.W., Clarke, H.
Detailed analysis of the online near-infrared spectra of pharmaceutical blend in a rotary tablet press feed frame.
J. Pharm. Biomed. Anal. 103C(0): 73–79 (2014)
- [129] Donoso, M., Kildsig, D.O., Ghaly, E.S.
Prediction of tablet hardness and porosity using near-infrared diffuse reflectance spectroscopy as a nondestructive method.
Pharm. Dev. Technol. 8(4): 357–366 (2003)
- [130] Tatavarti, A.S. et al.
Assessment of NIR spectroscopy for nondestructive analysis of physical and chemical attributes of sulfamethazine bolus dosage forms.
AAPS PharmSciTech 6(1): E91-9 (2005)
- [131] Morisseau, K.M., Rhodes, C.T.
Near-infrared spectroscopy as a nondestructive alternative to conventional tablet hardness testing.
Pharm. Res. 14(1): 108–111 (1997)
- [132] Moes, J.J., Ruijken, M.M., Gout, E., Frijlink, H.W., Ugwoke, M.I.
Application of process analytical technology in tablet process development using NIR spectroscopy: blend uniformity, content uniformity and coating thickness measurements.
Int. J. Pharm. 357(1-2): 108–118 (2008)
-

-
- [133] Gendre, C. et al.
Development of a Process Analytical Technology (PAT) for in-line monitoring of film thickness and mass of coating materials during a pan coating operation.
Eur. J. Pharm. Sci. 43(4): 244–250 (2011)
- [134] Kirsch, J.D., Drennen, J.K.
Near-infrared spectroscopic monitoring of the film coating process.
Pharm. Res. 13(2): 234–237 (1996)
- [135] Lee, M.-J. et al.
In line NIR quantification of film thickness on pharmaceutical pellets during a fluid bed coating process.
Int. J. Pharm. 403(1-2): 66–72 (2011)
- [136] Aldridge, P.K., Mushinsky, R.F., Andino, M.M., Evans, C.L.
Identification of tablet formulations inside blister packages by near-infrared spectroscopy.
Appl. spectrosc. 48(10): 1272–1276 (1994)
- [137] Herkert, T., Prinz, H., Kovar, K.-A.
One hundred percent online identity check of pharmaceutical products by near-infrared spectroscopy on the packaging line.
Eur. J. Pharm. Biopharm. 51(1): 9–16 (2001)
- [138] Dempster, M.A., MacDonald, B.F., Gemperline, P.J., Boyer, N.R.
A near-infrared reflectance analysis method for the noninvasive identification of film-coated and non-film-coated, blister-packed tablets.
Anal. Chim. Acta 310(1): 43–51 (1995)
- [139] Colón, Y.M., Florian, M.A., Acevedo, D., Méndez, R., Romañach, R.J.
Near Infrared Method Development for a Continuous Manufacturing Blending Process.
J. Pharm. Innov. 9(4): 291–301 (2014)
- [140] Martínez, L., Peinado, A., Liesum, L., Betz, G.
Use of near-infrared spectroscopy to quantify drug content on a continuous blending process: influence of mass flow and rotation speed variations.
Eur. J. Pharm. Biopharm. 84(3): 606–615 (2013)
-

-
- [141] Fonteyne, M. et al.
NIR spectroscopic method for the in-line moisture assessment during drying in a six-segmented fluid bed dryer of a continuous tablet production line: Validation of quantifying abilities and uncertainty assessment.
J. Pharm. Biomed. Anal. 100: 21–27 (2014)
- [142] Quiñones, L., Velazquez, C., Obregon, L.
A novel multiple linear multivariate NIR calibration model-based strategy for in-line monitoring of continuous mixing.
AIChE J. 60(9): 3123–3132 (2014)
- [143] Wikström, H., Romero-Torres, S., Wongweragiat, S., Williams, J.A., Grant, E.R., Taylor, L.S.
On-line content uniformity determination of tablets using low-resolution Raman spectroscopy.
Appl. spectrosc. 60(6): 672–681 (2006)
- [144] Fransson, M., Johansson, J., Sparén, A., Svensson, O.
Comparison of multivariate methods for quantitative determination with transmission Raman spectroscopy in pharmaceutical formulations.
J. Chemom. 24(11-12): 674–680 (2010)
- [145] Johansson, J., Pettersson, S., Folestad, S.
Characterization of different laser irradiation methods for quantitative Raman tablet assessment.
J. Pharm. Biomed. Anal. 39(3-4): 510–516 (2005)
- [146] Shah, R.B., Tawakkul, M.A., Khan, M.A.
Process analytical technology: chemometric analysis of Raman and near infra-red spectroscopic data for predicting physical properties of extended release matrix tablets.
J. Pharm. Sci. 96(5): 1356–1365 (2007)
- [147] Heigl, N. et al.
Potential of Raman Spectroscopy for Evaluating Crushing Strength of Tablets.
J. Pharm. Innov. 7(2): 76–86 (2012)
- [148] Müller, J., Knop, K., Thies, J., Uerpmann, C., Kleinebudde, P.
Feasibility of Raman spectroscopy as PAT tool in active coating.
Drug Dev. Ind. Pharm. 36(2): 234–243 (2010)
-

-
- [149] Roggo, Y., Degardin, K., Margot, P.
Identification of pharmaceutical tablets by Raman spectroscopy and chemometrics.
Talanta 81(3): 988–995 (2010)
- [150] Räsänen, E., Sandler, N.
Near infrared spectroscopy in the development of solid dosage forms.
J. Pharm. Pharmacol. 59(2): 147–159 (2007)
- [151] Rajalahti, T., Kvalheim, O.M.
Multivariate data analysis in pharmaceuticals: a tutorial review.
Int. J. Pharm. 417(1-2): 280–290 (2011)
- [152] Chang, B.S., Yeung, B.
Physical Stability of Protein Pharmaceuticals.
In: *Formulation and Process Development Strategies for Manufacturing Biopharmaceuticals* (Jameel, F., Hershenson, S., eds.): 69–104, John Wiley & Sons, Chichester (2010)
- [153] Tantipolphan, R., Rades, T., Medlicott, N.
Insights into the structure of protein by vibrational spectroscopy.
Curr. Pharm. Anal. 4(2): 53–68 (2008)
- [154] van de Weert, M.
Fourier Transform Infrared Spectroscopy.
In: *Methods for Structural Analysis of Protein Pharmaceuticals*, 1st ed. (Jiskoot, W., Crommelin, D., eds.): 131–66, Springer, New York (2005)
- [155] Provencher, S.W., Gloeckner, J.
Estimation of globular protein secondary structure from circular dichroism.
Biochem. 20(1): 33–37 (1981)
- [156] Snyder, D.A. et al.
Comparisons of NMR Spectral Quality and Success in Crystallization Demonstrate that NMR and X-ray Crystallography Are Complementary Methods for Small Protein Structure Determination.
J. Am. Chem. Soc. 127(47): 16505–16511 (2005)
- [157] Wishart, D.S., Sykes, B.D., Richards, F.M.
Simple techniques for the quantification of protein secondary structure by ¹H NMR spectroscopy.
FEBS Lett. 293(1-2): 72–80 (1991)
- [158] Barth, A.
Infrared spectroscopy of proteins.
Biochim. Biophys. Acta 1767(9): 1073–1101 (2007)
-

-
- [159] Kong, J., Yu, S.
Fourier Transform Infrared Spectroscopic Analysis of Protein Secondary Structures.
Acta Biochim. Biophys. Sin. 39(8): 549–559 (2007)
- [160] Fabian, H., Mäntele, W.
Infrared Spectroscopy of Proteins.
In: *Handbook of Vibrational Spectroscopy*, 1st ed. (Chalmers, J.M., Griffiths, P.R., eds.): 3399–425, John Wiley & Sons, Chichester (2002)
- [161] Singh, B.R.
Basic Aspects of the Technique and Applications of Infrared Spectroscopy of Peptides and Proteins.
In: *Infrared Analysis of Peptides and Proteins*, 1st ed. (Singh, B.R., ed.): 2–37, American Chemical Society, Washington DC (1999)
- [162] Chittur, K.K.
FTIR/ATR for protein adsorption to biomaterial surfaces.
Biomaterials 19(4-5): 357–369 (1998)
- [163] Luthra, S., Kalonia, D.S., Pikal, M.J.
Effect of hydration on the secondary structure of lyophilized proteins as measured by fourier transform infrared (FTIR) spectroscopy.
J. Pharm. Sci. 96(11): 2910–2921 (2007)
- [164] Prestrelski, S.J., Byler, D.M., Liebman, M.N.
Comparison of various molecular forms of bovine trypsin: correlation of infrared spectra with x-ray crystal structures: correlation of infrared spectra with x-ray crystal structures.
Biochem. 30(1): 133–143 (1991)
- [165] Haris, P.I.
Fourier transform infrared spectroscopic studies of peptides: potentials and pitfalls.
In: *Infrared Analysis of Peptides and Proteins*, 1st ed. (Singh, B.R., ed.): 54–95, American Chemical Society, Washington DC (1999)
- [166] Wang, Y., Boysen, R.I., Wood, B.R., Kansiz, M., McNaughton, D., Hearn, M.T.W.
Determination of the secondary structure of proteins in different environments by FTIR-ATR spectroscopy and PLS regression.
Biopolymers 89(11): 895–905 (2008)
-

-
- [167] Navea, S., Tauler, R., Goormaghtigh, E., de Juan, A.
Chemometric tools for classification and elucidation of protein secondary structure from infrared and circular dichroism spectroscopic measurements.
Proteins 63(3): 527–541 (2006)
- [168] Byler, D.M., Susi, H.
Examination of the secondary structure of proteins by deconvolved FTIR spectra.
Biopolymers 25(3): 469–487 (1986)
- [169] Cai, S., Singh, B.R.
A distinct utility of the amide III infrared band for secondary structure estimation of aqueous protein solutions using partial least squares methods.
Biochem. 43(9): 2541–2549 (2004)
- [170] Oberg, K.A., Ruysschaert, J.-M., Goormaghtigh, E.
The optimization of protein secondary structure determination with infrared and circular dichroism spectra.
Eur. J. Biochem. 271(14): 2937–2948 (2004)
- [171] Gowen, A.A., O'Donnell, C.P., Cullen, P.J., Bell, S.
Recent applications of chemical imaging to pharmaceutical process monitoring and quality control.
Eur. J. Pharm. Biopharm. 69(1): 10–22 (2008)
- [172] Amigo, J.M.
Practical issues of hyperspectral imaging analysis of solid dosage forms.
Anal. Bioanal. Chem. 398(1): 93–109 (2010)
- [173] Rios, M.
New dimensions in tablet imaging.
Pharm. Technol. 3(32) (2008)
- [174] Gendrin, C., Roggo, Y., Collet, C.
Pharmaceutical applications of vibrational chemical imaging and chemometrics: a review: a review.
J. Pharm. Biomed. Anal. 48(3): 533–553 (2008)
- [175] Amigo, J.M., Ravn, C.
Direct quantification and distribution assessment of major and minor components in pharmaceutical tablets by NIR-chemical imaging.
Eur. J. Pharm. Sci. 37(2): 76–82 (2009)
-

-
- [176] Boldrini, B., Kessler, W., Rebner, K., Kessler, R.
Hyperspectral imaging: a review of best practice, performance and pitfalls for inline and online applications.
J. Near Infrared Spectrosc. 20(5): 438 (2012)
- [177] Griffiths, P.R.
Infrared and Raman Instrumentation for Mapping and Imaging.
In: *Infrared and Raman Spectroscopic Imaging*, 1st ed.
(Salzer, R., Siesler, H.W., eds.): 3–64, Wiley-VCH, Weinheim (2009)
- [178] Gowen, A., O'Donnell, C.P., Cullen, R.J., Downey, G., Frias, J.M.
Hyperspectral imaging – an emerging process analytical tool for food quality and safety control.
Trends Food Sci. Technol. 18(12): 590–598 (2007)
- [179] Tatzer, P., Wolf, M., Panner, T.
Industrial application for inline material sorting using hyperspectral imaging in the NIR range.
Real-Time Imaging 11(2): 99–107 (2005)
- [180] Kulcke, A., Gurschler, C., Spöck, G., Leitner, R., Kraft, M.
On-line classification of synthetic polymers using near infrared spectral imaging.
J. Near Infrared Spectrosc. 11(1): 71 (2003)
- [181] Sacré, P.-Y., De Bleys, C., Chavez, P.-F., Netchacovitch, L., Hubert, P., Ziemons, E.
Data processing of vibrational chemical imaging for pharmaceutical applications.
J. Pharm. Biomed. Anal. 101(0): 123–140 (2014)
- [182] Geladi, P., Grahn, H.F., Burger, J.E.
Multivariate Images, Hyperspectral Imaging: Background and Equipment.
In: *Techniques and Applications of Hyperspectral Image Analysis*, 1st ed.
(Grahn, H.F., Geladi, P., eds.): 1–15, John Wiley & Sons, Chichester (2007)
- [183] Malik, I., Poonacha, M., Moses, J., Lodder, R.A.
Multispectral imaging of tablets in blister packaging.
AAPS PharmSciTech 2(2): E9 (2001)
- [184] Derganc, J., Likar, B., Bernard, R., Tomaževič, D., Pernuš, F.
Real-time automated visual inspection of color tablets in pharmaceutical blisters.
Real-Time Imaging 9(2): 113–124 (2003)
-

-
- [185] Carneiro, R.L., Poppi, R.J.
A quantitative method using near infrared imaging spectroscopy for determination of surface composition of tablet dosage forms: an example of spirolactone tablets.
J. Braz. Chem. Soc. 23(8): 1570–1576 (2012)
- [186] Franch-Lage, F., Amigo, J.M., Skibsted, E., Maspoch, S., Coello, J.
Fast assessment of the surface distribution of API and excipients in tablets using NIR-hyperspectral imaging.
Int. J. Pharm. 411(1-2): 27–35 (2011)
- [187] Palou, A., Cruz, J., Blanco, M., Tomàs, J., de los Ríos, Joaquín, Alcalà, M.
Determination of drug, excipients and coating distribution in pharmaceutical tablets using NIR-CI.
J. Pharm. Anal. 2(2): 90–97 (2012)
- [188] Rosas, J.G., Blanco, M.
A criterion for assessing homogeneity distribution in hyperspectral images. Part 2: application of homogeneity indices to solid pharmaceutical dosage forms.
J. Pharm. Biomed. Anal. 70: 691–699 (2012)
- [189] Cruz, J., Blanco, M.
Content uniformity studies in tablets by NIR-CI.
J. Pharm. Biomed. Anal. 56(2): 408–412 (2011)
- [190] Lee, E., Huang, W.X., Chen, P., Lewis, E.N., Vivilecchia, R.V.
High-throughput analysis of pharmaceutical tablet content uniformity by near-infrared chemical imaging.
Spectrosc. 21(11): 24–32 (2006)
- [191] Ropero, J., Colón, Y., Johnson-Restrepo, B., Romañach, R.J.
Near-infrared chemical imaging slope as a new method to study tablet compaction and tablet relaxation.
Appl. spectrosc. 65(4): 459–465 (2011)
- [192] Cairós, C., Amigo, J.M., Watt, R., Coello, J., Maspoch, S.
Implementation of enhanced correlation maps in near infrared chemical images: application in pharmaceutical research.
Talanta 79(3): 657–664 (2009)
- [193] Maurer, L., Leuenberger, H.
Terahertz pulsed imaging and near infrared imaging to monitor the coating process of pharmaceutical tablets.
Int. J. Pharm. 370(1-2): 8–16 (2009)
-

-
- [194] Hamilton, S.J., Lodder, R.A.
Hyperspectral Imaging Technology for Pharmaceutical Analysis.
Proc. SPIE 4626: 136–147 (2002)
- [195] Šašić, S.
Parallel imaging of active pharmaceutical ingredients in some tablets and blends on Raman and near-infrared mapping and imaging platforms.
Anal. Methods 3(4): 806 (2011)
- [196] Firkala, T., Farkas, A., Vajna, B., Farkas, I., Marosi, G.
Investigation of drug distribution in tablets using surface enhanced Raman chemical imaging.
J. Pharm. Biomed. Anal. 76: 145–151 (2013)
- [197] Vajna, B., Patyi, G., Nagy, Z., Bódis, A., Farkas, A., Marosi, G.
Comparison of chemometric methods in the analysis of pharmaceuticals with hyperspectral Raman imaging.
J. Raman Spectrosc. 42(11): 1977–1986 (2011)
- [198] Slipchenko, M.N., Chen, H., Ely, D.R., Jung, Y., Carvajal, M.T., Cheng, J.-X.
Vibrational imaging of tablets by epi-detected stimulated Raman scattering microscopy.
Analyst 135(10): 2613–2619 (2010)
- [199] Sasić, S.
Raman mapping of low-content API pharmaceutical formulations. I. Mapping of Alprazolam in Alprazolam/Xanax tablets.
Pharm. Res. 24(1): 58–65 (2007)
- [200] Boiret, M., de Juan, A., Gorretta, N., Ginot, Y.-M., Roger, J.-M.
Distribution of a low dose compound within pharmaceutical tablet by using multivariate curve resolution on Raman hyperspectral images.
J. Pharm. Biomed. Anal. 103C: 35–43 (2014)
- [201] Windbergs, M., Jurna, M., Offerhaus, H.L., Herek, J.L., Kleinebudde, P., Strachan, C.J.
Chemical imaging of oral solid dosage forms and changes upon dissolution using coherent anti-Stokes Raman scattering microscopy.
Anal. Chem. 81(6): 2085–2091 (2009)
- [202] Sasić, S.
An in-depth analysis of Raman and near-infrared chemical images of common pharmaceutical tablets.
Appl. spectrosc. 61(3): 239–250 (2007)
-

-
- [203] May, R.K. et al.
Hardness and density distributions of pharmaceutical tablets measured by terahertz pulsed imaging.
J. Pharm. Sci. 102(7): 2179–2186 (2013)
- [204] Ajito, K. et al.
Nondestructive Multicomponent Terahertz Chemical Imaging of Medicine in Tablets.
J. Electrochem. Soc. 161(9): B171–B175 (2014)
- [205] Fitzgerald, A.J., Cole, B.E., Taday, P.F.
Nondestructive analysis of tablet coating thicknesses using terahertz pulsed imaging.
J. Pharm. Sci. 94(1): 177–183 (2005)
- [206] Brock, D., Zeitler, J.A., Funke, A., Knop, K., Kleinebudde, P.
Evaluation of critical process parameters for intra-tablet coating uniformity using terahertz pulsed imaging.
Eur. J. Pharm. Biopharm. 85(3 Pt B): 1122–1129 (2013)
- [207] Brock, D., Zeitler, J.A., Funke, A., Knop, K., Kleinebudde, P.
Evaluation of critical process parameters for inter-tablet coating uniformity of active-coated GITS using Terahertz Pulsed Imaging.
Eur. J. Pharm. Biopharm. 88(2): 434–442 (2014)
- [208] Niwa, M., Hiraishi, Y., Terada, K.
Evaluation of coating properties of enteric-coated tablets using terahertz pulsed imaging.
Pharm. Res. 31(8): 2140–2151 (2014)
- [209] Zhong, S. et al.
Non-destructive quantification of pharmaceutical tablet coatings using terahertz pulsed imaging and optical coherence tomography.
Opt. Laser. Eng. 49(3): 361–365 (2011)
- [210] Zeitler, J.A., Shen, Y., Baker, C., Taday, P.F., Pepper, M., Rades, T.
Analysis of coating structures and interfaces in solid oral dosage forms by three dimensional terahertz pulsed imaging.
J. Pharm. Sci. 96(2): 330–340 (2007)
- [211] Elkhider, N., Chan, K.L.A., Kazarian, S.G.
Effect of moisture and pressure on tablet compaction studied with FTIR spectroscopic imaging.
J. Pharm. Sci. 96(2): 351–360 (2007)
-

-
- [212] Roggo, Y., Edmond, A., Chalus, P., Ulmschneider, M.
Infrared hyperspectral imaging for qualitative analysis of pharmaceutical solid forms.
Anal. Chim. Acta 535(1-2): 79–87 (2005)
- [213] Salzer, R., Siesler, H.W., eds.
Infrared and Raman Spectroscopic Imaging.
1st ed., Weinheim, Wiley-VCH (2009)
- [214] Strachan, C.J., Windbergs, M., Offerhaus, H.L.
Pharmaceutical applications of non-linear imaging.
Int. J. Pharm. 417(1-2): 163–172 (2011)
- [215] Vogt, F.G., Strohmeier, M.
Confocal UV and resonance Raman microscopic imaging of pharmaceutical products.
Mol. Pharm. 10(11): 4216–4228 (2013)
- [216] Zeitler, J.A., Taday, P.F., Newnham, D.A., Pepper, M., Gordon, K.C., Rades, T.
Terahertz pulsed spectroscopy and imaging in the pharmaceutical setting—a review.
J. Pharm. Pharmacol. 59(2): 209–223 (2007)
- [217] Amigo, J.
Emerging possibilities of near infrared spectroscopy and near infrared chemical imaging in the pharmaceutical manufacturing industry. The challenge of the process analytical technologies paradigm or just a research tool.
NIR news 24(8): 9 (2013)
- [218] Wu, J.X. et al.
Chemical imaging and solid state analysis at compact surfaces using UV imaging.
Int. J. Pharm. 477(1-2): 527–535 (2014)
- [219] Boetker, J.P. et al.
Insights into the early dissolution events of amlodipine using UV imaging and Raman spectroscopy.
Mol. Pharm. 8(4): 1372–1380 (2011)
- [220] Østergaard, J., Wu, J.X., Naelapää, K., Boetker, J.P., Jensen, H., Rantanen, J.
Simultaneous UV imaging and Raman spectroscopy for the measurement of solvent-mediated phase transformations during dissolution testing.
J. Pharm. Sci. 103(4): 1149–1156 (2014)
-

-
- [221] Gordon, S., Naelapää, K., Rantanen, J., Selen, A., Müllertz, A., Østergaard, J. Real-time dissolution behavior of furosemide in biorelevant media as determined by UV imaging. *Pharm. Dev. Technol.* 18(6): 1407–1416 (2013)
- [222] Wu, J.X., van den Berg, F., Rantanen, J., Rades, T., Yang, M. Current advances and future trends in characterizing poorly water-soluble drugs using spectroscopic, imaging and data analytical techniques. *Curr. Pharm. Des.* 20(3): 436–453 (2014)
- [223] Rinnan, Å., van den Berg, F., Engelsen, S.B. Review of the most common pre-processing techniques for near-infrared spectra. *Trends Anal. Chem* 28(10): 1201–1222 (2009)
- [224] Vidal, M., Amigo, J.M. Pre-processing of hyperspectral images. Essential steps before image analysis. *Chemom. Intell. Lab. Syst.* 117(0): 138–148 (2012)
- [225] Sacré, P.-Y. et al. A new criterion to assess distributional homogeneity in hyperspectral images of solid pharmaceutical dosage forms. *Anal. Chim. Acta* 818(0): 7–14 (2014)
- [226] Rinnan, Å. Pre-processing in vibrational spectroscopy – when, why and how. *Anal. Methods* 6(18): 7124 (2014)
- [227] Luo, W., Wu, J., Wang, X., Lin, X., Li, H. Near infrared spectroscopy combination with PLS to monitor the parameters of naproxen tablet preparation process. *Anal. Methods* 5(5): 1337 (2013)
- [228] Otsuka, M., Yamane, I. Prediction of tablet properties based on near infrared spectra of raw mixed powders by chemometrics: Scale-up factor of blending and tableting processes. *J. Pharm. Sci.* 98(11): 4296–4305 (2009)
- [229] Zhang, L., Henson, M.J., Sekulic, S.S. Multivariate data analysis for Raman imaging of a model pharmaceutical tablet. *Anal. Chim. Acta* 545(2): 262–278 (2005)
-

-
- [230] Bro, R., Smilde, A.K.
Centering and scaling in component analysis.
J. Chemom. 17(1): 16–33 (2003)
- [231] Wold, S., Esbensen, K., Geladi, P.
Principal component analysis.
Chemom. Intell. Lab. Syst. 2(1-3): 37–52 (1987)
- [232] Savolainen, M. et al.
Determination of amorphous content in the pharmaceutical process environment.
J. Pharm. Pharmacol. 59(2): 161–170 (2007)
- [233] Esbensen, K.H., Guyot, D., Westad, F., Houmoller, L.P.
Multivariate Data Analysis - In practice: An Introduction to Multivariate Data Analysis and Experimental Design.
5th ed., CAMO Software, Oslo (2010)
- [234] Gemperline, P.
Practical Guide to Chemometrics.
2nd ed., CRC Press, Boca Raton (2006)
- [235] Candolfi, A., De Maesschalck, R., Jouan-Rimbaud, D., Hailey, P.A., Massart, D.L.
The influence of data pre-processing in the pattern recognition of excipients near-infrared spectra.
J. Pharm. Biomed. Anal. 21(1): 115–132 (1999)
- [236] D'Antonio, J., Murphy, B.M., Manning, M.C., Al-Azzam, W.A.
Comparability of protein therapeutics: quantitative comparison of second-derivative amide I infrared spectra.
J. Pharm. Sci. 101(6): 2025–2033 (2012)
- [237] Barnes, R.J., Dhanoa, M.S., Lister, S.J.
Standard Normal Variate transformation and de-trending of near-infrared diffuse reflectance spectra.
Appl. spectrosc. 43(5): 772–777 (1989)
- [238] El-Hagrasy, A.S., Delgado-Lopez, M., Drennen, J.K.
A Process Analytical Technology approach to near-infrared process control of pharmaceutical powder blending: Part II: Qualitative near-infrared models for prediction of blend homogeneity.
J. Pharm. Sci. 95(2): 407–421 (2006)
-

-
- [239] Pérez-Ramos, J.D., Findlay, W.P., Peck, G., Morris, K.R.
Quantitative analysis of film coating in a pan coater based on in-line sensor measurements.
AAPS PharmSciTech 6(1): E127-36 (2005)
- [240] Drumm, C.A., Morris, M.D.
Microscopic Raman Line-Imaging with Principal Component Analysis.
Appl. spectrosc. 49(9): 1331–1337 (1995)
- [241] Lavine, B.K.
Clustering and Classification of Analytical Data.
In: Encyclopedia of Analytical Chemistry: Applications, Theory and Instrumentation (Meyers, R.A., ed.): 1–21, John Wiley & Sons, Chichester (2006)
- [242] Roussel, S., Preys, S., Chauchard, F., Lallemand, J.
Multivariate Data Analysis (Chemometrics).
In: Process Analytical Technology for the Food Industry, 1st ed. (O'Donnell, C.P., Fagan, C., Cullen, P., eds.): 7-59, Springer, New York (2014)
- [243] Pearson, K.
On lines and planes of closest fit to systems of points in space.
Philos. Mag. 2(11): 559–572 (1901)
- [244] Abdi, H., Williams, L.J.
Principal component analysis.
WIREs Comp. Stat. 2(4): 433–459 (2010)
- [245] Stockdale, G., Murphy, B.M., D'Antonio, J., Manning, M.C., Al-Azzam, W.
Comparability of higher order structure in proteins: chemometric analysis of second-derivative amide I fourier transform infrared spectra.
J. Pharm. Sci. 104(1): 25–33 (2015)
- [246] Eriksson, L.
Multi-and megavariate data analysis.
2nd ed., Umetrics AB, Umea (2006)
- [247] Kessler, W.
Multivariate Datenanalyse: für die Pharma-, Bio-und Prozessanalytik.
1st ed., Wiley-VCH, Weinheim (2007)
- [248] Berrueta, L.A., Alonso-Salces, R.M., Héberger, K.
Supervised pattern recognition in food analysis.
J. Chromatogr. A 1158(1-2): 196–214 (2007)
-

-
- [249] Wold, S., Martens, H., Wold, H.
The multivariate calibration problem in chemistry solved by the PLS method.
In: Matrix Pencils (Kågström, B., Ruhe, A., eds.): 286-293, Springer, Berlin Heidelberg (1983)
- [250] Wold, S., Ruhe, A., Wold, H., Dunn, III, W. J.
The Collinearity Problem in Linear Regression. The Partial Least Squares (PLS) Approach to Generalized Inverses.
SIAM J. Sci. Stat. Comput. 5(3): 735–743 (1984)
- [251] Wold, H.
Causal flows with latent variables.
Eur. Econ. Rev. 5(1): 67–86 (1974)
- [252] Abdi, H.
Partial least squares regression and projection on latent structure regression (PLS Regression).
WIREs Comp. Stat. 2(1): 97–106 (2010)
- [253] Dunn, W.J., Scott, D.R., Glen, W.G.
Principal components analysis and partial least squares regression.
Tetrahedron Comput. Methodol. 2(6): 349–376 (1989)
- [254] Bay, S.
Nearest neighbor classification from multiple feature subsets.
Intell. Data Anal. 3(3): 191–209 (1999)
- [255] Cover, T., Hart, P.
Nearest neighbor pattern classification.
IEEE Trans. Inf. Theory 13(1): 21–27 (1967)
- [256] Fix, E., Hodges Jr, J. L.
Discriminatory analysis-nonparametric discrimination: consistency properties.
Int. Stat. Rev. 57(3): 238–247 (1989)
- [257] Peterson, L.
K-nearest neighbor.
Scholarpedia 4(2): 1883 (2009)
- [258] Kowalski, B.R., Bender, C.F.
Pattern recognition. Powerful approach to interpreting chemical data.
J. Am. Chem. Soc. 94(16): 5632–5639 (1972)
-

-
- [259] Kowalski, B. R., Bender, C. F.
K-Nearest Neighbor Classification Rule (pattern recognition) applied to nuclear magnetic resonance spectral interpretation.
Anal. Chem. 44(8): 1405–1411 (1972)
- [260] Imandous, S.B., Bolandraftar, M.
Application of K-Nearest Neighbor (KNN) Approach for Predicting Economic Events: Theoretical Background.
Int. J. Eng. Res. Appl. 3(5): 605–610 (2013)
- [261] Cunningham, P., Delany, S.J.
k-Nearest neighbour classifiers. Technical Report UCD-CSI-2007-4, Artificial Intelligence Group, Dublin (2007)
- [262] Wold, S., Sjöström, M.
SIMCA: A Method for Analyzing Chemical Data in Terms of Similarity and Analogy.
In: *Chemometrics: Theory and Application* (Kowalski, B.R., ed.): 243-282, American Chemical Society, Washington DC (1977)
- [263] Wold, S.
Pattern recognition by means of disjoint principal components models.
Pattern Recogn. 8(3): 127–139 (1976)
- [264] Candolfi, A., De Maesschalck, R., Massart, D., Hailey, P., Harrington, A.
Identification of pharmaceutical excipients using NIR spectroscopy and SIMCA.
J. Pharm. Biomed. Anal. 19(6): 923–935 (1999)
- [265] Gemperline, P.J., Webber, L.D., Cox, F.O.
Raw materials testing using soft independent modeling of class analogy analysis of near-infrared reflectance spectra.
Anal. Chem. 61(2): 138–144 (1989)
- [266] De Beer, T.R.M. et al.
Raman spectroscopy as a process analytical technology (PAT) tool for the in-line monitoring and understanding of a powder blending process.
J. Pharm. Biomed. Anal. 48(3): 772–779 (2008)
- [267] De Maesschalck, R., Candolfi, A., Massart, D.L., Heuerding, S.
Decision criteria for soft independent modelling of class analogy applied to near infrared data.
Chemom. Intell. Lab. Syst. 47(1): 65–77 (1999)
-

-
- [268] Bylesjö, M., Rantalainen, M., Cloarec, O., Nicholson, J.K., Holmes, E., Trygg, J. OPLS discriminant analysis: combining the strengths of PLS-DA and SIMCA classification. *J. Chemom.* 20(8-10): 341–351 (2006)
- [269] Derde, M.P., Massart, D.L. Comparison of the performance of the class modelling techniques UNEQ, SIMCA, and PRIMA. *Chemom. Intell. Lab. Syst.* 4(1): 65–93 (1988)
- [270] Forina, M., Oliveri, P., Casale, M., Lanteri, S. Multivariate range modeling, a new technique for multivariate class modeling: the uncertainty of the estimates of sensitivity and specificity. *Anal. Chim. Acta* 622(1-2): 85–93 (2008)
- [271] van de Weert, M., Haris, P.I., Hennink, W.E., Crommelin, D.J. Fourier transform infrared spectrometric analysis of protein conformation: effect of sampling method and stress factors: Effect of sampling method and stress factors. *Anal. Biochem.* 297(2): 160–169 (2001)
- [272] Abdel-Hamid, S., Betz, G. Study of radial die-wall pressure changes during pharmaceutical powder compaction. *Drug Dev. Ind. Pharm.* 37(4): 387–395 (2011)
- [273] Gonzalez, R.C., Woods, R.E., Eddins, S.L. Digital image processing using MATLAB. 1st ed., Prentice Hall, Upper Saddle River (2004)
- [274] Fell, J.T., Newton, J.M. The tensile strength of lactose tablets. *J. Pharm. Pharmacol.* 20(8): 657–659 (1968)
- [275] Atherton, T.J., Kerbyson, D.J. Size invariant circle detection. *Image Vision Comput.* 17(11): 795–803 (1999)
- [276] Seitavuopio, P., Heinämäki, J., Rantanen, J., Yliruusi, J. Monitoring tablet surface roughness during the film coating process. *AAPS PharmSciTech* 7(2): E31 (2006)
- [277] Seitavuopio, P. The roughness and imaging characterisation of different pharmaceutical surfaces. PhD Thesis, University of Helsinki, Finland (2006)
-

-
- [278] Bittar, E.R., Caldeira, F.R., Santos, A., Günther, A.R., Rogana, E., Santoro, M.M.
Characterization of β -trypsin at acid pH by differential scanning calorimetry.
Braz. J. Med. Biol. Res. 36(12): 1621–1627 (2003)
- [279] Nasser Brumano, M.H., Rogana, E., Swaisgood, H.E.
Thermodynamics of unfolding of β -Trypsin at pH 2.8.
Arch. Biochem. Biophys. 382(1): 57–62 (2000)
- [280] Amigo, J.M., Ravn, C., Gallagher, N.B., Bro, R.
A comparison of a common approach to partial least squares-discriminant analysis and classical least squares in hyperspectral imaging.
Int. J. Pharm. 373(1-2): 179–182 (2009)
- [281] Ciurczak, E.
Uses of near-infrared spectroscopy in pharmaceutical analysis.
Appl. Spectrosc. Rev. 23(1-2): 147–163 (1987)
- [282] Kessler, R.W.
Sensitivity and selectivity in optical spectroscopy and imaging: A molecular approach.
In: OCM 2015 - optical characterization of materials: Conference proceedings (Beyerer, J., ed.): 89–102, KIT Scientific Publishing, Karlsruhe (2015)
- [283] Wu, J.X. et al.
A novel image analysis methodology for online monitoring of nucleation and crystal growth during solid state phase transformations.
Int. J. Pharm. 433(1-2): 60–70 (2012)
- [284] Canny, J.
A computational approach to edge detection.
IEEE T. Pattern Anal. PAMI-8(6): 679–698 (1986)
-

5 Appendix

A Curriculum vitae

The CV is not published for reasons of data protection.

B Conference contributions and publications

In context with this work, the following contributions have been presented at conferences and journal articles have been published.

Conference contributions - oral presentations

Klukkert, M., Sakmann, A., Rades, T., Leopold, C.S.
Investigation of the influence of tableting on the conformational and thermal stability of a model protein.
40th Annual Meeting of the Controlled Release Society, Honolulu, USA (2013)

Klukkert, M., Sakmann, A., Rehder, S., Carstensen, J.M., Rades, T., Leopold, C.S.
Multispectral UV imaging for high-speed quality control in the manufacturing process of tablets.
6th International Congress on Pharmaceutical Engineering, Graz, Austria (2014)

Klukkert, M., Wu, J.X., Carstensen, J.M., Rades, T., Leopold, C.S.
Multispectral UV imaging for quality control of tablets.
16th International Workshop on Physical Characterization of Pharmaceutical Solids, Prague, Czech (2014)

Klukkert, M., Wu, J.X., Rantanen, J., Carstensen, J.M., Rades, T., Leopold, C.S.
Multispectral UV imaging for fast and non-destructive quality control of tablets.
EuPAT 7 - Seventh pan-European QbD & PAT Science Conference, Graz, Austria (2015)

Conference contributions - poster presentations

Saniocki, I., Klukkert, M., Sakmann, A., Leopold, C.S.
Compaction of tablet formulations based on Ludipress® containing high-dose poorly compressible and pressure-sensitive drugs.
25th Annual Meeting of the American Association of Pharmaceutical Scientists
Washington DC, USA (2011)

Klukkert, M., Wu, J.X., Carstensen, J.M., Rades, T., Leopold, C.S.
Fast determination of API surface distribution in multicomponent enzyme tablet formulations by UV imaging.
27th Annual Meeting of the American Association of Pharmaceutical Scientists
San Antonio, USA (2013)

Biller, J., Klukkert, M., Morschheuser, L., Leopold, C.S., Trusch, M., Rohn, S.
Massenspektrometrische Charakterisierung von Enzym-Lactose-Derivaten.
47. Jahrestagung der Deutschen Gesellschaft für Massenspektrometrie
Frankfurt, Germany (2014)

Klukkert, M., Wu, J.X., Carstensen, J.M., Rades, T., Leopold, C.S.
High-throughput quality control of critical physical tablet attributes by UV multispectral imaging.
8th World Meeting on Pharmaceutics, Biopharmaceutics and Pharmaceutical Technology
Lisbon, Portugal (2014)

Klukkert, M., Wu, J.X., Carstensen, J.M., Rades, T., Leopold, C.S.
High-speed determination of the radial tensile strength of tablets by multispectral UV imaging.
28th Annual Meeting of the American Association of Pharmaceutical Scientists
San Diego, USA (2014)











Klukkert, M., Wu, J.X., Carstensen, J.M., Rades, T., Leopold, C.S.
Multispectral imaging for determination of an interaction between protein API and excipient during tableting and storage - a multifactorial approach.
28th Annual Meeting of the American Association of Pharmaceutical Scientists
San Diego, USA (2014)




Klukkert, M., Doreth, M., Grohgan, H., Rades, T., Leopold, C.S.
Role of water sorption capacity of tableting excipients to protect protein drugs from structural changes during storage using infrared spectroscopy.
41st Annual Meeting of the Controlled Release Society, Chicago, USA (2014)

Journal articles with authors contributions and reference chapters.

Title	Journal	Authors	Contribution to the work	Percentage	Reference chapters
Influence of tableting on the conformation and thermal stability of trypsin as a model protein	Journal of Pharmaceutical Sciences (accepted)	Klukkert, M. Van de Weert, M. Fanø, M. Rades, T. Leopold, C.S.	Project plan, experiments, data analysis, publication Supervisor Supervisor Supervisor Supervisor	100 %	2.3; 3.1;
Rapid assessment of tablet film coating quality by multispectral UV imaging	AAPS PharmSciTech (accepted)	Klukkert, M. Wu, J.X. Rantanen, J. Rehder, S.C. Carstensen, J.M. Rades, T. Leopold, C.S.	Project plan, experiments, data analysis, publication Data analysis Supervisor Supervisor Supervisor Supervisor Supervisor	95 % 5 %	1.4.3.4; 2.2.2; 2.6; 3.4;
Non-destructive quality control of tablets and blister packs by UV imaging	Pharmazeutische Industrie (accepted)	Klukkert, M. Wu, J.X. Rantanen, J. Rehder, S.C. Carstensen, J.M. Rades, T. Leopold, C.S.	Project plan, experiments, data analysis, publication Data analysis Supervisor Supervisor Supervisor Supervisor Supervisor	95 % 5 %	2.2.5; 2.5; 3.3;
Multispectral UV Imaging for fast and non-destructive quality control of chemical and physical tablet attributes	European Journal of Pharmaceutical sciences (submitted)	Klukkert, M. Wu, J.X. Rantanen, J. Carstensen, J.M. Rades, T. Leopold, C.S.	Project plan, experiments, data analysis, publication Data analysis Supervisor Supervisor Supervisor Supervisor	95 % 5 %	2.2.5; 2.4; 3.2;

C Hazardous materials

Substance	Supplier	Danger symbol	Hazard statements	Precautionary statements
Acetylsalicylic acid	Fagron Germany		H302, H315, H319, H335	P261, P305+P338+P351
Amylase	Extrakt Chemie Germany		H334	P261, P311+P342
Febantel	Bayer HealthCare Germany	  	H302, H360D, H410	P264, P273, P281, P301+P310, P308+P313, P330
Hydrochloric acid	Roth Germany		H290	P234, P390
Lipase	Extrakt Chemie Germany	 	H315, H319, H334	P261, P280, P302+P352, P313+P337
Praziquantel	Bayer HealthCare Germany		H312, H412	P273, P280, P302, P350
Pyrantel pamoate	Bayer HealthCare Germany		H317, H334, H412	P260, P273, P281, P303+P353+P361, P304+P341, P313+P333

Sodium hydroxide	Roth Germany		H290, H314	P280, P303+P353+P361, P305+P338+P351, P310
Trypsin	Biozym Germany	 	H315, H319, H334, H335	P261, P264

D Declaration on oath / Eidesstattliche Versicherung

Hiermit erkläre ich an Eides statt, dass ich die vorliegende Dissertationsschrift selbst verfasst und keine als die angegebenen Quellen und Hilfsmittel benutzt habe. Ich versichere zudem, keinen weiteren Promotionsversuch an einer anderen Einrichtung unternommen zu haben.

Hamburg, den

Marten Klukkert
